HIGH ORDER $\mathcal{H}(\mathbf{DIV})$ DISCONTINUOUS GALERKIN METHODS FOR MHD EQUATIONS

by

Jian Wu

A dissertation submitted to the faculty of
The University of North Carolina at Charlotte
in partial fulfillment of the requirements
for the degree of Doctor of Philosophy in
Applied Mathematics

Charlotte

2016

Approved by:

_____

Dr. Wei Cai

_____

Dr. Shaozhong Deng

_____

Dr. Duan Chen

_____

Dr. Zhengchang Su

ABSTRACT

JIAN WU. High order $\mathcal{H}(\mathbf{div})$ discontinuous Galerkin methods for MHD equations. (Under the direction of DR. WEI CAI)

In this dissertation, we investigate the divergence-free discontinuous Galerkin method using the $\mathcal{H}(\mathbf{div})$ basis, to solve the nonlinear ideal magnetohydrodynamics (MHD) equations. This is a novel approach to ensure the divergence-free condition on the magnetic field. The idea is to add on each element extra bubble functions from the same order hierarchical $\mathcal{H}(\mathbf{div})$-conforming basis to reduce the higher order divergence, and then extra constant edge functions to remove the constant term of divergence. As a consequence, this method has a smaller computational cost than the traditional discontinuous Galerkin method with standard piecewise polynomial spaces. We formulate the discontinuous Galerkin method using the $\mathcal{H}(\mathbf{div})$-conforming basis and perform extensive two-dimensional numerical experiments for both smooth solutions and solutions with discontinuities. The computational results show that the global divergence is largely reduced, but with a relatively small increase on the error of the numerical solution.

ACKNOWLEDGMENTS

Firstly, I would like to express my sincere gratitude to my advisor Prof. Wei Cai for the continuous support of my Ph.D study and related research, for his patience, motivation, and immense knowledge. His guidance helped me in all the time of research and writing of this thesis. I could not have imagined having a better advisor and mentor for my Ph.D study.

Besides my advisor, I would like to thank the rest of my dissertation committee: Prof. Shaozhong Deng, Prof. Duan Chen, and Dr. Zhengchang Su, for their insightful comments and encouragement, but also for the hard question which incented me to widen my research from various perspectives. I also need to offer special appreciation to Professor Joel Avrin and Shaozhong Deng, who served as graduate coordinator during my time in this program. Their insightful suggestions enabled me to success-fully finish this program.

My sincere thanks also goes to Dr. Changhao Yan and Dr. Jun Yang, who helped me to improve and debug my codes, and inspired me in many other aspects. I also need to thank Marshall Hamrick to help me set up the research facilities. Without their precious support it would not be possible to conduct this research.

Last but not least, I would not forget our team members, Brian Zinzer, Yijing Zhou, Caylah Retz, Kelly Smalenberger and Xingjie Li, for their weekly discussions that helped broaden my academic horizon.

I dedicate my dissertation to my parents, Huijuan Zou and Weiming Wu, for their patience, generosity and sacrifice along my growing path.

TABLE OF CONTENTS

LIST OF FIGURES

LIST OF TABLES

CHAPTER 1: INTRODUCTION

Magnetohydrodynamics (MHD) is the study of the magnetic properties of electrically conducting fluids. Examples of such magneto-fluids include plasmas, liquid metals, and salt water or electrolytes. The field of MHD was initiated by Hannes Alfvn [2], for which he received the Nobel Prize in Physics in 1970.

The simplest form of MHD, Ideal MHD, assumes that the fluid has so little resistivity that it can be treated as a perfect conductor. This is the limit of infinite magnetic Reynolds number. In ideal MHD, Lenz's law dictates that the fluid is in a sense tied to the magnetic field lines. To explain, in ideal MHD a small rope-like volume of fluid surrounding a field line will continue to lie along a magnetic field line, even as it is twisted and distorted by fluid flows in the system. This is sometimes referred to as the magnetic field lines being "frozen" in the fluid. The connection between magnetic field lines and fluid in ideal MHD fixes the topology of the magnetic field in the fluid. For example, if a set of magnetic field lines are tied into a knot, then they will remain so as long as the fluid/plasma has negligible resistivity. This difficulty in reconnecting magnetic field lines makes it possible to store energy by moving the fluid or the source of the magnetic field. The energy can then become available if the conditions for ideal MHD break down, allowing magnetic reconnection that releases the stored energy from the magnetic field.

Many physical problems arising in a modeling process can be described by the MHD

equations, the simplest self-constrained model. The fundamental concept behind MHD is that magnetic fields can induce currents in a moving conductive fluid, which in turn polarizes the fluid and reciprocally changes the magnetic field itself. The set of equations that describe MHD are a combination of the Navier-Stokes equations of fluid dynamics and Maxwell's equations of electromagnetism. These differential equations must be solved simultaneously, either analytically or numerically. The equations are highly nonlinear, and analytic solutions are not available. We will focus on the ideal MHD equations which form a hyperbolic conservation law but are constrained as the magnetic field of the system is evolved with the constraint of zero divergence, namely, $\nabla \cdot B = 0$. On an analytic level the involution constraint is always fulfilled, but numerical experiments indicate that negligence in dealing with the divergence constraint leads to numerical instabilities and nonphysical solutions. Besides, solving such a nonlinear system introduces another numerical challenge.

Various attemps have been made to numerically solve the hyperbolic conservation law. Finite Volume Method (FVM) and Finite Element Method (FEM) are two of the most popular methods. In this dissertation, we will focus on the Discontinuous Galerkin (DG) Method which combines the flexibility of FEM and the physical influence of FVM. A discontinuous basis, normally piecewise polynomials or normal continuous $\mathcal{H}(\mathbf{div})$ basis in our work, are used in DG method for the numerical solution and the test functions. Due to the discontinuity, the scheme is more flexible compared to standard Finite Element methods. The discontinuities at the element interfaces allow the design of suitable inter-element boundary treatments, namely, numerical fluxes, to obtain highly accurate and stable methods in many difficult cases.

The allowance of arbitrary unstructured grids can have its own polynomial degree independent of its neighbors. Moreover, the DG scheme has a extremely high parallel efficiency, since the local elements only depend on their immediate neighbors.

The first discontinuous Galerkin method was introduced by Reed and Hill [35] in 1973, when neutron transport was studied. Cockburn and Shu [6][10][11][12][24] developed a framework to solve nonlinear time dependent problems. For temporal integration, explicit, nonlinearly stable high order Runge-Kutta time discretizations are used. For the DG spatial integration, exact or approximate Riemann solvers as interface fluxes are applied. Also, total variation bounded nonlinear limiters are introduced to avoid oscillations near shocks [37].

In terms of numerical influence of the divergence free condition, many attempts have been made in the literature to satisfy the constraint or at least reduce the negative impact on the numerical solution. In the following we will review some of the divergence "cleaning" techniques in the context of MHD equations.

One way for the divergence correction is by projection, first proposed by Brackbill and Barnes [7] in 1980. The numerical magnetic field $\mathbf{B}$ is projected into a zero divergence vector space and the projected $\mathbf{B}$ is used in the next time step. Since the projection is based on solving a global Poisson equation, the scheme increases the computational cost a lot.

Another way is Powell's source term formulation [32][47] in 1994. It is derived from the physical laws if $\nabla \cdot \mathbf{B} = 0$ is not used. In order to symmetrize the MHD equations, source terms proportional to $\nabla \cdot \mathbf{B}$ are added to the equations. The source terms make the system well behaved but nonconservative.

In 2002 Dedner et. al. [36] introduced their hyperbolic divergence cleaning technique which has several advantages over the Powell's source terms. A generalized Lagrangian multiplier was introduced to the MHD equations, along with some control parameters. While the Powell source terms only propagates the divergence with fluid velocity, Dedner's method allows the divergence error to be transported to the domain boundaries with certain speed and damped at the same time.

Powell's and Dedner's methods are not able to reduce the divergence to zero, like the projection method of Brackbill and Barnes does, but these methods are local and easy to implement. To ensure an exact zero divergence, the follow approaches have been proposed.

Another class of numerical schemes preserving the divergence of the magnetic fields are often referred to as "constrained transport methods", which was first brought by Yee [45] in electromagnetics, and then adapted to MHD equations by Brecht et al. [18], Evans and Hawley [17], Stone and Norman [40], etc. In the approach, a staggered mesh is used, and a suitably defined discrete approximation to the divergence of the solution can be maintained exactly zero. This method has been further developed recently by combining with the higher order Godunov type schemes by Dai and Woodward [14], Ryu et al. [21], Balsara and Spicer [5], etc. In [3][4], Balsara developed such divergence-free reconstruction strategy in an adaptive mesh setting. In [41], Toth compared some of the methods mentioned above and introduced the field/flux-interpolated central difference (CD) approaches, in which no staggered mesh in needed. These shemes are restriced to structured grids and require large stencils for the spatial discretization.

In [27][44], Li introduced a DG scheme which is local and preserves the zero divergence of the magnetic field. This is done by first discretizing the normal components of the magnetic field along the edges of the elements, followed by a locally divergence free reconstruction inside the elements. This method is restricted to cartesian grids, since it uses the information of the normal components of the elements.

Recently, Li and Shu also introduced in [26] a DG scheme which uses a locally divergence free basis for the magnetic field, followed the approach in context of Stokes equations and the stationary Navier-Stokes equations, Baker et al.[22][23]. Li and Shu use the locally divergence-free piecewise polynomials as the solution space in the discontinuous Garlerkin method to solve ideal MHD equations. Because the space is smaller, it can save computational cost when using the locally divergence-free piecewise polynomial space compared with the standard piecewise polynomial space, while enhancing the accuracy and stability in many cases. However, since the locally divergence-free piecewise polynomials are used, it is hard to maintain the divergence free condition globally.

In this dissertation, using on the high order divergence-free $\mathcal{H}(\mathbf{div})$-conforming hierarchical bases for MHD equations proposed by Cai, et, al.[43], we follow the discontinuous Galerkin method to solve two dimensional nonlinear ideal MHD equations. The idea of the method is that the divergence-free $\mathcal{H}(\mathbf{div})$-conforming hierarchical bases is applied to the magnetic field $\mathbf{B}$ only, which will solve the magnetic filed equation globally. Then divergence cleaning treatments are introduced based on the $\mathcal{H}(\mathbf{div})$-conforming hierarchical bases to clean up the divergence of magnetic field, on the global basis. For other variables in the MHD equations, standard hierarchichal

basis function will be used, and it can maintain the computation at an efficient level. The method can be applied to three dimensional cases with no essential difficulty, but will not be considered in this dissertation.

This dissertation is organized as follows. In Section 2.1, we describe the ideal MHD equations along with their involution constraint. In Section 2.2, we will derive the discontinuous scheme for ideal MHD equations. In Section 2.3, we will introduce the construction of solving a two dimensional MHD equations using discontinuous Galerkin method. In Chapter 3, high order divergence-free $\mathcal{H}(\mathbf{div})$-conforming hierarchical bases are introduced, in both two dimension and three dimension cases. In Chapter 4, we will introduce the divergence cleaning treatment using the high order divergence-free $\mathcal{H}(\mathbf{div})$-conforming hierarchical bases, in both two dimension and three dimension cases. In Chapter 5, the numerical results are presented. In Chapter 6, concluding remarks are made. Finally, Chapter 7 is the appendix. In appendix, the mathematical derivation of the construction, the examples of basis functions, and other detailed parameters are included.

CHAPTER 2: MHD EQUATIONS AND DISCONTINUOUS GALERKIN METHOD

2.1   Ideal MHD Equations

Ideal MHD is only strictly applicable when the plasma is strongly collisional, so that the time scale of collisions is shorter than the other characteristic times in the system, and the particle distributions are therefore close to Maxwellian.

Electrically conducting fluid flow in which the electromagnetic forces can be of the same order or even greater than the hydrodynamic ones is often modeled by MHD equations. The ideal MHD equations consist of a set of nonlinear hyperbolic equations,

$$\frac{\partial \rho}{\partial t} + \nabla \cdot (\rho \mathbf{u}) = 0$$

$$\frac{\partial (\rho \mathbf{u})}{\partial t} + \nabla \cdot \left(\rho \mathbf{u} \mathbf{u}^T + \left(p + \frac{1}{2} |\mathbf{B}|^2 \right) \cdot I - \mathbf{B} \mathbf{B}^T \right) = 0$$

$$(2.1)$$

$$\frac{\partial E}{\partial t} + \nabla \cdot \left(\left(E + p + \frac{1}{2} |\mathbf{B}|^2 \right) \mathbf{u} - \mathbf{B} \left(\mathbf{u} \cdot \mathbf{B} \right) \right) = 0$$

$$\frac{\partial \mathbf{B}}{\partial t} + \nabla \cdot \left(\mathbf{u} \mathbf{B}^T - \mathbf{B} \mathbf{u}^T \right) = 0$$

with the additional divergence constraint

$$\nabla \cdot \mathbf{B} = 0 \qquad\qquad (2.2)$$

Here ρ, p, $\mathbf{u} = (u_x, u_y, u_z)$, $\mathbf{B} = (B_x, B_y, B_z)$ and E denote the mass density, the hydrodynamic presure, the velocity field, the magnetic field, and the total energy, respectively. The ratio of the specific heats is given by γ and

$$E = \frac{1}{2}\rho|\mathbf{u}|^2 + \frac{1}{2}|\mathbf{B}|^2 + \frac{p}{\gamma - 1} \tag{2.3}$$

This system combines the equations of gas dynamics with Maxwell equations for problems in which relativistic, viscous, and resistive effects can be neglected; the permeability is set to be unity. If the initial magnetic field satisfies the divergence-free condition (2.2), the exact solution will automatically satisfy the constraint (2.2) for all time.

We rewrite (2.1) in the conservation form

$$\mathbf{U}_t + \nabla \cdot \mathbf{F}(\mathbf{U}) = 0 \tag{2.4}$$

where

$$\mathbf{U} = (\rho, \rho u_x, \rho u_y, \rho u_z, B_x, B_y, B_z, E)^T$$

$$F_1(\mathbf{U}) = \left(\rho u_x, \rho u_x^2 + p + \frac{1}{2}|\mathbf{B}|^2 - B_x^2, \rho u_x u_y \right.$$

$$-B_x B_y, \rho u_x u_z - B_x B_z, 0, u_x B_y - u_y B_x, u_x B_z$$

$$\left. -u_z B_x, u_x \left(E + p + \frac{1}{2}|\mathbf{B}|^2 \right) - B_x \left(u_x B_x + u_y B_y + u_z B_z \right) \right)^T$$

$$F_2(\mathbf{U}) = \left(\rho u_y, \rho u_y u_x - B_y B_x, \rho u_y^2 + p + \frac{1}{2}|\mathbf{B}|^2 - B_y^2, \right.$$

$$\rho u_y u_z - B_y B_z, u_y B_x - u_x B_y, 0, u_y B_z - u_z B_y,$$

$$\left. u_y \left(E + p + \frac{1}{2}|\mathbf{B}|^2 \right) - B_y \left(u_x B_x + u_y B_y + u_z B_z \right) \right)^T$$

2.2   Discontinuous Galerkin Method for MHD Equations

Starting with a triangulation Γ_h of the domain Ω, with the element being denoted by K, the edge by e, and the outward unit normal by $\mathbf{n} = \mathbf{n}_{e,K} = (n_1, n_2)$, following the usual definition of discontinuous Galerkin methods for conservation laws, [12][6], we obtain the Runge-Kutta Discontinuous Galerkin formulation for (2.4) Find $\mathbf{U}_h \in \mathbf{V}_h$, such that for all $\mathbf{v} \in \mathbf{V}_h$,

$$\int_K \mathbf{U}_{ht} \cdot \mathbf{v} dx + \sum_{e \in \partial K} \int_e \mathbf{h}_{e,K}\left(\mathbf{U}_h^{int(K)}, \mathbf{U}_h^{ext(K)}, \mathbf{n}_{e,K}\right) \cdot \mathbf{v} ds - \int_K \mathbf{F}(\mathbf{U}_h) \cdot \nabla \mathbf{v} dx = 0, \ \forall K$$

$$(2.5)$$

holds, where $\mathbf{V}_h$ is the solution space, which is the same as the test function space and given by

$$\mathbf{V}_h = \mathbf{V}_h^k = \left\{ \mathbf{v} : \mathbf{v}|_K \in \mathbf{P}^k(K), \begin{pmatrix} v_5 \\ v_6 \end{pmatrix} \in H^k(div) \right\}$$

$$(2.6)$$

with $\mathbf{P}^k(K) = (P^k(K))^8$, and $P^k(K)$ denotes the space of polynomials in K of degree at most k.

In (2.5), $\mathbf{h}_{e,K}\left(\mathbf{U}_h^{int(K)}, \mathbf{U}_h^{ext(K)}, \mathbf{n}_{e,K}\right)$ is the numerical flux, which is an exact or approximate Riemann solver, consistent with $\mathbf{F}(\mathbf{U}_h) \cdot \mathbf{n}_{e,K}$ and conservative,

$$\mathbf{h}_{e,K}\left(\mathbf{v}_h^{int(K)}, \mathbf{v}_h^{ext(K)}, \mathbf{n}_{e,K}\right) + \mathbf{h}_{e,K'}\left(\mathbf{v}_h^{int(K')}, \mathbf{v}_h^{ext(K')}, \mathbf{n}_{e,K'}\right) = 0, \ K \cap K' = e \quad (2.7)$$

where $\mathbf{v}_h^{int(K)}, \mathbf{v}_h^{ext(K)}$ are the limits of $\mathbf{v}$ at the interface e from the interior and exterior of K, respectively. The one we will use in our numerical examples is the

Lax-Friedrichs flux,

$$\mathbf{h}_{e,K}(\mathbf{a}, \mathbf{b}, \mathbf{n}_{e,k}) = \frac{1}{2}[F(\mathbf{a}) \cdot \mathbf{n}_{e,k} + F(\mathbf{b}) \cdot \mathbf{n}_{e,k} - \alpha_{e,K}(\mathbf{b} - \mathbf{a})] \tag{2.8}$$

where $\alpha_{e,K}$ is an estimate of the largest absolute value of eigenvalues of the Jacobi $\frac{\partial}{\partial \mathbf{v}}\mathbf{F}(\mathbf{v}) \cdot \mathbf{n}_{e,K}$ in the neighborhood of the edge e.

For discontinuous Galerkin methods applied to nonlinear systems such as (2.1), nonlinear limiters are often needed. We use the minmod TVB slope limiter by Shu [37] and Cockburn *et al.* [6][11], which has a parameter M related to the magnitude of the second derivatives of the solution at smooth extrema.

To construct the minmod TVB slope limiter for triangular elements, we proceed as follows. We start by making a simple observation. Consider the triangles in Figure ??, where m_1 is the mid-point of the edge on the boundary of K_0, and bI_i denotes the barycenter of the triangle K_i for $i = 0, 1, 2, 3$.
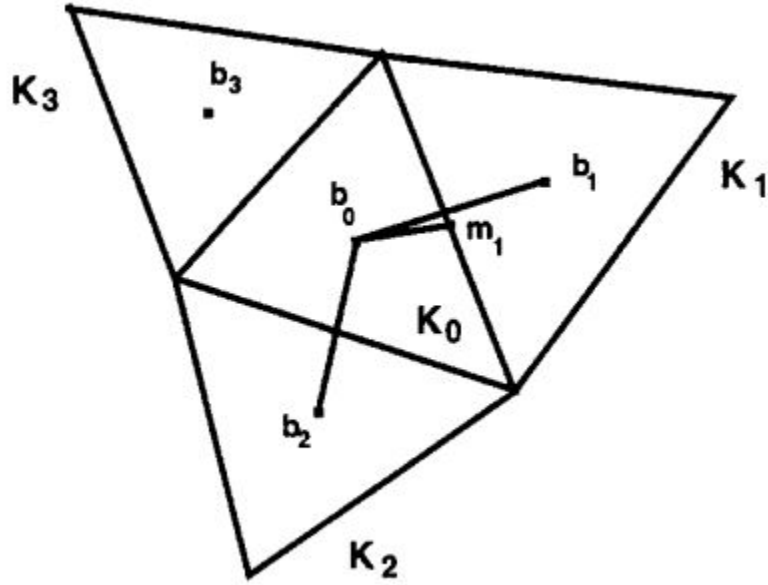
Figure 1: The 2D MINMOD limiter diagram.

Since we have that

$$m_1 - b_0 = \alpha_1(b_1 - b_0) + \alpha_2(b_2 - b_0) \tag{2.9}$$

for some nonnegative coefficients α_1, α_2 which depend only on m_1 and the geometry, we can write for any linear function u_h

$$u_h(m_1) - u_h(b_0) = \alpha_1(u_h(b_1) - u_h(b_0)) + \alpha_2(u_h(b_2) - u_h(b_0)) \tag{2.10}$$

and since

$$\overline{u}_{K_i} = \frac{1}{|K_i|} \int_{K_i} u_h = u_h(b_i), \ i = 0, 1, 2, 3, \tag{2.11}$$

we have that

$$\widetilde{u}_h(m_1, K_0) \equiv u_h(m_1) - \overline{u}_{K_0} \tag{2.12}$$

and

$$\Delta\overline{u}(m_1, K_0) \equiv \alpha_1(\overline{u}_{K_1} - \overline{u}_{K_0}) + \alpha_2(\overline{u}_{K_2} - \overline{u}_{K_0}) \tag{2.13}$$

Now, we are ready to describe the slope limiting. Let us consider a piecewise linear function u_h, and let $m_i, i = 1, 2, 3$ be the three mid-points of the edges of the triangle K_0. We then can write for $(x, y) \in K_0$

$$u_h(x, y) = \sum_{i=1}^{3} u_h(m_i)\psi_i(x, y) = \overline{u}_{K_0} + \sum_{i=1}^{3} \widetilde{u}_h(m_i, K_0)\psi_i(x, y) \tag{2.14}$$

where $\psi_i, i = 1, 2, 3$ are first order basis functions.

To compute $\Lambda\Pi_h u_h$, we first compute the quantities

$$\Delta_i = \overline{m}(\widetilde{u}_h(m_i, K_0), \nu\Delta\overline{u}(m_i, K_0)) \tag{2.15}$$

where $\overline{m}$ is the TVB modified *minmod* function defined as

$$\overline{m}(a_1, \cdots, a_m) = \begin{cases} a_1, & \text{for } |a_1| \leq M\Delta x^2, \\ m(a_1, \cdots, a_m), & \text{otherwise} \end{cases} \tag{2.16}$$

with the *minmod* function m defined by

$$m(a_1, \cdots, a_m) = \begin{cases} s \ \min_i |a_i|, & \text{if } s = \text{sign}(a_1) = \cdots = \text{sign}(a_m), \\ 0, & \text{otherwise} \end{cases} \tag{2.17}$$

The TVB correction is needed to avoid unnecessary limiting near smooth extrema. For an estimate of the TVB constant M in terms of the second derivatives of the function, see [10]. Usually, the numerical results are sensitive to the choice of limiters. In all calculation in this dissertation, we take M to be 50.

Also we take $\nu = 1.5$ in our computation. Then, if $\sum\limits_{i=1}^{3} \Delta_i = 0$, we simply set

$$\Lambda\Pi_h u_h(x, y) = \overline{u}_{K_0} + \sum_{i=1}^{3} \Delta_i \psi_i(x, y) \tag{2.18}$$

If $\sum\limits_{i=1}^{3} \Delta_i \neq 0$, we compute

$$\text{pos} = \sum_{i=1}^{3} \max(0, \Delta_i), \ \text{neg} = \sum_{i=1}^{3} \max(0, -\Delta_i) \tag{2.19}$$

and set

$$\theta^+ = \min\left(1, \frac{\text{neg}}{\text{pos}}\right), \ \theta^- = \min\left(1, \frac{\text{pos}}{\text{neg}}\right) \tag{2.20}$$

Then, we define

$$\Lambda\Pi_h u_h(x, y) = \overline{u}_{K_0} + \sum_{i=1}^{3} \widehat{\Delta}_i \psi_i(x, y) \tag{2.21}$$

where

$$\widehat{\Delta}_i = \theta^+ \max(0, \Delta_i) - \theta^- \max(0, \Delta_i) \qquad (2.22)$$

It is very easy to see that this slope-limiting operator satisfies the following three properties:

- Accuracy: if piecewise function u_h is linear, then $\Lambda\Pi_h u_h = u_h$.

- Conservation of mass: for every element K of the triangulation Γ_h, we have

$$\int_K \Lambda\Pi_h u_h = \int_K u_h \qquad (2.23)$$

- Slope limiting: on each element K of the triangulation Γ_h, the gradient of $\Lambda\Pi_h u_h$ is not larger than that of u_h.

2.3   MHD Equations in Two Dimensions

In two dimensional case, we rewrite (2.4) in the form of

$$\frac{\partial}{\partial t}\begin{bmatrix} \rho \\ \rho u_x \\ \rho u_y \\ E \\ B_x \\ B_y \end{bmatrix} + \frac{\partial}{\partial x}\begin{bmatrix} \rho u_x \\ \rho u_x^2 + p + \frac{1}{2}|\mathbf{B}|^2 - B_x^2 \\ \rho u_x u_y - B_x B_y \\ u_x \left(E + p + \frac{1}{2}|\mathbf{B}|^2\right) - B_x\left(\mathbf{u}\cdot\mathbf{B}\right) \\ 0 \\ u_x B_y - B_x u_y \end{bmatrix} + \frac{\partial}{\partial y}\begin{bmatrix} \rho u_y \\ \rho u_x u_y - B_x B_y \\ \rho u_y^2 + p + \frac{1}{2}|\mathbf{B}|^2 - B_y^2 \\ u_y \left(E + p + \frac{1}{2}|\mathbf{B}|^2\right) - B_y\left(\mathbf{u}\cdot\mathbf{B}\right) \\ u_y B_x - B_y u_x \\ 0 \end{bmatrix} = 0$$

$$(2.24)$$

where $p = (\gamma - 1)\left(E - \frac{1}{2}\rho\left(u_x^2 + u_y^2\right) - \frac{1}{2}\left(B_x^2 + B_y^2\right)\right)$.

In order to apply DG method, set

$$\mathbf{B} = \sum_{i=1}^{n} \alpha_i \vec{\psi}_i$$

$$\rho = \sum_{i=1}^{n} \beta_i \phi_i$$

$$\rho u_x = \sum_{i=1}^{n} \gamma_{x,i} \phi_i \qquad (2.25)$$

$$\rho u_y = \sum_{i=1}^{n} \gamma_{y,i} \phi_i$$

$$E = \sum_{i=1}^{n} \eta_i \phi_i$$

$\{\psi\}_i^n$ is the $\mathcal{H}(\mathbf{div})$-conforming basis, and $\{\phi\}_i^n$ is the regular orthonormal hierarchical basis.

$\mathcal{H}(\mathbf{div})$-conforming basis will be discussed in the next chapter. For regular orthonormal hierarchical basis in 2-D triangles $\{\phi\}_i^n$, the following form can be adapted, see [9]:

- Zeroth-order

$$\phi_{0,0} = \sqrt{2}$$

- First-order

$$\phi_{1,0} = 3(2x_1 - 1)$$

$$\phi_{0,1} = 2\sqrt{3}(x_1 + 2x_2 - 1)$$

- Second-order:

$$\phi_{2,0} = \sqrt{6}(1 - 8x_1 + 10x_1^2)$$

$$\phi_{0,2} = \sqrt{30}(1 - 2x_1 + x_1^2 - 6x_2 + 6x_1x_2 + 6x_2^2)$$

$$\phi_{1,1} = 3\sqrt{2}(x_1 + 2x_2 - 1)(5x_1 - 1)$$

- Third-oder:

$$\phi_{3,0} = 2\sqrt{2}(15x_1 - 45x_1^2 + 35x_1^3 - 1)$$

$$\phi_{0,3} = 2\sqrt{14}(3x_1 - 3x_1^2 + 12x_2 + x_1^3 - 24x_1x_2 - 30x_2^2 + 20x_2^3 + 12x_2x_1^2 + 30x_1x_2^2 - 1)$$

$$\phi_{2,1} = 2\sqrt{6}(x_1 + 2x_2 - 1)(1 - 12x_1 + 21x_1^2)$$

$$\phi_{1,2} = 2\sqrt{10}(7x_1 - 1)(1 - 2x_1 + x_1^2 - 6x_2 + 6x_1x_2 + 6x_2^2)$$

For future simplification, we define mass matrix M_ϕ, and stiffness matrix S_ϕ, for basis $\{\phi\}_i^n$

$$M_\phi = \int_K \phi_i\phi_j dx, \tag{2.26}$$

and

$$S_\phi = \int_K \left(u_x\phi_i\frac{\partial\phi_j}{\partial x} + u_y\phi_i\frac{\partial\phi_j}{\partial y} \right) dx. \tag{2.27}$$

This set of orthonormal basis functions will make the mass matrix

$$M_\phi = |J| \cdot I, \tag{2.28}$$

where $|J|$ is the Jacobian of the mapping from the reference triangle to the global triangle.

In order to perform integration on triangles and their edges, numerical integration

will be applied. We include the details of numerical integration for 1-D intervals and

2-D triangles in the appendix 7.3.

Now we will show the finite element construction of 2-D MHD equation.

First, for equation of ρ, the DG formulation is

$$\int_K \frac{\partial \rho}{\partial t} \phi_j dx = \int_K \rho \vec{u} \cdot \nabla \phi_j dx - \int_{\partial K} F^*(\rho) \cdot \phi_j ds \qquad (2.29)$$

For each term, we can rewrite them as

$$
\begin{aligned}
\int_K \frac{\partial \rho}{\partial t} \phi_j dx &= \frac{\partial}{\partial t} \int_K \sum_{i=1}^{n} \beta_i \phi_i \phi_j dx \\
&= \frac{\partial}{\partial t} \sum_{i=1}^{n} \beta_i \int_K \phi_i \phi_j dx \\
&= M_\phi \cdot \frac{d}{dt} \vec{\beta}^{\perp}
\end{aligned}
\qquad (2.30)
$$

$$
\begin{aligned}
\int_K \rho \vec{u} \cdot \nabla \phi_j dx &= \int_K \rho \left(u_x \cdot \frac{\partial \phi_j}{\partial x} + u_y \cdot \frac{\partial \phi_j}{\partial y} \right) d\vec{x} \\
&= \sum_{i=1}^{n} \beta_i \int_K \left(u_x \phi_i \frac{\partial \phi_j}{\partial x} + u_y \phi_i \frac{\partial \phi_j}{\partial y} \right) d\vec{x} \\
&= S_\phi \cdot \vec{\beta}^{\perp}
\end{aligned}
\qquad (2.31)
$$

After applying Lax-Friedrichs flux, the flux term becomes

$$
\begin{aligned}
\int_{\partial K} F^*(\rho) \cdot \phi_j ds &= \frac{1}{2} \int_{\partial K} (F(\rho^{int}) \cdot \vec{n} + F(\rho^{ext}) \cdot \vec{n} - C(\rho^{ext} - \rho^{int})) \cdot \phi_j ds \\
&= \frac{1}{2} \sum_{r=1}^{3} \int_{\partial \Gamma_r} (F(\rho^{int}) \cdot \vec{n} + F(\rho^{ext}) \cdot \vec{n} - C(\rho^{ext} - \rho^{int})) \cdot \phi_j ds
\end{aligned}
$$
$$(2.32)$$

where Γ_r is the edges of the triangle element.

On each edge, the flux term can be further expressed as

$$\frac{1}{2} \int_{\partial \Gamma_r} \left(F(\rho^{int}) \cdot \overrightarrow{n} + F(\rho^{ext}) \cdot \overrightarrow{n} \right) \cdot \phi_j ds$$

$$= \frac{1}{2} \int_{\partial \Gamma_r} \left(\rho^{int} \overrightarrow{u}^{int} \cdot \overrightarrow{n} + \rho^{ext} \overrightarrow{u}^{ext} \cdot \overrightarrow{n} \right) \cdot \phi_j ds \qquad (2.33)$$

$$= C_{avg,\rho}$$

$$\frac{1}{2} C \int_{\partial \Gamma_r} \left(\rho^{ext} - \rho^{int} \right) \cdot \phi_j ds = J_\rho \qquad (2.34)$$

The corresponding boundary condition is applied in the above flux term, which the edges lies on the boundary.

Second, for equation of $\overrightarrow{u}$, the DG formulation is

$$\int_K \frac{\partial \rho \overrightarrow{u}}{\partial t} \overrightarrow{\phi}_j dx = \int_K \left(\rho \overrightarrow{u} \overrightarrow{u}^T + \left(p + \tfrac{1}{2} |\overrightarrow{B}|^2 \right) \cdot I - \overrightarrow{B} \overrightarrow{B}^T \right) \cdot \nabla \overrightarrow{\phi}_j dx - \int_{\partial K} F^*(\rho \overrightarrow{u}) \cdot \overrightarrow{\phi}_j ds \quad (2.35)$$

For the first component u_x, we can rewrite each term as

$$\int_K \frac{\partial \rho \overrightarrow{u}_x}{\partial t} \overrightarrow{\phi}_j dx \;=\; \frac{\partial}{\partial t} \int_K \sum_{i=1}^n \gamma_{x,i} \phi_i \phi_j dx$$

$$= \frac{\partial}{\partial t} \sum_{i=1}^n \gamma_{x,i} \int_K \phi_i \phi_j dx \qquad (2.36)$$

$$= M_\phi \cdot \frac{d}{dt} \overrightarrow{\gamma_x}^\perp$$

$$\int_K \left(\rho u_x \overrightarrow{u} + \left(p + \frac{1}{2} |\overrightarrow{B}|^2 \right) \cdot \begin{pmatrix} 1 \\ 0 \end{pmatrix} - B_x \overrightarrow{B} \right) \cdot \nabla \phi_j dx$$

$$= \int_K \left\{ \left(\rho u_x u_x + \left(p + \frac{1}{2} |\overrightarrow{B}|^2 \right) - B_x B_x \right) \cdot \frac{\partial \phi_j}{\partial x} + \left(\rho u_x u_y - B_x B_y \right) \cdot \frac{\partial \phi_i}{\partial y} \right\} dx$$

$$= \int_K \left\{ \left(\sum_{i=1}^n \gamma_{x,i} \phi_i u_x + \left(p + \frac{1}{2} |\overrightarrow{B}|^2 \right) - B_x B_x \right) \cdot \frac{\partial \phi_j}{\partial x} + \left(\sum_{i=1}^n \gamma_{x,i} \phi_i u_y - B_x B_y \right) \cdot \frac{\partial \phi_i}{\partial y} \right\} dx \qquad (2.37)$$

$$= \sum_{i=1}^n \gamma_{x,i} \int_K \left(\phi_i u_x \cdot \frac{\partial \phi_j}{\partial x} + \phi_i u_y \cdot \frac{\partial \phi_j}{\partial y} \right) dx + \int_K \left\{ \left(p + \tfrac{1}{2} |\overrightarrow{B}|^2 - B_x - B_x \right) \cdot \frac{\partial \phi_j}{\partial x} - B_x B_y \cdot \frac{\partial \phi_j}{\partial y} \right\} dx$$

$$= S_\phi \cdot \overrightarrow{\gamma}_x^T + V_{\rho u_x}$$

After applying Lax-Friedrichs flux, the flux term becomes

$$\int_{\partial K} F^*(\rho u_x) \cdot \phi_j ds$$

$$= \frac{1}{2} \int_{\partial K} \{ (F((\rho u_x)^{int}) \cdot \overrightarrow{n} + F((\rho u_x)^{ext}) \cdot \overrightarrow{n} - C((\rho u_x)^{ext} - (\rho u_x)^{int})) \cdot \phi_j \} ds$$

$$= \frac{1}{2} \sum_{r=1}^{3} \int_{\partial \Gamma_r} \{ (F((\rho u_x)^{int}) \cdot \overrightarrow{n} + F((\rho u_x)^{ext}) \cdot \overrightarrow{n} - C((\rho u_x)^{ext} - (\rho u_x)^{int})) \cdot \phi_j \} ds$$

$$(2.38)$$

where Γ_r is the edges of the triangle element.

On each edge, the flux term can be further expressed as

$$\frac{1}{2} \int_{\partial \Gamma_r} (F((\rho u_x)^{int}) \cdot \overrightarrow{n} + F((\rho, u_x)^{ext}) \cdot \overrightarrow{n}) \cdot \phi_j ds$$

$$= \frac{1}{2} \int_{\partial \Gamma_r} \left\{ \left((\rho u_x)^{int} \overrightarrow{u}^{int} + \left(p^{int} + \frac{1}{2} |\overrightarrow{B}^{int}|^2 \right) \cdot \begin{pmatrix} 1 \\ 0 \end{pmatrix} - B_x^{int} \overrightarrow{B}^{int} \right) \cdot \overrightarrow{n} \right.$$

$$\left. + \left((\rho u_x)^{ext} \overrightarrow{u}^{ext} + \left(p^{ext} + \frac{1}{2} |\overrightarrow{B}^{ext}|^2 \right) \cdot \begin{pmatrix} 1 \\ 0 \end{pmatrix} - B_x^{ext} \overrightarrow{B}^{ext} \right) \cdot \overrightarrow{n} \right\} \cdot \phi_j ds$$

$$(2.39)$$

$$= C_{avg,\rho u_x}$$

$$\frac{1}{2} C \int_{\partial \Gamma_r} ((\rho u_x)^{ext} - (\rho u_x)^{int})) \cdot \phi_j ds = J_{\rho u_x} \tag{2.40}$$

The corresponding boundary condition is applied in the above flux term, which the edges lies on the boundary.

In the same manner, the second component of $\overrightarrow{u}$, u_y is calculated as follows.

$$\int_K \frac{\partial \rho \overrightarrow{u}_y}{\partial t} \overrightarrow{\phi}_j dx = \frac{\partial}{\partial t} \int_K \sum_{i=1}^{n} \gamma_{y,i} \phi_i \phi_j dx$$

$$= \frac{\partial}{\partial t} \sum_{i=1}^{n} \gamma_{y,i} \int_K \phi_i \phi_j dx \tag{2.41}$$

$$= M_\phi \cdot \frac{d}{dt} \overrightarrow{\gamma_y}^\perp$$

$$\int_K \left(\rho u_y \overrightarrow{u} + \left(p + \frac{1}{2}|\overrightarrow{B}|^2\right) \cdot \begin{pmatrix} 0 \\ 1 \end{pmatrix} - B_y \overrightarrow{B} \right) \cdot \nabla \phi_j dx$$

$$= \int_K \left\{ (\rho u_y u_x - B_y B_x) \cdot \frac{\partial \phi_i}{\partial x} + \left(\rho u_y u_y + \left(p + \frac{1}{2}|\overrightarrow{B}|^2\right) - B_y B_y\right) \cdot \frac{\partial \phi_j}{\partial y} \right\} dx$$

$$= \int_K \left\{ \left(\sum_{i=1}^{n} \gamma_{y,i} \phi_i u_x - B_y B_x\right) \cdot \frac{\partial \phi_i}{\partial x} + \left(\sum_{i=1}^{n} \gamma_{y,i} \phi_i u_y + \left(p + \frac{1}{2}|\overrightarrow{B}|^2\right) - B_y B_y\right) \cdot \frac{\partial \phi_j}{\partial y} \right\} dx \qquad (2.42)$$

$$= \sum_{i=1}^{n} \gamma_{y,i} \int_K \left(\phi_i u_x \cdot \frac{\partial \phi_j}{\partial x} + \phi_i u_y \cdot \frac{\partial \phi_j}{\partial y} \right) dx + \int_K \left\{ \left(p + \frac{1}{2}|\overrightarrow{B}|^2 - B_y - B_y\right) \cdot \frac{\partial \phi_j}{\partial x} - B_y B_x \cdot \frac{\partial \phi_j}{\partial x} \right\} dx$$

$$= S_\phi \cdot \overrightarrow{\gamma}_y^T + V_{\rho u_y}$$

After applying Lax-Friedrichs flux, the flux term becomes

$$\int_{\partial K} F^*(\rho u_y) \cdot \phi_j ds$$

$$= \frac{1}{2} \int_{\partial K} \left(F((\rho u_y)^{int}) \cdot \overrightarrow{n} + F((\rho u_y)^{ext}) \cdot \overrightarrow{n} - C((\rho u_y)^{ext} - (\rho u_y)^{int}) \right) \cdot \phi_j ds$$

$$= \frac{1}{2} \sum_{r=1}^{3} \int_{\partial \Gamma_r} \left(F((\rho u_y)^{int}) \cdot \overrightarrow{n} + F((\rho u_y)^{ext}) \cdot \overrightarrow{n} - C((\rho u_y)^{ext} - (\rho u_y)^{int}) \right) \cdot \phi_j ds$$

$$(2.43)$$

where Γ_r is the edges of the triangle element.

On each edge, the flux term can be further expressed as

$$\frac{1}{2} \int_{\partial \Gamma_r} \left(F((\rho u_y)^{int}) \cdot \overrightarrow{n} + F((\rho, u_y)^{ext}) \cdot \overrightarrow{n} \right) \cdot \phi_j ds$$

$$= \frac{1}{2} \int_{\partial \Gamma_r} \left\{ \left((\rho u_y)^{int} \overrightarrow{u}^{int} + \left(p^{int} + \frac{1}{2}|\overrightarrow{B}^{int}|^2\right) \cdot \begin{pmatrix} 0 \\ 1 \end{pmatrix} - B_y^{int} \overrightarrow{B}^{int} \right) \cdot \overrightarrow{n} \right.$$

$$+ \left. \left((\rho u_y)^{ext} \overrightarrow{u}^{ext} + \left(p^{ext} + \frac{1}{2}|\overrightarrow{B}^{ext}|^2\right) \cdot \begin{pmatrix} 0 \\ 1 \end{pmatrix} - B_y^{ext} \overrightarrow{B}^{ext} \right) \cdot \overrightarrow{n} \right\} \cdot \phi_j ds \qquad (2.44)$$

$$= C_{avg,\rho u_y}$$

$$\frac{1}{2} C \int_{\partial \Gamma_r} \left((\rho u_y)^{ext} - (\rho u_y)^{int} \right) \cdot \phi_j ds = J_{\rho u_y} \qquad (2.45)$$

The corresponding boundary condition is applied in the above flux term, which the edges lies on the boundary.

Third, for equation of E, the DG formulation is

$$\int_K \frac{\partial E}{\partial t} \cdot \phi_j dx = \int_K \left(\left(E + p + \frac{1}{2}|\vec{B}|^2 \right) \cdot \vec{u} - \vec{B}(\vec{u} - \vec{B}) \right) \cdot \nabla \phi_j dx - \int_{\partial K} F^*(E) \cdot \phi_j ds$$

$$(2.46)$$

For each term, we can rewrite into

$$
\begin{aligned}
\int_K \frac{\partial E}{\partial t} \vec{\phi}_j dx &= \frac{\partial}{\partial t} \int_K \sum_{i=1}^n \eta_i \phi_i \phi_j dx \\
&= \frac{\partial}{\partial t} \sum_{i=1}^n \eta_i \int_K \phi_i \phi_j dx \\
&= M_\phi \cdot \frac{d}{dt} \vec{\eta}^T
\end{aligned}
$$

$$(2.47)$$

$$
\begin{aligned}
&\int_K \left(\left(E + p + \frac{1}{2}|\vec{B}|^2 \right) \cdot \vec{u} - \vec{B}(\vec{u} - \vec{B}) \right) \cdot \nabla \vec{\phi}_j dx \\
&= \int_K \left\{ \left(\left(E + p + \frac{1}{2}|\vec{B}|^2 \right) u_x - B_x(\vec{u} - \vec{B}) \right) \cdot \frac{\partial \phi_j}{\partial x} \right. \\
&\left. + \left(\left(E + p + \frac{1}{2}|\vec{B}|^2 \right) u_y - B_y(\vec{u} - \vec{B}) \right) \cdot \frac{\partial \phi_j}{\partial y} \right\} dx \\
&= \int_K \left\{ \left(\left(\sum_{i=1}^n \eta_j \phi_i + p + \frac{1}{2}|\vec{B}|^2 \right) u_x - B_x(\vec{u} - \vec{B}) \right) \cdot \frac{\partial \phi_j}{\partial x} \right. \\
&\left. + \left(\left(\sum_{i=1}^n \eta_j \phi_i + p + \frac{1}{2}|\vec{B}|^2 \right) u_y - B_y(\vec{u} - \vec{B}) \right) \cdot \frac{\partial \phi_j}{\partial y} \right\} dx \\
&= \sum_{i=1}^n \eta_j \int_K \left(u_x \phi_i \cdot \frac{\partial \phi_j}{\partial x} + u_y \phi_i \cdot \frac{\partial \phi_j}{\partial y} \right) dx \\
&+ \int_K \left\{ \left(\left(p + \frac{1}{2}|\vec{B}|^2 \right) u_x - B_x(\vec{u} - \vec{B}) \right) \cdot \frac{\partial \phi_j}{\partial x} + \left(\left(p + \frac{1}{2}|\vec{B}|^2 \right) u_y - B_y(\vec{u} - \vec{B}) \right) \cdot \frac{\partial \phi_j}{\partial y} \right\} dx \\
&= S_\phi \cdot \vec{\eta}^T + V_E
\end{aligned}
$$

$$(2.48)$$

After applying Lax-Friedrichs flux, the flux term becomes

$$
\begin{aligned}
&\int_{\partial K} F^*(E) \cdot \phi_j ds \\
&= \frac{1}{2} \int_{\partial K} \left(F(E^{int}) \cdot \vec{n} + F(E^{ext}) \cdot \vec{n} - C(E^{ext} - E^{int}) \right) \cdot \phi_j ds \\
&= \frac{1}{2} \sum_{r=1}^3 \int_{\partial \Gamma_r} \left(F(E^{int}) \cdot \vec{n} + F(E^{ext}) \cdot \vec{n} - C(E^{ext} - E^{int}) \right) \cdot \phi_j ds
\end{aligned}
$$

$$(2.49)$$

where Γ_r is the edges of the triangle element.

On each edge, the flux term can be further expressed as

$$
\begin{aligned}
&\frac{1}{2}\int_{\partial\Gamma_r}\left(F(E^{int})\cdot\overrightarrow{n}+F(E^{ext})\cdot\overrightarrow{n}\right)\cdot\phi_j ds\\
&=\frac{1}{2}\int_{\partial\Gamma_r}\left\{\left(\left(E^{int}+p^{int}+\tfrac{1}{2}|\overrightarrow{B}^{int}|^2\right)\cdot\overrightarrow{u}^{int}-\overrightarrow{B}^{int}(\overrightarrow{u}^{int}\cdot\overrightarrow{B}^{int})\right)\cdot\overrightarrow{n}\right.\\
&\left.+\left(\left(E^{ext}+p^{ext}+\tfrac{1}{2}|\overrightarrow{B}^{ext}|^2\right)\cdot\overrightarrow{u}^{ext}-\overrightarrow{B}^{ext}(\overrightarrow{u}^{ext}\cdot\overrightarrow{B}^{ext})\right)\cdot\overrightarrow{n}\right\}\cdot\phi_j ds\\
&=C_{avg,E}
\end{aligned}
\tag{2.50}
$$

$$
\frac{1}{2}C\int_{\partial\Gamma_r}\left(E^{ext}-E^{int}\right)\cdot\phi_j ds=J_E
\tag{2.51}
$$

The corresponding boundary condition is applied in the above flux term, which the

edges lies on the boundary.

Fianlly, for equation of $\overrightarrow{B}$, the DG formulation is

$$
\int_K\frac{\partial\overrightarrow{B}}{\partial t}\cdot\overrightarrow{\psi}_j dx=\int_K\left(\overrightarrow{B}\cdot\overrightarrow{u}^T-\overrightarrow{u}\cdot\overrightarrow{B}^T\right)\cdot\nabla\overrightarrow{\psi}_j dx-\int_{\partial K}F^*\cdot\overrightarrow{\psi}_j ds
\tag{2.52}
$$

For each term, we can rewrite into

$$
\begin{aligned}
\int_K\frac{\partial\overrightarrow{B}}{\partial t}\overrightarrow{\psi}_j dx&=\frac{\partial}{\partial t}\int_K\sum_{i=1}^n\alpha_i\overrightarrow{\psi}_i\overrightarrow{\psi}_j dx\\
&=\frac{\partial}{\partial t}\sum_{i=1}^n\alpha_i\int_K\overrightarrow{\psi}_i\overrightarrow{\psi}_j dx\\
&=M_\psi\cdot\frac{d}{dt}\overrightarrow{\alpha}^T
\end{aligned}
\tag{2.53}
$$

$$
\begin{aligned}
&\int_K\left(\overrightarrow{B}\cdot\overrightarrow{u}^T-\overrightarrow{u}\cdot\overrightarrow{B}^T\right)\cdot\nabla\overrightarrow{\psi}_j dx\\
&=\int_K\left\{(\overrightarrow{B}u_x-\overrightarrow{u}B_x)\cdot\frac{\partial\overrightarrow{\psi}_j}{\partial x}+(\overrightarrow{B}u_y-\overrightarrow{u}B_y)\cdot\frac{\partial\overrightarrow{\psi}_j}{\partial y}\right\}dx\\
&=\int_K\left\{\left(\sum_{i=1}^n\alpha_i\overrightarrow{\psi}_iu_x-\sum_{i=1}^n\alpha_i\psi_{i,x}\overrightarrow{u}\right)\cdot\frac{\partial\overrightarrow{\psi}_j}{\partial x}+\left(\sum_{i=1}^n\alpha_i\overrightarrow{\psi}_iu_y-\sum_{i=1}^n\alpha_i\psi_{i,y}\overrightarrow{u}\right)\cdot\frac{\partial\overrightarrow{\psi}_j}{\partial y}\right\}dx\\
&=\sum_{i=1}^n\alpha_i\int_K\left\{(\overrightarrow{\psi}_iu_x-\psi_{i,x}\overrightarrow{u})\cdot\frac{\partial\overrightarrow{\psi}_j}{\partial x}+(\overrightarrow{\psi}_iu_y-\psi_{i,y}\overrightarrow{u})\cdot\frac{\partial\overrightarrow{\psi}_j}{\partial y}\right\}dx\\
&=S_B\cdot\overrightarrow{\alpha}^T
\end{aligned}
\tag{2.54}
$$

After applying Lax-Friedrichs flux, the flux term becomes

$$\int_{\partial K} F^* \cdot \vec{\psi}_j ds$$

$$= \frac{1}{2} \int_{\partial K} \left(\vec{F}(\vec{B}^{int}) \cdot \vec{n} + \vec{F}(\vec{B}^{ext}) \cdot \vec{n} - C(\vec{B}^{ext} - \vec{B}^{int}) \right) \cdot \vec{\psi}_j ds \qquad (2.55)$$

$$= \frac{1}{2} \sum_{r=1}^{3} \int_{\gamma_r} \left(\vec{F}(\vec{B}^{int}) \cdot \vec{n} + \vec{F}(\vec{B}^{ext}) \cdot \vec{n} - C(\vec{B}^{ext} - \vec{B}^{int}) \right) \cdot \vec{\psi}_j ds$$

where Γ_r is the edges of the triangle element.

On each edge, the flux term can be further expressed as

$$\frac{1}{2} \int_{\partial \Gamma_r} \left(\vec{F}(\vec{B}^{int}) \cdot \vec{n} + \vec{F}(\vec{B}^{ext}) \cdot \vec{n} \right) \cdot \vec{\psi}_j ds$$

$$= \frac{1}{2} \int_{\partial \Gamma_r} \left\{ \left(\vec{B}^{int} u_x^{int} - \vec{u}^{int} B_x^{int} + \vec{B}^{ext} u_x^{ext} - \vec{u}^{ext} B_x^{ext} \right) \cdot n_x \cdot \vec{\psi}_j \right.$$

$$\left. + \left(\vec{B}^{int} u_y^{int} - \vec{u}^{int} B_y^{int} + \vec{B}^{ext} u_y^{ext} - \vec{u}^{ext} B_y^{ext} \right) \cdot n_y \cdot \vec{\psi}_j \right\} ds \qquad (2.56)$$

$$= C_{avg,B}$$

$$\frac{1}{2} C \int_{\partial \Gamma_r} \left(\vec{B}^{ext} - \vec{B}^{int} \right) \cdot \vec{\psi}_j ds = J_B \qquad (2.57)$$

The corresponding boundary condition is applied in the above flux term, which the

edges lies on the boundary.

MHD Equations in time space

Next, we construction our equations with all the matrices above

$$M_\phi \cdot \frac{d}{dt} \vec{\beta}^T = S_\phi \cdot \vec{\beta}^T - \sum_{r=1}^{3} (C_{avg,\rho} - J_\rho)$$

$$M_\phi \cdot \frac{d}{dt} \vec{\gamma}_x^T = S_\phi \cdot \vec{\gamma}_x^T + V_{\rho u_x} - \sum_{r=1}^{3} (C_{avg,\rho u_x} - J\rho u_x)$$

$$M_\phi \cdot \frac{d}{dt} \vec{\gamma}_y^T = S_\phi \cdot \vec{\gamma}_y^T + V_{\rho u_y} - \sum_{r=1}^{3} (C_{avg,\rho u_y} - J\rho u_y) \qquad (2.58)$$

$$M_\phi \cdot \frac{d}{dt} \vec{\eta}^T = S_\phi \cdot \vec{\eta}^T + V_E - \sum_{r=1}^{3} (C_{avg,E} - J_E)$$

$$M_B \cdot \frac{d}{dt} \vec{\alpha}^T = S_B \cdot \vec{\alpha}^T - \sum_{r=1}^{3} (C_{avg,B} - J_B)$$

- Forward Euler scheme

Euler method is a first-order numerical procedure for solving ordinary differential equations (ODEs) with a given initial value. It is the most basic explicit method for numerical integration of ordinary differential equations and is the simplest Runge-Kutta method. Euler method has error of order $O(h)$.

$$\vec{\beta}^{T(N+1)} = \vec{\beta}^{T(N)} + \Delta h \cdot M_\phi^{-1} \cdot \left\{ S_\phi^{(N)} \cdot \vec{\beta}^{T(N)} - \sum_{r=1}^{3} (C_{avg,\rho}^{(N)} - J_\rho^{(N)}) \right\}$$

$$\vec{\gamma}_x^{T(N+1)} = \vec{\gamma}_x^{T(N)} + \Delta h \cdot M_\phi^{-1} \cdot \left\{ S_\phi^{(N)} \cdot \vec{\gamma}_x^{T(N)} + V_{\rho u_x}^{(N)} - \sum_{r=1}^{3} (C_{avg,\rho u_x}^{(N)} - J_{\rho u_x}^{(N)}) \right\}$$

$$\vec{\gamma}_y^{T(N+1)} = \vec{\gamma}_y^{T(N)} + \Delta h \cdot M_\phi^{-1} \cdot \left\{ S_\phi^{(N)} \cdot \vec{\gamma}_y^{T(N)} + V_{\rho u_y}^{(N)} - \sum_{r=1}^{3} (C_{avg,\rho u_y}^{(N)} - J_{\rho u_y}^{(N)}) \right\}$$

$$\vec{\eta}^{T(N+1)} = \vec{\eta}^{T(N)} + \Delta h \cdot M_\phi^{-1} \cdot \left\{ S_\phi^{(N)} \cdot \vec{\eta}^{T(N)} + V_E^{(N)} - \sum_{r=1}^{3} (C_{avg,E}^{(N)} - J_E^{(N)}) \right\}$$

$$\vec{\alpha}^{T(N+1)} = \vec{\alpha}^{T(N)} + \Delta h \cdot M_B^{-1} \cdot \left\{ S_B^{(N)} \cdot \vec{\alpha}^{T(N)} - \sum_{r=1}^{3} (C_{avg,B}^{(N)} - J_B^{(N)}) \right\}$$

$$(2.59)$$

where Δh is the size of each time step.

- 3rd order Runge-Kutta scheme

RungeKutta methods are a family of implicit and explicit iterative methods, which includes the well-known routine called the Euler Methods, used in temporal discretization for the approximate solutions of ordinary differential equations.

$$\vec{\beta}^{T(N+1)} = \vec{\beta}^{T(N)} + \frac{1}{6}\Delta h \cdot (K_1^\beta + 4K_2^\beta + K_3^\beta)$$

$$\vec{\gamma}_x^{T(N+1)} = \vec{\gamma}_x^{T(N)} + \frac{1}{6}\Delta h \cdot (K_1^{\gamma_x} + 4K_2^{\gamma_x} + K_3^{\gamma_x})$$

$$\vec{\gamma}_y^{T(N+1)} = \vec{\gamma}_y^{T(N)} + \frac{1}{6}\Delta h \cdot (K_1^{\gamma_y} + 4K_2^{\gamma_y} + K_3^{\gamma_y}) \qquad (2.60)$$

$$\vec{\eta}^{T(N+1)} = \vec{\eta}^{T(N)} + \frac{1}{6}\Delta h \cdot (K_1^\eta + 4K_2^\eta + K_3^\eta)$$

$$\vec{\alpha}^{T(N+1)} = \vec{\alpha}^{T(N)} + \frac{1}{6}\Delta h \cdot (K_1^\alpha + 4K_2^\alpha + K_3^\alpha)$$

where

$$K_1^\beta = M_\phi^{-1} \cdot \left\{ S_\phi^{(N)} \cdot \overrightarrow{\beta}^{T(N)} - \sum_{r=1}^{3} (C_{avg,\rho}^{(N)} - J_\rho^{(N)}) \right\}$$

$$K_2^\beta = M_\phi^{-1} \cdot \left\{ S_\phi^{(N)} \cdot \left(\overrightarrow{\beta}^{T(N)} + \frac{\Delta h K_1^\beta}{2} \right) - \sum_{r=1}^{3} (C_{avg,\rho}^{(N)} - J_\rho^{(N)}) \right\}$$

$$K_3^\beta = M_\phi^{-1} \cdot \left\{ S_\phi^{(N)} \cdot \left(\overrightarrow{\beta}^{T(N)} - \Delta h K_1^\beta + 2\Delta h K_2^\beta \right) - \sum_{r=1}^{3} (C_{avg,\rho}^{(N)} - J_\rho^{(N)}) \right\}$$

$$(2.61)$$

and

$$K_1^{\gamma_x} = M_\phi^{-1} \cdot \left\{ S_\phi^{(N)} \cdot \overrightarrow{\gamma}_x^{T(N)} + V_{\rho u_x}^{(N)} - \sum_{r=1}^{3} (C_{avg,\rho u_x}^{(N)} - J_{\rho u_x}^{(N)}) \right\}$$

$$K_2^{\gamma_x} = M_\phi^{-1} \cdot \left\{ S_\phi^{(N)} \cdot \left(\overrightarrow{\gamma}_x^{T(N)} + \frac{\Delta h K_1^{\gamma_x}}{2} \right) + V_{\rho u_x}^{(N)} - \sum_{r=1}^{3} (C_{avg,\rho u_x}^{(N)} - J_{\rho u_x}^{(N)}) \right\}$$

$$K_3^{\gamma_x} = M_\phi^{-1} \cdot \left\{ S_\phi^{(N)} \cdot \left(\overrightarrow{\gamma}_x^{T(N)} - \Delta h K_1^{\gamma_x} + 2\Delta h K_2^{\gamma_x} \right) + V_{\rho u_x}^{(N)} - \sum_{r=1}^{3} (C_{avg,\rho u_x}^{(N)} - J_{\rho u_x}^{(N)}) \right\}$$

$$(2.62)$$

and

$$K_1^{\gamma_y} = M_\phi^{-1} \cdot \left\{ S_\phi^{(N)} \cdot \overrightarrow{\gamma}_y^{T(N)} + V_{\rho u_y}^{(N)} - \sum_{r=1}^{3} (C_{avg,\rho u_y}^{(N)} - J_{\rho u_y}^{(N)}) \right\}$$

$$K_2^{\gamma_y} = M_\phi^{-1} \cdot \left\{ S_\phi^{(N)} \cdot \left(\overrightarrow{\gamma}_y^{T(N)} + \frac{\Delta h K_1^{\gamma_y}}{2} \right) + V_{\rho u_y}^{(N)} - \sum_{r=1}^{3} (C_{avg,\rho u_y}^{(N)} - J_{\rho u_y}^{(N)}) \right\}$$

$$K_3^{\gamma_y} = M_\phi^{-1} \cdot \left\{ S_\phi^{(N)} \cdot \left(\overrightarrow{\gamma}_y^{T(N)} - \Delta h K_1^{\gamma_y} + 2\Delta h K_2^{\gamma_y} \right) + V_{\rho u_y}^{(N)} - \sum_{r=1}^{3} (C_{avg,\rho u_y}^{(N)} - J_{\rho u_y}^{(N)}) \right\}$$

$$(2.63)$$

and

$$K_1^\eta = M_\phi^{-1} \cdot \left\{ S_\phi^{(N)} \cdot \overrightarrow{\eta}^{T(N)} + V_E^{(N)} - \sum_{r=1}^{3} (C_{avg,E}^{(N)} - J_E^{(N)}) \right\}$$

$$K_2^\eta = M_\phi^{-1} \cdot \left\{ S_\phi^{(N)} \cdot \left(\overrightarrow{eta}^{T(N)} + \frac{\Delta h K_1^\eta}{2} \right) + V_E^{(N)} - \sum_{r=1}^{3} (C_{avg,E}^{(N)} - J_E^{(N)}) \right\}$$

$$K_3^\eta = M_\phi^{-1} \cdot \left\{ S_\phi^{(N)} \cdot \left(\overrightarrow{\eta}^{T(N)} - \Delta h K_1^\eta + 2\Delta h K_2^\eta \right) + V_E^{(N)} - \sum_{r=1}^{3} (C_{avg,E}^{(N)} - J_E^{(N)}) \right\}$$

$$(2.64)$$

and

$$K_1^\alpha = M_B^{-1} \cdot \left\{ S_B^{(N)} \cdot \overrightarrow{\alpha}^{T(N)} - \sum_{r=1}^{3}(C_{avg,B}^{(N)} - J_B^{(N)}) \right\}$$

$$K_2^\alpha = M_B^{-1} \cdot \left\{ S_B^{(N)} \cdot \left(\overrightarrow{\alpha}^{T(N)} + \frac{\Delta h K_1^\alpha}{2} \right) - \sum_{r=1}^{3}(C_{avg,B}^{(N)} - J_B^{(N)}) \right\}$$

$$K_3^\alpha = M_B^{-1} \cdot \left\{ S_B^{(N)} \cdot \left(\overrightarrow{\alpha}^{T(N)} - \Delta h K_1^\alpha + 2\Delta h K_2^\alpha \right) - \sum_{r=1}^{3}(C_{avg,B}^{(N)} - J_B^{(N)}) \right\}$$

$$(2.65)$$

where M_B^{-1} will be calculated by Gauss elimination method.

CHAPTER 3: $\mathcal{H}(\mathbf{DIV})$ BASIS FUNCTIONS

3.1 $\mathcal{H}(\mathbf{div})$ Basis Functions for the Triangular Element

Any point in the reference triangular element is uniquely located in terms of the local coordinate system (ξ, η). The vertexes are numbered as $v_0(0,0), v_1(1,0), v_2(0,1)$, in Figure **??**. The barycentric coordinates are given as

$$\lambda_0 := 1 - \xi - \eta$$
$$\lambda_1 := \xi \qquad\qquad (3.1)$$
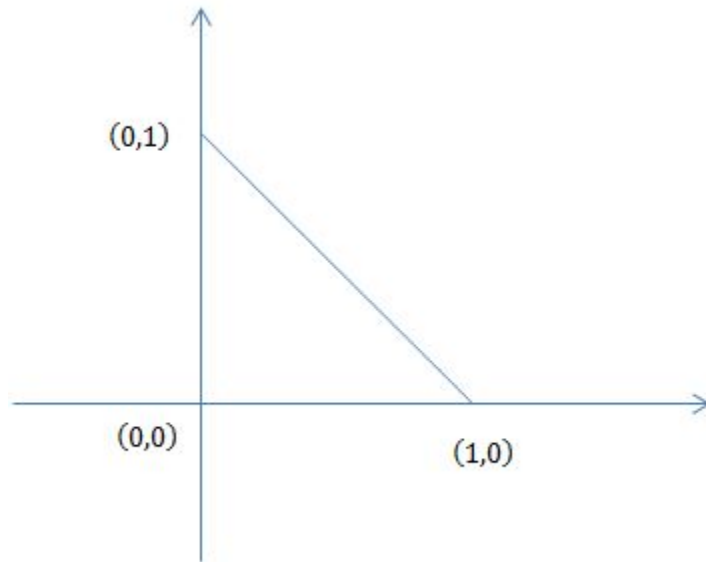$$\lambda_2 := \eta$$

Figure 2: Two dimensional reference triangular element

The directed tangent on a generic edge $e_j = [j_1, j_2]$ is similarly defined as in (3.19)

for the three dimensional case. In the same manner the edge is also parameterized as in (3.20). A generic edge can be uniquely identified with

$$\mathbf{e}_j := [j_1, j_2], \; j_1 = \{0, 1\}, \; j_1 < j_2 \le 2, \; j = j_1 + j_2 \tag{3.2}$$

The two-dimensional vectorial curl operator of a scalar quantity, which is used in our construction, needs a proper definition. We use the one given in the book [15], *viz.*

$$\mathbf{curl}(u) := \nabla \times u := \left[\frac{\partial u}{\partial \eta}, -\frac{\partial u}{\partial \xi} \right]^T \tag{3.3}$$

Based upon the newly created shape functions for the three-dimensional $H(div)$-conforming tetrahedral elements and using the technique of dimension reduction we construct the basis for the $H(div)$-conforming triangular elements in two dimensions. However, it is easy to see that the two groups for the face functions cannot be appropriately modified for our purpose. Instead we borrow the idea of Zaglmayr in the dissertation [46], viz, we combine the edge-based shape functions in [46] with our newly constructed edge-based and bubble interior functions. In [46] Zaglmayr had applied the so-called scaled integrated Legendre polynomial in the construction, *viz.*

$$L_n^s(x, t) := t^{n-1} \int_{-t}^{x} l_{n-1}\left(\frac{\xi}{t}\right) d\xi, \; n \ge 2, \; t \in (0, 1], \tag{3.4}$$

where $l_n(x)$ is the n-th order Legendre polynomial.

- Edge functions

  Associated with each edge the formulas for these functions are given as

$$\boldsymbol{\Phi}_{e[k_1, k_2]}^{N_0} = \lambda_{k_2} \nabla \times \lambda_{k_1} - \lambda_{k_1} \nabla \times \lambda_{k_2} \tag{3.5}$$

for the zeroth order approximation,

$$\mathbf{\Phi}^{N_1}_{e[k_1,k_2]} = \lambda_{k_2} \nabla \times \lambda_{k_1} + \lambda_{k_1} \nabla \times \lambda_{k_2} \tag{3.6}$$

for the first order approximation, and

$$\mathbf{\Phi}^{j}_{e[k_1,k_2]} = L^s_{j-1} \left(\lambda_{k_2} - \lambda_{k_1}\right) \mathbf{\Phi}^{N_1}_{e[k_1,k_2]} + L^s_{j-2} \left(\lambda_{k_2} - \lambda_{k_1}\right) \mathbf{\Phi}^{N_0}_{e[k_1,k_2]}, \; j \geq 2 \tag{3.7}$$

for higher-order approximations.

- Interior functions

  The interior functions are further classified into two categories: edge-based and bubble interior functions. By construction the normal component of each interior function vanishes on either edge of the reference triangular element, *viz.*

  $$\mathbf{n}^{\mathbf{e}_j} \cdot \mathbf{\Phi}^t = 0, \; j = 1\{1, 2, 3\}, \tag{3.8}$$

  where $\mathbf{n}^{\mathbf{e}_j}$ is the unit outward normal vector to edge $\mathbf{e}_j$.

  Edge-based interior functions

  The tangential component of each edge-based function does not vanish on the associated only edge $\mathbf{e}_k := [k_1, k_2]$ but vanishes on the other two edges, *viz.*

  $$\tau^{\mathbf{e}_j} \cdot \mathbf{\Phi}^{\mathbf{t},\mathbf{i}}_{\mathbf{e_k}:=[\mathbf{k_1},\mathbf{k_2}]} = 0, \; \mathbf{e}_j \neq \mathbf{e}_k, \tag{3.9}$$

  where $\tau^{\mathbf{e}_j}$ is the directed tangent along the edge $\mathbf{e}_j := [j_1, j_2]$. The following basis functions are proposed here as

  $$\mathbf{\Phi}^{\mathbf{t},\mathbf{i}}_{\mathbf{e_k}:=[\mathbf{k_1},\mathbf{k_2}]} = C_i \lambda_{k_1} \lambda_{k_2} (1 - \lambda_{k_1})^i P^{0,2}_i \left(\frac{2\lambda_{k_2}}{1 - \lambda_{k_1}} - 1\right) \frac{\tau^{\mathbf{e}_k}}{|\tau^{\mathbf{e}_k}|} \tag{3.10}$$

where the function $P_i^{(0,2)}(\bullet)$ is the classical un-normalized Jacobi polynomial of degree i with a single variable [30], and the scaling coefficient is given by

$$C_i = \sqrt{2(i+2)(i+3)(2i+3)(2i+5)}, \ i = 0, 1, \cdots, p-2 \qquad (3.11)$$

The following orthonormal property of edge-based interior functions can be proved

$$\langle \boldsymbol{\Phi}^{\mathbf{t,m}}_{\mathbf{e_k}:=[\mathbf{k_1},\mathbf{k_2}]}, \boldsymbol{\Phi}^{\mathbf{t,n}}_{\mathbf{e_k}:=[\mathbf{k_1},\mathbf{k_2}]} \rangle|_{K^2} = \delta_{mn}, \ \{m, n\} = 0, 1, \cdots, p-2. \qquad (3.12)$$

Interior bubble functions:

The interior bubble funtions vanish on the entire boundary of the reference triangular element. The formulas of these functions are given as

$$\boldsymbol{\Phi}^{\mathbf{t},\vec{e}_i}_{m,n} = C_{m,n} \lambda_0 \lambda_1 \lambda_2 (1 - \lambda_0)^m P_m^{(2,2)}\left(\frac{\lambda_1 - \lambda_2}{1 - \lambda_0}\right) P_n^{(2m+5,2)}(2\lambda_0 - 1)\vec{e}_i, \ i = 1, 2,$$

$$(3.13)$$

where

$$C_{m,n} = \sqrt{\frac{(m+3)(m+4)(2m+5)(2m+n+6)(2m+n+7)(2m+2n+8)}{(m+1)(m+2)(n+1)(n+2)}}$$

$$(3.14)$$

and

$$0 \leq \{m, n\}, \ m + n \leq p - 3 \qquad (3.15)$$

One can again prove the orthonormal property of the interior bubble functions

$$\langle \boldsymbol{\Phi}^{\mathbf{t},\vec{e}i}_{m_1,n_1}, \boldsymbol{\Phi}^{\mathbf{t},\vec{e}j}_{m_2,n_2} \rangle|_{K^2} = \delta_{m_1 m_2} \delta_{n_1 n_2}, \qquad (3.16)$$

where

$$0 \leq \{m_1, m_2, n_1, n_2\}, \; m_1 + n_1, m_2 + n_2 \leq p - 3, \; \{i, j\} = 1, 2 \qquad (3.17)$$

The following table shows the decomposition of the space $(\mathbf{P}_n(K))^2$ for the $H(div)$-conforming triangular element.

Decomposition	Dimension
Edge functions	$3(n+1)$
Edge-based interior functions	$3(n-1)$
Interior bubble functions	$(n-2)(n-1)$
Total	$(n+1)(n+2)$

3.2 $\mathcal{H}(\mathbf{div})$ Basis Functions for the Tetrahedral Element

Our construction [43] is motivated by the work on the construction of $\mathcal{H}(\mathbf{div})$-conforming hierarchical bases for tetrahedral elements [1]. We construct shape functions for the $\mathcal{H}(\mathbf{div})$-conforming tetrahedral element on the canonical reference tetrahedral element, as shown in Figure **??**. The shape functions are grouped into several categories based upon their geometrical entities on the reference tetrahedral element [1]. The basis functions in each category are constructed so that they are orthonormal on the reference element.

Any point in the tetrahedral element K^3 is uniquely located in terms of the local coordinate system (ξ, η, ζ). The vertexes are numbered as $v_0(0, 0, 0)$, $v_1(1, 0, 0)$,
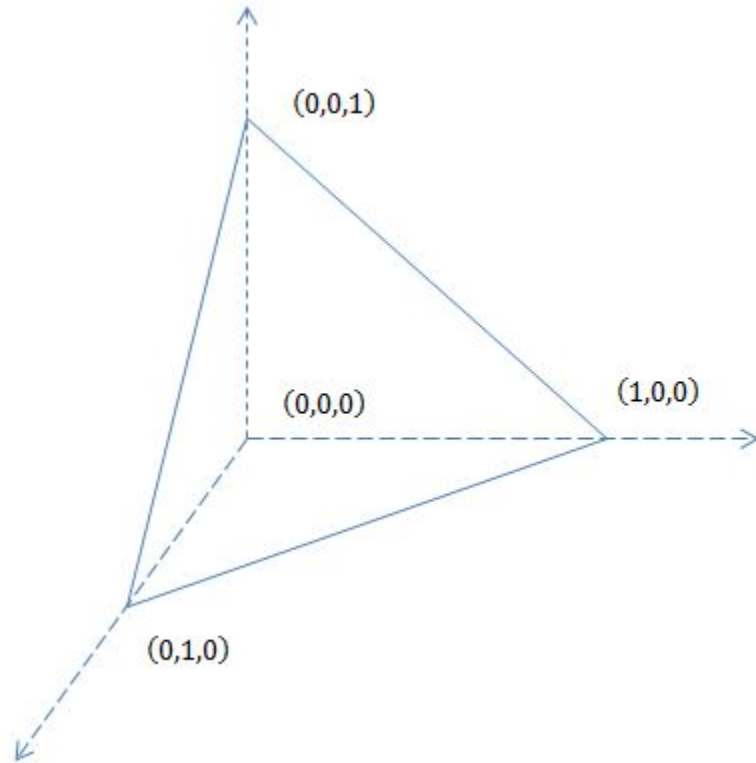
Figure 3: Three dimensional reference tetrahedral elements

$v_2(0, 1, 0)$, $v_3(0, 0, 1)$. The barycentric coordinates are given as

$$
\begin{aligned}
\lambda_0 &:= 1 - \xi - \eta - \zeta \\
\lambda_1 &:= \xi \\
\lambda_2 &:= \eta \\
\lambda_3 &:= \zeta
\end{aligned}
\tag{3.18}
$$

The directed tangent on a generic edge $\mathbf{e}_j = [j_1, j_2]$ is defined as

$$
\tau^{\mathbf{e}_j} := \tau^{[j_1, j_2]} = \mathbf{v}_{j_2} - \mathbf{v}_{j_1}, \ j_1 < j_2.
\tag{3.19}
$$

The edge is parameterized as

$$
\gamma_{\mathbf{e}_j} := \lambda_{j_2} - \lambda_{j_1}, \ j_1 < j_2.
\tag{3.20}
$$

A generic edge can be uniquely identified with

$$\mathbf{e}_j := [j_1, j_2], \ j_1 = 0, 1, 2, \ j_1 < j_2 \le 3, \ j = j_1 + j_2 + sign(j_1), \qquad (3.21)$$

where $sign(0) = 0$. Each face on the tetrahedral element K^3 can be identified by the associated three vetexes, and is uniquely defined as

$$\mathbf{f}_{j_1} := [j_2, j_3, j_4], \ 0 \le \{j_1, j_2, j_3, j_4\} \le 3, \ j_2 \le j_3 \le j_4. \qquad (3.22)$$

The standard bases in $\mathbb{R}^n$ are noted as $\overrightarrow{e}_i$, $i = 1, \cdots, n$, and $n = 1\{2, 3\}$.

- Face functions The face functions are further grouped into two categories: edge based face functions and face bubble functions.

Edge-based face functions:

These functions are associated with the three edges of a certain face $\mathbf{f}_{j_1}$, and by construction all have non-zero normal components only on the associated face $\mathbf{f}_{j_1}$, *viz.*

$$\mathbf{n}^{\mathbf{f}_{j_k}} \cdot \mathbf{\Phi}_{\mathbf{e}[k_1, k_2]}^{\mathbf{f}_{j_1}, i} = 0, \ j_k \neq j_1, \qquad (3.23)$$

where $\mathbf{n}^{\mathbf{f}_{j_k}}$ is the unit outward normal vector to face $\mathbf{f}_{j_k}$.

The edge-based face functions for higher order have been proposed in [1] as follows:

$$\widetilde{\mathbf{\Phi}}_{\mathbf{e}[k_1, k_2]}^{\mathbf{f}_{j_1}, i} = l_i(\gamma_{\mathbf{e}_k}) \lambda_{k_1} \nabla \lambda_{k_2} \times \nabla \lambda_{k_3}, \ i = 0, \cdots, p - 1. \qquad (3.24)$$

For instance, for the face opposite to the vertex $v_0(0, 0, 0)$, $\mathbf{f}_0 := [1, 2, 3]$, the

face functions related to edge $\mathbf{e}[1,2]$ are given by

$$\widetilde{\mathbf{\Phi}}^{\mathbf{f}_0,i}_{\mathbf{e}[1,2]} = l_i(\lambda_3 - \lambda_2)\lambda_1 \nabla\lambda_2 \times \nabla\lambda_3, \ i = 0, \cdots, p-1 \qquad (3.25)$$

However, it can be easily checked that the basis functions given in (3.24) in fact are not independent for $p = 2$ (for example, the sum of all the basis functions on a given face in fact equals to zero) and thus the proposed basis function is not complete. To remedy this degeneracy, two types of constructions of new hierarchical high-order independent edge-based face functions will be presented here.

- **Type One:** high-order independent edge-based face functions

  In [8], the following orthonormal basis functions are given as

  $$\mathbf{\Phi}^{\mathbf{f}_{j_1},i}_{\mathbf{e}[k_1,k_2]} = C_i \lambda_{k_3}(1 - \lambda_{k_1})^i P_i^{(3,0)}\left(\frac{2\lambda_{k_2}}{1-\lambda_{k_1}} - 1\right)\frac{\nabla\lambda_{k_1} \times \nabla\lambda_{k_2}}{|\nabla\lambda_{k_1} \times \nabla\lambda_{k_2}|}, \quad (3.26)$$

  where

  $$C_i = \sqrt{3(2i+4)(2i+5)}, \ i = 0, 1, \cdots, p-1, \qquad (3.27)$$

  and

  $$k_1 = \{j_2, j_3\}, \ k_2 = \{j_3, j4\}, \ k_1 < k_2, \ k_3 = \{j_2, j_3, j_4\}\backslash\{k_1, k_2\}. \qquad (3.28)$$

  One can prove the orthonormal property of these edge-based face functions

  $$\langle\mathbf{\Phi}^{\mathbf{f}_{j_1},m}_{\mathbf{e}[k_1,k_2]}, \mathbf{\Phi}^{\mathbf{f}_{j_1},n}_{\mathbf{e}[k_1,k_2]}\rangle|_{K^3} = \delta_{mn}, \ \{m, n\} = 0, 1, \cdots, p-1. \qquad (3.29)$$

  Note that with our new construction, the edge-based face functions are all linearly independent, which is also verified by the fact that in the spectrum

of the mass (Gram) matrix, none of the eigenvalues is zero.

– **Type Two:** high-order independent edge-based face functions

An alternative approach using the idea of recursion from [1] can also be

used to construct independent edge-based face functions as follows.

For $p = 1$, for each edge we have one face function for this edge as proposed

in [1],

$$\mathbf{\Phi}^{\mathbf{f}_{j_1},0}_{\mathbf{e}[k_1,k_2]} = \lambda_{k_1} \nabla \lambda_{k_2} \times \nabla \lambda_{k_3}, \tag{3.30}$$

and for $p = 2$, one additional new basis function can be constructed as

$$\mathbf{\Phi}^{\mathbf{f}_{j_1},1}_{\mathbf{e}[k_1,k_2]} = \lambda_{k_1} \lambda_{k_2} \nabla \lambda_{k_3} \times \nabla \lambda_{k_1}, \tag{3.31}$$

which can be shown to satisfy the condition (3.23), and for $p > 3$, the basis

functions are given by

$$\begin{aligned}
\widetilde{\mathbf{\Phi}}^{\mathbf{f}_{j_1},i+1}_{\mathbf{e}[k_1,k_2]} &\equiv l_i(\gamma_{\mathbf{e}_k}) \widetilde{\mathbf{\Phi}}^{\mathbf{f}_{j_1},1}_{\mathbf{e}[k_1,k_2]} + l_{i-1}(\gamma_{\mathbf{e}_k}) \widetilde{\mathbf{\Phi}}^{\mathbf{f}_{j_1},0}_{\mathbf{e}[k_1,k_2]} \\
&= l_i(\gamma_{\mathbf{e}_k}) [\lambda_{k_1} \lambda_{k_2} \nabla \lambda_{k_3} \times \nabla \lambda_{k_1}] + l_{i-1}(\gamma_{\mathbf{e}_k}) [\lambda_{k_1} \nabla \lambda_{k_2} \times \nabla \lambda_{k_3}], \\
&\quad i = 1, \cdots, p-2
\end{aligned} \tag{3.32}$$

It can be shown again numerically that there are exactly p functions that

are independent and only whose normal component is non-zero only on

the associated edge $\mathbf{e}_k$.

Face bubble functions:

The face bubble functions which belong to each specific group are associated

with a particular face $\mathbf{f}_{j_1}$. They vanish on all edges of the reference tetrahedral

element K^3, and the normal components of which vanish on other three faces, *viz.*

$$\mathbf{n}^{\mathbf{f}_{j_k}} \cdot \mathbf{\Phi}_{m,n}^{\mathbf{f}_{j_1}} = 0, \ j_k \neq j_1 \tag{3.33}$$

The explicit formula is given as

$$\mathbf{\Phi}_{m,n}^{\mathbf{f}_{j_1}} = \iota(1-\lambda_{j_2})^m(1-\lambda_{j_2}-\lambda_{j_3})^n P_m^{(2n+3,2)}\left(\frac{2\lambda_{j_3}}{1-\lambda_{j_2}}-1\right) P_n^{(0,2)}\left(\frac{2\lambda_{j_4}}{1-\lambda_{j_2}-\lambda_{j_3}}-1\right)\frac{\nabla\lambda_{j_3}\times\nabla\lambda_{j_4}}{|\nabla\lambda_{j_3}\times\nabla\lambda_{j_4}|}$$

$$\tag{3.34}$$

where

$$\iota = C_m^n \lambda_{j_2}\lambda_{j_3}\lambda_{j_4} \tag{3.35}$$

where

$$C_m^n = \frac{\sqrt{(2n+3)(m+n+3)(m+2n+4)(m+2n+5)(m+2n+7)(m+2n+8)(m+2n+9)}}{\sqrt{(m+1)(m+2)}} \tag{3.36}$$

and

$$0 \leq \{m,n\}, \ m+n \leq p-3 \tag{3.37}$$

By construction the face bubble functions share again the orthonormal property on the reference tetrahedral element K^3:

$$\langle \mathbf{\Phi}_{m_1,n_1}^{\mathbf{f}_{j_1}}, \mathbf{\Phi}_{m_2,n_2}^{\mathbf{f}_{j_1}}\rangle|_{K^3} = \delta_{m_1,m_2}\delta_{n_1,n_2} \tag{3.38}$$

- Interior functions

  The interior functions are classified into three categories: edge-based, face-based and bubble interior functions. By construction the normal component of each interior function vanishes on either face of the reference tetrahedral element K^3,

viz.

$$\mathbf{n^{f_j}} \cdot \mathbf{\Phi^t} = 0, \ j = \{0, 1, 2, 3\}. \tag{3.39}$$

Edge-based interior functions:

The tangential component of each edge-based function does not vanish on the associated only edge $\mathbf{e}_k := [k_1, k_2]$, but vanishes on all other five edges, *viz.*

$$\tau^{\mathbf{f}_j} \cdot \mathbf{\Phi^{t,i}_{e[k_1,k_2]}} = 0, \ \mathbf{e}_j \neq \mathbf{e}_k, \tag{3.40}$$

where $\tau^{\mathbf{f}_j}$ is the directed tangent along the edge $\mathbf{e}_j := [j_1, j_2]$. The shape functions are given as

$$\mathbf{\Phi^{t,i}_{e[k_1,k_2]}} = C_i \lambda_{k_1} \lambda_{k_2} (1 - \lambda_{k_1})^i P_i^{(1,2)} \left(\frac{2\lambda_{k_2}}{1 - \lambda_{k_1}} - 1 \right) \frac{\tau^{\mathbf{e}_k}}{|\tau^{\mathbf{e}_k}|}, \tag{3.41}$$

where

$$C_i = (i + 3) \sqrt{\frac{(2i + 4)(2i + 5)(2i + 7)}{i + 1}}, \ i = 0, 1, \cdots, p - 2. \tag{3.42}$$

Again one can prove the orthonormal property of edge-based interior functions:

$$\langle \mathbf{\Phi^{t,m}_{e[k_1,k_2]}}, \mathbf{\Phi^{t,n}_{e[k_1,k_2]}} \rangle |_{K^3} = \delta_{mn}, \ \{m, n\} = 0, 1, \cdots, p - 2. \tag{3.43}$$

Face-based interior functions:

These functions which are associated with a particular face $\mathbf{f}_{j_1}$ have non-zero tangential components on their associated face only, and have no contribution to be the tangential components on all other three faces, *viz.*

$$\mathbf{n^{f_{j_k}}} \times \mathbf{\Phi^{t,f_{j_1}}_{m,n}} = 0, \ j_k \neq j_1, \tag{3.44}$$

Further each face-based interior function vanishes on all the egdges of the tetra-

hedral element K^3, *viz.*

$$\tau^{\mathbf{e}_k} \cdot \mathbf{\Phi}_{m,n}^{\mathbf{t},\mathbf{f}_{j_1}} = 0. \tag{3.45}$$

The formulas of these functions are given as

$$\mathbf{\Phi}_{m,n}^{\mathbf{t},\mathbf{f}_{j_1}^1} = \iota(1-\lambda_{j_2})^m(1-\lambda_{j_2}-\lambda_{j_3})^n P_m^{(2n+3,2)}\left(\frac{2\lambda_{j_3}}{1-\lambda_{j_2}}-1\right) P_n^{0,2}\left(\frac{2\lambda_{j_4}}{1-\lambda_{j_2}-\lambda_{j_3}}-1\right)\frac{\tau^{[j_2,j_3]}}{|\tau^{[j_2,j_3]}|},$$

$$\mathbf{\Phi}_{m,n}^{\mathbf{t},\mathbf{f}_{j_1}^2} = \iota(1-\lambda_{j_2})^m(1-\lambda_{j_2}-\lambda_{j_3})^n P_m^{(2n+3,2)}\left(\frac{2\lambda_{j_3}}{1-\lambda_{j_2}}-1\right) P_n^{0,2}\left(\frac{2\lambda_{j_4}}{1-\lambda_{j_2}-\lambda_{j_3}}-1\right)\frac{\tau^{[j_2,j_4]}}{|\tau^{[j_2,j_4]}|},$$

$$\tag{3.46}$$

where ι is given in (3.35) and $0 \leq \{m,n\}$, $m+n \leq p-3$. The face based

interior functions enjoy the orthonormal property on the reference tetrahedral

element K^3:

$$\langle \mathbf{\Phi}_{m_1,n_1}^{\mathbf{t},\mathbf{f}_{j_1}^i}, \mathbf{\Phi}_{m_2,n_2}^{\mathbf{t},\mathbf{f}_{j_1}^i}\rangle|_{K^3} = \delta_{m_1 m_2}\delta_{n_1 n_2},$$

$$\tag{3.47}$$

$$i = \{1,2\},\ 0 \leq \{m_1, m_2, n_1, n_2\},\ m_1 + n_1, m_2 + n_2 \leq p-3.$$

Interior bubble functions:

The interior bubble functions vanish on the entire boundary ∂K^3 of the reference

tetrahedral element K^3. The formulas of these functions are given as

$$\mathbf{\Phi}_{l,m,n}^{\mathbf{t},\vec{e}_i} = \chi P_l^{(2m+2n+8,2)}(2\lambda_1 - 1)P_m^{(2n+5,2)}\left(\frac{2\lambda_2}{1-\lambda_1}-1\right) P_n^{(2,2)}\left(\frac{2\lambda_3}{1-\lambda_1-\lambda_2}-1\right)\vec{e}_i, i = 1,2,3,$$

$$\tag{3.48}$$

where

$$\chi = C_{l,m,n}\lambda_0\lambda_1\lambda_2\lambda_3(1-\lambda_1)^m(1-\lambda_1-\lambda_2)^n \tag{3.49}$$

where

$$C_{l,m,n} = C_{l,m,n}^1 C_{l,m,n}^2, \tag{3.50}$$

where

$$C^1_{l,m,n} = \sqrt{\frac{(l+2m+2n+9)(l+2m+2n+10)(l+2m+2n+11)(m+2n+6)}{(l+1)(m+1)(n+1)}}$$

$$C^2_{l,m,n} = \sqrt{\frac{(m+2n+7)(m+2n+8)(n+3)(n+4)(2n+5)}{(l+2)(m+2)(n+2)}}$$

(3.51)

and

$$0 \leq \{l, m, n\}, \ l + m + n \leq p - 4. \tag{3.52}$$

Again, one can show the orthonormal property of the interior bubble functions

$$\langle \mathbf{\Phi}^{\mathbf{t},\vec{e}_i}_{l_1,m_1,n_1}, \mathbf{\Phi}^{\mathbf{t},\vec{e}_j}_{l_2,m_2,n_2} \rangle |_{K^3} = \delta_{l_1,l_2}\delta_{m_1,m_2}\delta_{n_1,n_2}, \tag{3.53}$$

where

$$0 \leq \{l_1, l_2, m_1, m_2, n_1, n_2\}, \ l_1 + m_1 + n_1, l_2 + m_2 + n_2 \leq p - 4, \ \{i, j\} = 1, 2, 3.$$

(3.54)

In the following table we summarize the decomposition of the space $(\mathbf{P}_n(K))^3$ for the $H(div)$-conforming tetrahedral element.

Decomposition	Dimension
Edge-based face functions	$12n$
Face bubble functions	$2(n-2)(n-1)$
Edge-based interior functions	$6(n-1)$
Face-based interior functions	$4(n-2)(n-1)$
Interior bubble functions	$(n-3)(n-2)(n-1)/2$
Total	$(n+1)(n+2)(n+3)/2$

CHAPTER 4: GLOBAL DIVERGENCE-FREE TREATMENT

4.1 Treatment on 2-D Triangle Mesh

In solving the MHD equations, the divergence free condition needs to be satisfied. However, the time evolution from a fulling discretized DG finite element method will render the divergence of $\mathbf{B}$ to be non-zero. There are many ways to remove the non-zero divergence in the magnetic field such as the projection method through Helmholtz decomposition. In this dissertation, we will use the interior functions in the $\mathcal{H}(\mathbf{div})$ basis set to correct the non-zero divergence element by element. Due to the vanishing property of the normal components of the interior basis functions, such a local correction will still keep the corrected finite element solution in $\mathcal{H}(\mathbf{div})$ in the whole domain.

First, we will study 2-dimensional case. The $\mathcal{H}(\mathbf{div})$ basis functions can be expressed as

$$\mathcal{H}(\mathbf{div}) = \left\{ \mathbf{u} = \begin{pmatrix} u_1 \\ u_2 \end{pmatrix}, [\mathbf{u} \cdot \mathbf{n}]|_\Gamma = 0 \right\} \in \mathbf{P}_n^2(K), \qquad (4.1)$$

where $\mathbf{n}$ is the outer unit normal vector on the interface Γ of the triangle, and $\mathbf{P}_n^2(K)$ denotes the space of polynomials in K of degree at most n. There are $(n+1)(n+2)$ of basis functions of degree at most n.

For example, on edge e_{12}, for edge-based interior function $\psi^{\mathbf{t},i}_{[k_1,k_2]}$, we have

$$\psi^{\mathbf{t},i}_{[k_1,k_2]} \cdot \mathbf{n}_i = 0 \qquad (4.2)$$

for $i = 1, 2$, but it has non-zero tangential components on its associated edge only

$$\psi^{\mathbf{t},i}_{[k_1,k_2]} \cdot \mathbf{n}_0 \neq 0 \qquad (4.3)$$

For interior bubble functions, such as $\psi^{\mathbf{t},\overrightarrow{e}_i}_{m,n} = \lambda_1\lambda_2\lambda_0\overrightarrow{e}_i$, $i = 1, 2$, it vanishes on the entire boundary of the reference triangle.

For future convenience, we define a collection of bubble functions which is consisted of edge-based interior functions and interior bubble functions.

$$\Sigma_{int} = \left\{\psi^b_i\right\}^{n_b}_{i=1} \qquad (4.4)$$

where $n_b = 3(n-1) + (n-2)(n-1)$.

In solving the 2-D equation

$$\frac{\partial \mathbf{B}}{\partial t} + \nabla \cdot \left(\mathbf{u}\mathbf{B}^T - \mathbf{B}\mathbf{u}^T\right) = 0 \qquad (4.5)$$

The magnetic field $\mathbf{B} \in \mathcal{H}(\mathbf{div})$, but $\nabla\mathbf{B} \neq 0$.

The ability of using only the interior functions to reduce the non-divergence error in the following lemma.

Lemma 4.1. *The span of the divergence of the bubble functions of order n is equivalent to the span of the polynomial space $n - 1$ excluding the constant term. That is,* $Div\Sigma_{int} = \mathbf{P}_{n-1}(K)\backslash\{1\} = \{1\}^{\perp}.$

Proof. We will prove the result by subspace inclusion argument. First, we will show

$Div\Sigma_{int} \subset \{1\}^{\perp}.$

For $\forall \mathbf{b} \in \Sigma_n$, we have

$$\int_K div\mathbf{b}dx = \int_K 1 \cdot div\mathbf{b}dx = \int_{\partial K} \mathbf{b} \cdot \mathbf{n}ds = 0, \tag{4.6}$$

due to the fact that the normal component of interior function vanishes on the edge of the element K.

Thus, $Div\Sigma_{int} \subset \{1\}^{\perp}$.

On the other hand, we will show $Div\Sigma_{int} \supset \{1\}^{\perp}$ by showing that $(Div\Sigma_{int})^{\perp} \subset \{1\}$, instead.

Let $v \in (Div\Sigma_{int})^{\perp} \subset P_{p-1}(K)$, then we have

$$\int_K v \cdot Div\mathbf{b}_i dx = 0, \tag{4.7}$$

for $\forall \mathbf{b}_i \in \Sigma_{int}$.

After integration by parts, we get

$$\int_{\partial K} \mathbf{b}_i \cdot \mathbf{n} \cdot vds - \int_K \nabla v \cdot \mathbf{b}_i dx = 0 \tag{4.8}$$

Since $\int_{\partial K} \mathbf{b}_i \cdot \mathbf{n} \cdot vds = 0$ by the design of the $\mathbf{b}_i$'s, then

$$\int_K \nabla v \cdot \mathbf{b}_i dx = 0, \tag{4.9}$$

for $\forall \mathbf{b}_i \in \Sigma_{int}$.

We can see $\nabla v \in \mathbf{P}_{n-2}^2(K)$.

Let $\mathbf{t}_{01}, \mathbf{t}_{02}$ be the tangential vectors of the two edges sharing the common vertex $\mathbf{v}_0$. We can see easily that the following vector functions are also interior functions

(with zero normal components on all faces),

$$\lambda_0\lambda_1 g_1 \mathbf{t}_{01}, \lambda_0\lambda_1 g_2 \mathbf{t}_{02} \in \Sigma_{int} \tag{4.10}$$

where the scalar functions $g_i, i = 1, 2$ are polynomials of degree $p - 2$.

Next we construct two bi-orthogonal vectors $\mathbf{s}_1, \mathbf{s}_2$, with respect to $\mathbf{t}_{01}, \mathbf{t}_{02}$ with the following property

$$\mathbf{s}_j \cdot \mathbf{t}_{0i} = \delta_{ij}. \tag{4.11}$$

Now we can express the vector field $\nabla \cdot \mathbf{v}$ using the basis vector $\mathbf{s}_1, \mathbf{s}_2$ as follows

$$\nabla v = g_{01}\mathbf{s}_1 + g_{02}\mathbf{s}_2, \tag{4.12}$$

where $\mathbf{g}_{01}, \mathbf{g}_{02}, \in \mathbf{P}_{n-2}(K)$.

Pick $\mathbf{b} = g_{01}\lambda_0\lambda_1\mathbf{t}_{01}$, and $\mathbf{b} \in \Sigma_{int}$, since

$$\mathbf{t}_{01} \perp \mathbf{e}_{01},$$

$$\lambda_0 = 0 \text{ on } \mathbf{e}_{12}, \tag{4.13}$$

$$\lambda_1 = 0 \text{ on } \mathbf{e}_{02}.$$

Plugging ∇v and $\mathbf{b}$ into equation (4.9), we can get

$$\int_K \nabla v \cdot \mathbf{b} dx = 0 \tag{4.14}$$

$$\int_K (g_{01}\mathbf{s}_1 + g_{02}\mathbf{s}_2) \cdot (g_{01}\lambda_0\lambda_1\mathbf{t}_{01}) = 0 \tag{4.15}$$

$$\int_K \lambda_0\lambda_1 g_{01}^2 \cdot \mathbf{s}_1\mathbf{t}_{01} dx = 0 \tag{4.16}$$

The integration equals to zero only when $g_{01} = 0$. By the same argument, $g_{02} = 0$.

Thus, $\nabla v = 0$. That is, $v = constant$.

Thus, $(Div\Sigma_{int})^{\perp} \subset \{1\}$ is proved.

$\square$

4.2   Treatment on 3-D Tetrahedral Mesh

In 3-dimensional case, the H(div) basis functions can be expressed as

$$H(div) = \left\{ \mathbf{u} = \begin{pmatrix} u_1 \\ u_2 \\ u_3 \end{pmatrix}, [\mathbf{u} \cdot \mathbf{n}]|_{\Gamma} = 0 \right\} \subset \mathbf{P}_n^3(K), \qquad (4.17)$$

where $\mathbf{n}$ is the outer unit normal vector on face Γ of the tetrahedron, and $\mathbf{P}_n^3(K)$ denotes the space of polynomials in K of degree at most n. There are $\dfrac{(n+1)(n+2)(n+3)}{2}$ number of basis functions of degree at most n.

For example, on face f_0, for face-based interior function $\psi_{m,n}^{\mathbf{t},f_0}$, we have

$$\psi_{m,n}^{\mathbf{t},f_0} \cdot \mathbf{n}_i = 0 \qquad (4.18)$$

for $i = 1, 2, 3$, but it has non-zero tangential components on its associated face only

$$\psi_{m,n}^{\mathbf{t},f_0} \cdot \mathbf{n}_0 \neq 0 \qquad (4.19)$$

For edge-based interior functions, such as $\psi_{[k_1,k_2]}^{\mathbf{t},i} = \lambda_1 \nabla \lambda_2 \times \nabla \lambda_3$ on edge $\mathbf{e}_{12}$, its tangential component does not vanish on the associated only edge e_{12}, but vanishes all other five edges.

For future convenience, we define a collection of bubble functions which is consisted of edge-based interior functions, face-based interior functions and interior bubble

functions.

$$\Sigma_{int} = \left\{\psi_i^b\right\}_{i=1}^{n_b} \tag{4.20}$$

where $n_b = 6(n-1) + 4(n-2)(n-1) + \dfrac{(n-3)(n-2)(n-1)}{2}$.

In solving the 3-D equation

$$\frac{\partial \mathbf{B}}{\partial t} + \nabla \cdot \left(\mathbf{u}\mathbf{B}^T - \mathbf{B}\mathbf{u}^T\right) = 0 \tag{4.21}$$

The magnetic field $\mathbf{B} \in H(div)$, but $\nabla\mathbf{B} \neq 0$.

Our goal is to make $\nabla \cdot \mathbf{B}^* = 0$. To achieve it, we need a proved theorem [19].

Lemma 4.2. *The span of the divergence of the bubble functions of order n is equivalent to the span of the polynomial space $n-1$ excluding the constant term. That is,*

$Div\Sigma_{int} = \mathbf{P}_{n-1}(K)\backslash\{1\} = \{1\}^{\perp}.$

Proof. We will prove the result by subspace inclusion argument. First, we will show

$Div\Sigma_n \subset \{1\}^{\perp}.$

For $\forall \mathbf{b} \in \Sigma_{int}$, we have

$$\int_K Div\mathbf{b}dx = \int_K 1 \cdot Div\mathbf{b}dx = \int_{\partial K} \mathbf{b} \cdot \mathbf{n}ds = 0, \tag{4.22}$$

due to the fact that the normal component of interior function vanishes on the edge of the element K.

Thus, $Div\Sigma_{int} \subset \{1\}^{\perp}$.

On the other hand, we will show $Div\Sigma_{int} \supset \{1\}^{\perp}$ by showing that $(Div\Sigma_{int})^{\perp} \subset \{1\}$, instead.

Let $v \in (Div\Sigma_n)^{\perp} \subset P_{p-1}(K)$, then we have

$$\int_K v \cdot \nabla \mathbf{b}_i dx = 0, \tag{4.23}$$

for $\forall \mathbf{b}_i \in \Sigma_{int}$.

After integration by parts, we get

$$\int_{\partial K} \mathbf{b}_i \cdot \mathbf{n} \cdot v ds - \int_K \nabla v \cdot \mathbf{b}_i dx = 0 \tag{4.24}$$

Since $\int_{\partial K} \mathbf{b}_i \cdot \mathbf{n} \cdot v ds = 0$ by the design of the $\mathbf{b}_i$'s, then

$$\int_K \nabla v \cdot \mathbf{b}_i dx = 0, \tag{4.25}$$

for $\forall \mathbf{b}_i \in \Sigma_{int}$.

We can see $\nabla v \in \mathbf{P}_{n-2}^3(K)$.

Let $\mathbf{t}_{01}, \mathbf{t}_{02}, \mathbf{t}_{02}$ be the tangential vectors of the three edges sharing the common vertex $\mathbf{v}_0$. We can see easily that the following vector functions are also interior functions (with zero normal components on all faces),

$$\lambda_0 \lambda_1 g_1 \mathbf{t}_{01}, \ \lambda_0 \lambda_1 g_2 \mathbf{t}_{02}, \ \lambda_0 \lambda_1 g_2 \mathbf{t}_{03} \in \Sigma_{int} \tag{4.26}$$

where the scalar functions $g_i, i = 1, 2, 3$ are polynomials of degree $p - 2$.

Next we construct two bi-orthogonal vectors $\mathbf{s}_1, \mathbf{s}_2, \mathbf{s}_3$, with respect to $\mathbf{t}_{01}, \mathbf{t}_{02}, \mathbf{t}_{03}$ with the following property

$$\mathbf{s}_j \cdot \mathbf{t}_{0i} = \delta_{ij}. \tag{4.27}$$

Now we can express the vector field $\nabla \cdot \mathbf{v}$ using the basis vector $\mathbf{s}_1, \mathbf{s}_2, \mathbf{s}_3$ as follows

$$\nabla v = g_{01} \mathbf{s}_1 + g_{02} \mathbf{s}_2 + g_{03} \mathbf{s}_3, \tag{4.28}$$

where $\mathbf{g}_{01}, \mathbf{g}_{02}, \mathbf{g}_{03} \in \mathbf{P}_{n-2}(K)$.

Pick $\mathbf{b} = g_{01}\lambda_0\lambda_1\mathbf{t}_{01}$, and $\mathbf{b} \in \Sigma_{int}$, since

$$\mathbf{t}_{01} \perp f_2, f_3,$$
$$\lambda_0 = 0 \text{ on } f_0, \tag{4.29}$$
$$\lambda_1 = 0 \text{ on } f_1.$$

Plugging ∇v and $\mathbf{b}$ into equation (4.23), we can get

$$\int_K \nabla v \cdot \mathbf{b} dx = 0 \tag{4.30}$$

$$\int_K (g_{01}\mathbf{s}_1 + g_{02}\mathbf{s}_2 + g_{03}\mathbf{s}_3) \cdot (g_{01}\lambda_0\lambda_1\mathbf{t}_{01}) = 0 \tag{4.31}$$

$$\int_K \lambda_0\lambda_1 g_{01}^2 \cdot \mathbf{s}_1\mathbf{t}_{01} dx = 0 \tag{4.32}$$

The integration equals to zero only when $g_{01} = 0$. By the same argument, $g_{02} = 0, g_{03} = 0$.

Thus, $\nabla v = 0$. That is, $v = constant$.

Thus, $(Div\Sigma_{int})^\perp \subset \{1\}$ is proved.

$\square$

4.3   Algorithm of Cleaning the Divergence of Magnetic Field

Next, we propose the following algorighm to remove the non-divergence in the numerical solution for the magnetic field $\mathbf{B}$ in the numerical solution for the magnetic field on a triangle.

- Step 1 (local correction) Element-wise normal removal of high order terms in $Div\mathbf{B}$.

Due to Lemma 1, we can use the interior function in Σ_{int} to remove higher order terms in $Div\mathbf{B}$, the remaining component in $Div\mathbf{B}$ will be a constant on each element. We proceed to find a vector function

$$\mathbf{\Phi} = \sum_{i=1}^{n_i} \alpha_i \Phi_i \in \Sigma_n \tag{4.33}$$

such that

$$\mathbf{B}_1 = \mathbf{B} + \mathbf{\Phi}, \tag{4.34}$$

$$Div(\mathbf{B} + \mathbf{\Phi}) = c \tag{4.35}$$

where $Div(\mathbf{B} + \mathbf{\Phi}) \in (Div\Sigma_n)^{\perp}$, which gives the following linear system

$$\sum_{i=1}^{n_i} \alpha_i \int_K Div\Phi_i \cdot Div\Phi_j dx = -\int_K Div\mathbf{B} \cdot Div\Phi_j dx \tag{4.36}$$

where $1 \leq j \leq n_i$. α_i's can be solved in least square measure.

- Step 2 (global correction) Remove the constant term in $Div\mathbf{B}_1$ in the whole domain.

  Due to the result of Lemma 1, we will have a residual constant term left in the corrected magnetic field $Div\mathbf{B}_1$, which can only be removed by a global correction with the first order $\mathcal{H}(\mathbf{div})$ basis defined in Chapter 3. We proceed as follows by finding a function $\mathbf{\Psi} \in \mathcal{H}(\mathbf{div}, \Omega)$ using the first order $\mathcal{H}(\mathbf{div})$ basis functions

$$\mathbf{\Psi} = \sum_{i=1}^{N_1} \beta_i \Phi_i \tag{4.37}$$

such that

$$\mathbf{B}^* = \mathbf{B}_1 + \mathbf{\Psi} \tag{4.38}$$

$$\int_\Omega Div\mathbf{B}^* \cdot Div\Phi_j dx = 0, \ for 1 \le j \le N_1, \tag{4.39}$$

resulting into the following linear system for the coefficient $\{\beta_i\}_{i=1}^{N_1}$,

$$\sum_{i=1}^{n_i} \beta_i \int_K Div\Phi_i \cdot Div\Phi_j dx = -\int_K Div\mathbf{B}_1 \cdot Div\Phi_j dx. \tag{4.40}$$

CHAPTER 5: NUMERICAL EXAMPLES

5.1 Approximation Accuracy of Basis Functions

In order to check the convergence rate of the $\mathcal{H}(\mathbf{div})$-conforming basis functions, we design this example to fully test it.

Assume $\mathbf{B}_h = \sum_{i=1}^{n} \alpha_i \psi_i$, and $\mathbf{B}_h = \mathbf{B}_0$. n is the number of basis functions. Use Discontinuous Galerkin method, we obtain

$$\int_K \mathbf{B}_h \cdot \psi_j d\mathbf{x} = \int_K \mathbf{B}_0 \cdot \psi_j d\mathbf{x} \tag{5.1}$$

and plugging $\mathbf{B}_h$, one can obtain

$$\sum_{i=1}^{n} \alpha_i \int_K \psi_i \cdot \psi_j d\mathbf{x} = \int_K \mathbf{B}_0 \cdot \psi_j d\mathbf{x} \tag{5.2}$$

Write it in the form of matrices:

$$M_k \cdot \alpha = \mathbf{b}_k \tag{5.3}$$

where $M_k = \int_K \psi_i \cdot \psi_j d\mathbf{x}$ and $\mathbf{b}_k = \int_K \mathbf{B}_0 \cdot \psi_j d\mathbf{x}$.

α can be solved from the above equation, in the domain $[0, 10] \times [0, 10]$, and the domain is discretized by triangular elements in Figure **??**. K is one of the triangular elements in the mesh.

The novelty of our method is that when patching M_k and b_k together, the edge functions of the common edge on two neighboring elements will have the same coefficient
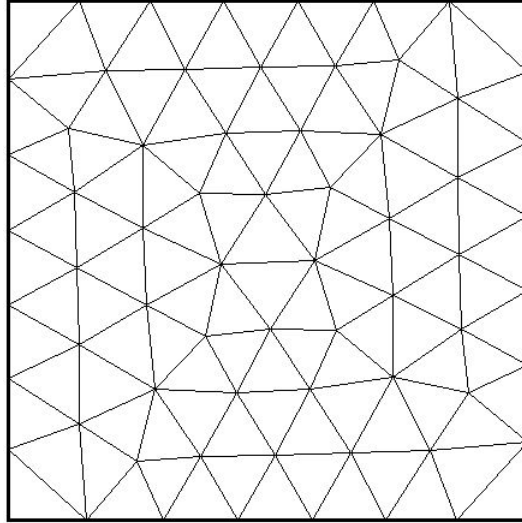
Figure 4: An example triangular mesh on a square domain

α_i, to ensure the continuity on normal component. This can be shown numerically that the normal component of the edge functions only depends on the two vertices of the edge AB, see Figure **??**. Therefore, the edge functions of the same order p on the the common edge AB of two neighboring elements K_1 and K_2 have the same magnitude on the normal direction. By ensuring the edge functions share the same coefficient on neighboring elements, the continuity of the normal direction across the interface can be well preserved.

Aggregate the M_k and b_k, ensuring that the edge functions of each edge are shared, and thus the corresponding entries are overlapped in M and $\mathbf{b}$, with

$$M = \sum_{i=1}^{N} M_k, \ \mathbf{b} = \sum_{i=1}^{N} \mathbf{b}_k \tag{5.4}$$
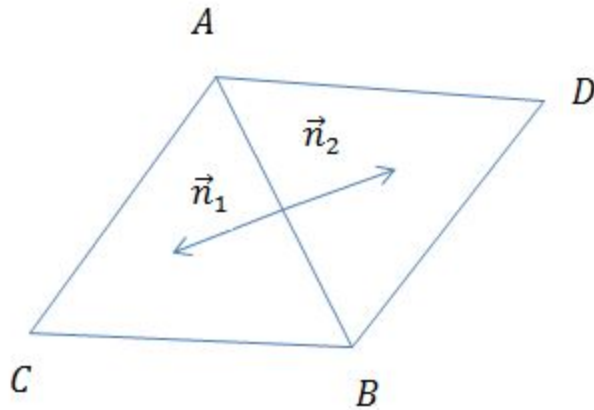
where N is the number of elements in the domain.

Figure 5: An example of patching two triangular elements

Let

$$\mathbf{B}_0 = \begin{pmatrix} \sin(x+y) \\ \cos(x+y) \end{pmatrix} \tag{5.5}$$

and we check the error of the numerical solution $\mathbf{B}_h$,

$$\epsilon = ||\mathbf{B}_h - \mathbf{B}_0||_2 \tag{5.6}$$

Theoretically, for basis functions of order p, as the length of the element edge decreases by half, the numerical error will go down by a rate of 2^{p+1}, which is also called as convergence rate. In Table 1, The numerical result shows that for basis function of order p, the numerical convergence rate is close to the theoretical rate.

Moreover, Figure 6, as a better illustration of Table 1, shows that the error goes down not only as the mesh is finer, but also as the order of basis functions increases. Therefore, the $\mathcal{H}(\mathbf{div})$ basis functions enjoy a good convergence property while ensuing the normal components are continuous across the interface of the triangular elements.

Table 1: Numerical error and convergence rate of using $H(div)$ basis functions of different order, compared to the theoretical convergence rate

Mesh	$p = 0$		$p = 1$		$p = 2$		$p = 3$		$p = 4$	
	Error	Rate	Error	Rate	Error	Rate	Error	Rate	Error	Rate
2	3.0E-00	-	1.0E-00	-	1.2E-00	-	1.0E-00	-	7.0E-01	-
8	1.0E-00	1.6	6.9E-01	0.5	4.6E-01	1.4	1.2E-01	8.3	4.5E-02	4.0
34	5.7E-01	0.8	4.0E-01	0.8	7.1E-02	2.8	1.9E-02	6.3	2.6E-03	4.1
142	2.3E-01	1.3	7.7E-02	2.4	8.1E-03	3.1	7.4E-04	25.7	6.5E-05	5.3
average	-	1.3	-	2.8	-	1.5	-	3.7	-	4.6
theoretical	-	1	-	2	-	8	-	4	-	5
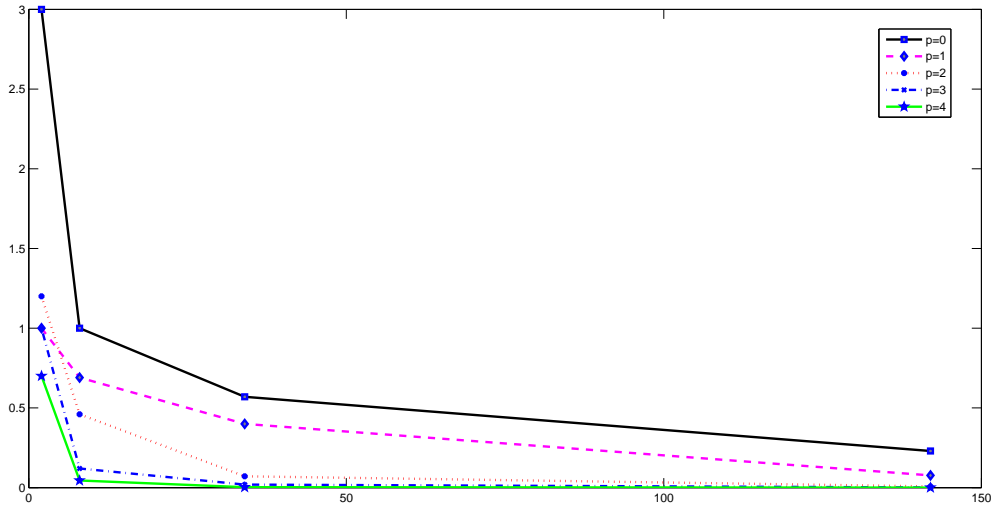
Figure 6: Numerical error of using $\mathcal{H}(\mathbf{div})$ basis functions of different order

5.2   Example with Smooth Solution

This two dimensional vortex problem was originally suggest by Shu [38] in the hydrodynamical system, and was adapted to the MHD equations by Balsara [4]. The solution is a smooth vortex stably convected with the velocity field and the magnetic field. The unperturbed magnetohydrodynaimic flow with $(\rho, u_x, u_y, B_x, B_y, p) = (1, 1, 1, 0, 0, 1)$ is initialized on the computational domain $[-10, 10] \times [-10, 10]$ with $\gamma = 5/3$. The vortex is introduced through the fluctuation in the velocity and mag-

netic fields given by

$$(\partial u_x, \partial u_y) = \frac{\eta}{2\pi} \nabla \times \exp\{0.5(1 - r^2)\} \tag{5.7}$$

$$(\partial B_x, \partial B_y) = \frac{\xi}{2\pi} \nabla \times \exp\{0.5(1 - r^2)\} \tag{5.8}$$

where $r^2 = x^2 + y^2$, and the dynamical balance is obtained through the perturbation

on pressure by

$$\partial p = (\xi^2(1 - r^2) - \eta^2)\frac{1}{8\pi^2} \exp(1 - r^2) \tag{5.9}$$

In our computation of equation (2.1), we set $\eta = 1, \xi = 1$. Periodical boundary

conditions are used. The exact solution is just the one obtained from the initial

configuration propagating with speed $(1, 1)$, or mathematically given by $\mathbf{U}^p(x, y, t) = \mathbf{U}_0^p(x - t, y - t)$.

We choose the $\mathcal{H}(\mathbf{div})$-conforming basis function for magnetic filed $\mathbf{B}$, and the third

order regular orthonormal hierarchical basis for other components. As our major

task is to test the property of $\mathcal{H}(\mathbf{div})$-conforming basis, we will keep the regular

orthonormal hierarchical basis, and focus on the impact of $\mathcal{H}(\mathbf{div})$-conforming basis

of different orders.

Table 2 shows the L^2 errors and accuracy for all the components of MHD equations

at $t = 0$. The L^2 errors are computed within the domain $[-10, 10] \times [-10, 10]$.

We can see that the third order regular orthonormal hierarchical basis obtain third

order accuracy. $\mathcal{H}(\mathbf{div})$-conforming basis of order p obtain p-th order accuracy when

$p = 2, 3$. When $p = 4, 5$, the convergence rate definitely improves, but is a little

short to the p-th order convergence, which was limited by the third order regular

orthonormal hierarchical basis that we use. Nevertheless, our results show again that the $\mathcal{H}(\mathbf{div})$-conforming basis enjoys a well-behaved convergence property, and it can work very well with other type of basis functions, such as regular orthonormal hierarchical basis. The convergence rates are proportionally adjusted to the size of the elements, so that they are comparable to the theoretical values.

Table 2: L^2 errors of all the components and the convergence rate with smooth solution at time $t = 0$

	ρ		$\mathbf{u}$		E		$\mathbf{B}$	
Mesh	Error	Order	Error	Order	Error	Order	Error	Order
			$p = 3$				$p = 2$	
2	5.55E-16		5.39E-02		1.33E-03		3.16E-02	
14	4.84E-16	-	8.00E-03	1.94	2.70E-04	1.49	1.40E-02	0.37
44	4.29E-16	-	1.05E-03	3.28	1.35E-03	-2.00	3.35E-03	2.41
106	4.64E-16	-	2.05E-04	3.09	1.98E-04	3.50	1.12E-03	2.31
			$p = 3$				$p = 3$	
2	5.55E-16		5.39E-02		1.33E-03		5.39E-02	
14	4.84E-16	-	8.00E-03	1.94	2.70E-04	1.49	8.92E-03	1.79
44	4.29E-16	-	1.05E-03	3.28	1.35E-03	-2.00	1.24E-03	3.20
106	4.64E-16	-	2.05E-04	3.09	1.98E-04	3.50	2.35E-04	3.13
			$p = 3$				$p = 4$	
2	5.55E-16		5.39E-02		1.33E-03		9.37E-02	
14	4.84E-16	-	8.00E-03	1.94	2.70E-04	1.49	6.00E-03	3.16
44	4.29E-16	-	1.05E-03	3.28	1.35E-03	-2.00	9.78E-04	2.97
106	4.64E-16	-	2.05E-04	3.09	1.98E-04	3.50	1.59E-04	3.35
			$p = 3$				$p = 5$	
2	5.55E-16		5.39E-02		1.33E-03		1.23E-01	
14	4.84E-16	-	8.00E-03	1.94	2.70E-04	1.49	4.10E-03	4.10
44	4.29E-16	-	1.05E-03	3.28	1.35E-03	-2.00	1.92E-04	4.76
106	4.64E-16	-	2.05E-04	3.09	1.98E-04	3.50	2.69E-05	3.57

Figure 7 shows clearly the above relation at $t = 0$. As we increase the granularity of the mesh, the L^2 error of the magnetic field $\mathbf{B}$ will decay, for $p = 2, 3, 4, 5$, respectively. As we increase the order of $\mathcal{H}(\mathbf{div})$-conforming basis, the numerical solution will converge to the exact solution. For other components, using third order regular

orthonormal hierarchical basis, as the mesh is finer, the error typically gets smaller.
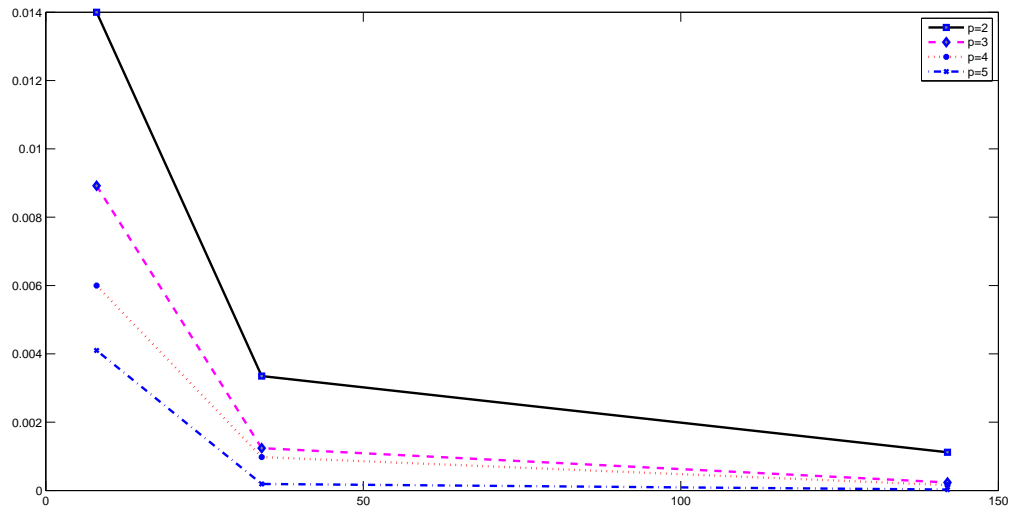
(a) Magnetic field **B** using $H(div)$ basis functions
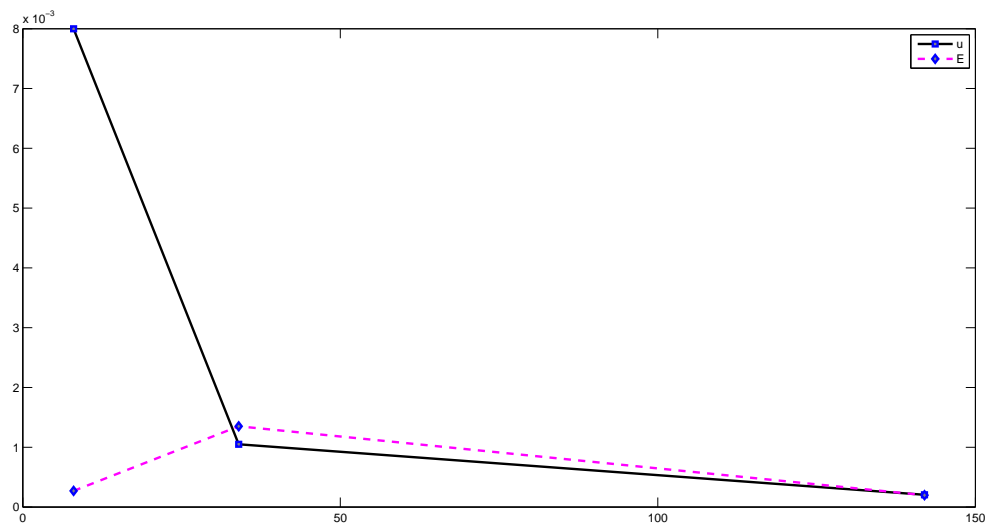
(b) Speed **u** and energy E

Figure 7: Numerical error of different components using different size of meshes at $t = 0$

Table 3 shows the L^2 errors and accuracy for all the components of MHD equations at $t = 1.0$, using third order Runge-Kutta temporal scheme. The spatial L^2 error is still calculated over the domain $[-10, 10] \times [-10, 10]$. As the error from the temporal discretization kicks in, the convergence rate of $\mathcal{H}(\mathbf{div})$-conforming basis at $t = 1.0$ can no longer obtain p-th order accuracy. However, there is still a trend for the numerical solution converging to the exact solution as higher order of $\mathcal{H}(\mathbf{div})$-conforming basis is used or the mesh gets finer. The errors are contained well by our third order Runge-Kutta time scheme. The third order regular orthonormal hierarchical basis shows a similar behavior as $\mathcal{H}(\mathbf{div})$-conforming basis. Again, the convergence rates are proportionally adjusted to the size of the elements, so that they are comparable to the theoretical values.

Agian, Figure 8 shows a clear illustration of the above relation at $t = 1.0$. As we increase the granularity of the mesh, the L^2 error of the magnetic field $\mathbf{B}$ will decay, for $p = 2, 3, 4, 5$, respectively. As we increase the order of $\mathcal{H}(\mathbf{div})$-conforming basis, the numerical solution will converge to the exact solution. For other components, using third order regular orthonormal hierarchical basis, as the mesh is more granule, the error typically gets smaller. The error of ρ is not shown at $t = 0$ since it is a constant at $t = 0$, and only presents machine error. At time $t = 1.0$, the effect of the temporal error brings the error of ρ in sight, but it goes down by finer mesh.

Table 3: L^2 errors of all the components and the convergence rate with smooth solution at time $t = 1.0$

Mesh	ρ Error	Order	**u** Error	Order	E Error	Order	**B** Error	Order
			$p = 3$				$p = 2$	
2	1.69E-06		1.32E-01		3.60E-03		1.30E-01	
14	2.46E-03	-10.51	4.97E-03	3.92	5.76E-03	-1.47	3.54E-03	4.39
44	1.59E-03	0.98	3.34E-03	0.92	5.89E-03	0.31	3.60E-03	0.32
106	8.96E-04	1.56	1.26E-03	2.14	2.81E-03	1.80	2.58E-03	1.21
			$p = 3$				$p = 3$	
2	2.30E-06		1.32E-01		3.60E-03		1.20E-01	
14	2.25E-03	-9.93	4.96E-03	3.93	5.89E-3	-1.51	4.86E-03	3.82
44	1.44E-03	0.99	3.26E-03	0.96	5.58E-03	0.42	2.28E-03	1.44
106	7.21E-04	1.73	1.22E-03	2.15	2.43E-03	1.93	8.86E-04	2.09
			$p = 3$				$p = 4$	
2	4.35E-06		1.32E-01		3.60E-03		1.10E-01	
14	2.30E-03	-9.05	4.97E-03	3.92	5.98E-03	-1.56	1.44E-03	5.45
44	1.38E-03	1.08	3.29E-03	0.94	5.54E-03	0.45	9.78E-04	0.90
106	7.28E-04	1.66	1.21E-03	2.17	2.45E-03	1.91	5.11E-04	1.67
			$p = 3$				$p = 5$	
2	5.98E-06		1.32E-01		3.60E-03		9.65E-02	
14	2.41E-03	-8.65	4.96E-03	3.93	6.15E-03	-1.60	2.34E-03	4.56
44	1.37E-03	1.16	3.28E-03	0.94	5.55E-03	0.50	7.70E-04	1.95
106	7.31E-03	1.64	1.23E-03	2.15	2.45E-03	1.91	7.19E-04	0.83

Now we will show the results after we apply the divergence cleaning technique described in Chapter 4. After the magnetic filed $\mathbf{B}_h$ is numerically solved from the MHD equations, we will apply our divergence cleaning technique as a post process. To clean the divergence of the magnetic field, we follow two steps. First step to use the bubble function to eliminate the higher order terms in $\nabla \cdot \mathbf{B}_h$; then the second step is to use the edge functions from order $p = 0$ to eliminate the constant term. Although, we find that the divergence of the edge function of order 0 are linear dependent, it may not completely eliminate the remaining constant term of the divergence. Our numerical experiment below shows that our two-step divergence cleaning technique
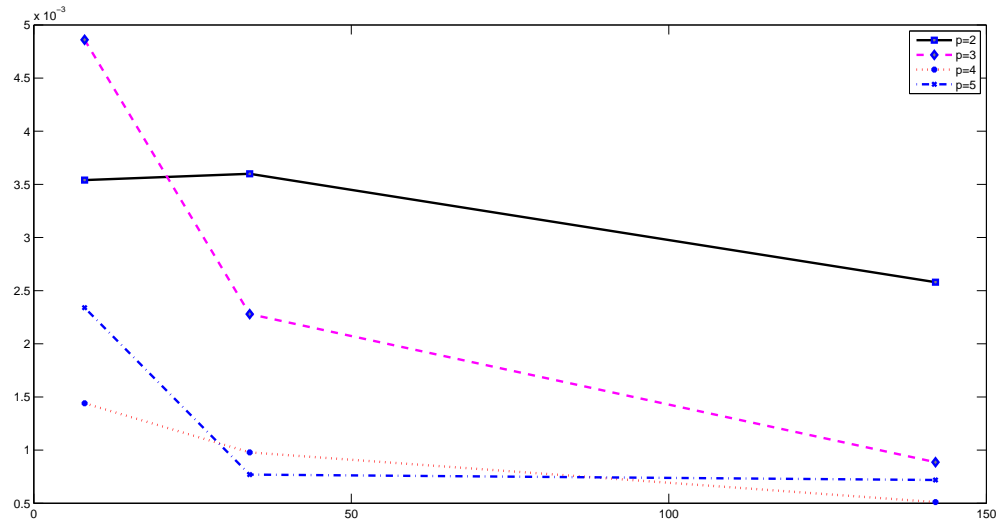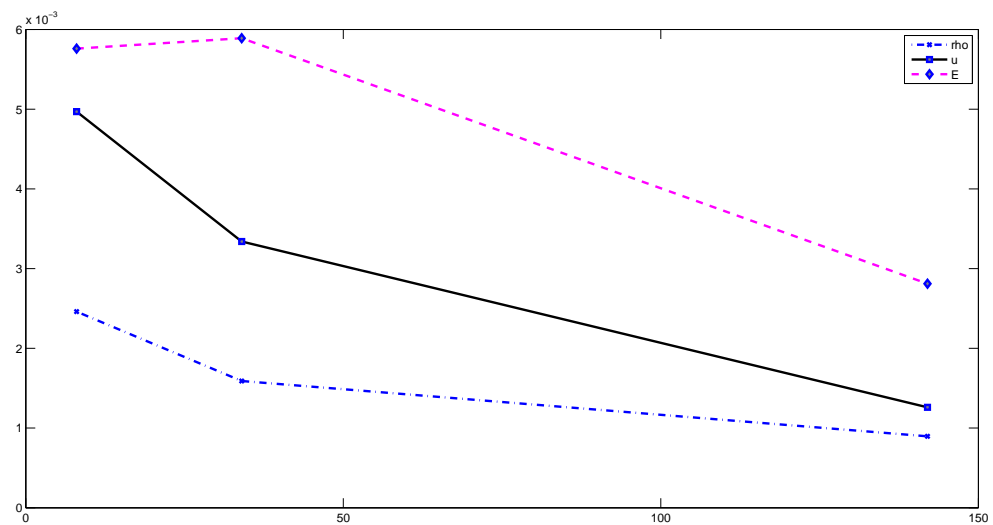
(a) Magnetic field $\mathbf{B}$ using $H(div)$ basis functions

(b) Speed $\mathbf{u}$ and energy E

Figure 8: Numerical error of different components using different size of meshes at $t = 1.0$

can largely reduce the divergence of magnetic field to a very low level.

Table 4, 5, 6 and 7 show the L^2 error and the divergence of the magnetic field $\mathbf{B}$ before and after each cleaning step, at time $t = 0$ and $t = 1.0$, for $\mathcal{H}(\mathbf{div})$-conforming basis of order $p = 2, 3, 4, 5$. The error and divergence are computed on

over the domain $[-10, 10] \times [-10, 10]$ with diferent sizes of mesh. The results show that at time $t = 0$ without sacrificing too much accuracy of the solution of magnetic field $\mathbf{B}_h$, the divergence can be significantly reduced by fifth or sixth orders. At time $t = 1.0$, this divergence cleaning technique also works well with the time scheme, and have a similar effect in reducing divergence. We notice that in some cases, the divergence can be completely eliminated (to machine error), but in some cases it can only be largely reduced. The effect is caused by the following reason. Since the edge functions are shared on common edges when patching the triangular elements together, the actual number edge functions of order 0 in the global scope is less than the needed freedom of the equation(the number of triangular elements), which makes our equation system (4.40) under-determined. At $t = 0$, when all the components start with nicely defined polynomials or other special functions, we might have the luck to completely eliminate all the constant divergence with fewer edge functions of order 0. However, we will not going to have the same luck when the temporal error kicks in and the linear combination of the numerical solutions get more complicated.

Table 4: Error of magnetic field $\mathbf{B}$ and divergence of magnetic field at $t = 0$ and $t = 1.0$, using $\mathcal{H}(\mathbf{div})$ basis of order 2

$p = 2$ Mesh		$t = 0$		$t = 1.0$	
		$\mathbf{B} - \mathbf{B}_h$	$\nabla\mathbf{B}_h$	$\mathbf{B} - \mathbf{B}_h$	$\nabla\mathbf{B}_h$
2	original	3.16E-02	1.11E-16	1.30E-01	2.05E-09
	step 1	2.14E-01	4.39E-17	1.22E-01	3.77E-10
	step 2	2.14E-01	4.26E-18	1.22E-01	3.77E-10
14	original	1.40E-02	4.24E-04	3.54E-03	6.28E-04
	step 1	1.70E-02	5.36E-04	4.41E-03	7.10E-04
	step 2	1.92E-02	2.45E-18	1.94E-02	3.06E-07
44	original	3.35E-03	6.74E-04	3.60E-03	1.89E-03
	step 1	3.86E-03	5.36E-04	6.31E-03	1.60E-03
	step 2	6.14E-03	2.08E-06	1.52E-02	7.55E-06
106	original	1.12E-03	3.85E-04	2.58E-03	1.85E-03
	step 1	2.01E-03	2.72E-04	4.43E-03	1.26E-03
	step 2	5.80E-03	6.04E-09	5.80E-02	4.38E-07

Table 5: Error of magnetic field $\mathbf{B}$ and divergence of magnetic field at $t = 0$ and $t = 1.0$, using $\mathcal{H}(\mathbf{div})$ basis of order 3

$p = 3$ Mesh		$t = 0$		$t = 1.0$	
		$\mathbf{B} - \mathbf{B}_h$	$\nabla\mathbf{B}_h$	$\mathbf{B} - \mathbf{B}_h$	$\nabla\mathbf{B}_h$
2	original	5.39E-02	3.88E-16	1.20E-01	3.35E-05
	step 1	5.51E-01	8.20E-17	1.93E-01	1.02E-05
	step 2	5.51E-01	7.37E-18	1.93E-01	3.68E-06
14	original	8.92E-03	5.50E-04	4.86E-03	1.16E-03
	step 1	1.46E-02	8.10E-05	1.85E-01	6.11E-04
	step 2	1.47E-02	3.79E-18	1.95E-01	5.29E-07
44	original	1.24E-03	4.93E-04	2.28E-03	1.55E-03
	step 1	3.26E-03	3.50E-04	7.89E-03	1.17E-03
	step 2	5.41E-03	1.55E-06	1.29E-02	2.75E-06
106	original	2.35E-04	3.03E-04	8.86E-04	8.90E-04
	step 1	7.14E-04	1.25E-04	4.06E-03	8.34E-04
	step 2	3.30E-03	3.90E-10	1.36E-02	7.58E-08

Table 8 and Table 9 show the error and accuracy for the divergence-cleaned magnetic field $\mathbf{B}^*$, at $t = 0$ and $t = 1.0$, respectively. We can see that the magnetic field after correction $\mathbf{B}^*$ at $t = 0$ typically has a better convergence rate than that of $t = 1.0$. Although in either of the cases, the convergence rate is short of the

Table 6: Error of magnetic field $\mathbf{B}$ and divergence of magnetic field at $t = 0$ and $t = 1.0$, using $H(div)$ basis of order 4

$p = 4$ Mesh		$t = 0$ $\mathbf{B} - \mathbf{B}_h$	$\nabla\mathbf{B}_h$	$t = 1.0$ $\mathbf{B} - \mathbf{B}_h$	$\nabla\mathbf{B}_h$
2	original	9.37E-02	1.96E-15	1.10E-01	6.86E-04
	step 1	2.11E-01	3.25E-17	5.53E-02	1.85E-05
	step 2	2.11E-01	1.19E-17	5.53E-02	1.85E-05
14	original	6.00E-03	4.04E-04	1.44E-03	1.76E-03
	step 1	2.61E-02	5.85E-04	2.54E-02	7.16E-04
	step 2	2.76E-02	1.60E-17	3.08E-02	1.26E-06
44	original	9.78E-04	3.38E-04	9.78E-04	1.66E-03
	step 1	1.11E-02	1.99E-04	9.73E-03	5.99E-04
	step 2	1.23E-02	2.19E-07	1.05E-02	4.91E-07
106	original	1.59E-04	5.19E-05	5.11E-04	1.03E-03
	step 1	8.71E-04	5.27E-05	6.07E-03	6.04E-04
	step 2	1.46E-03	4.54E-11	1.45E-02	2.13E-08

Table 7: Error of magnetic field $\mathbf{B}$ and divergence of magnetic field at $t = 0$ and $t = 1.0$, using $\mathcal{H}(\mathbf{div})$ basis of order 5

$p = 5$ Mesh		$t = 0$ $\mathbf{B} - \mathbf{B}_h$	$\nabla\mathbf{B}_h$	$t = 1.0$ $\mathbf{B} - \mathbf{B}_h$	$\nabla\mathbf{B}_h$
2	original	1.23E-01	1.39E-15	9.65E-02	4.86E-04
	step 1	2.94E-01	5.46E-17	7.78E-02	1.61E-05
	step 2	2.94E-01	5.46E-17	7.78E-02	1.45E-05
14	original	4.10E-03	2.94E-04	2.34E-03	7.21E-04
	step 1	1.60E-01	1.87E-04	1.71E-01	4.34E-04
	step 2	1.63E-01	1.10E-17	1.72E-01	7.56E-09
44	original	1.92E-04	1.75E-04	7.70E-04	6.90E-04
	step 1	1.31E-02	7.42E-05	8.20E-02	5.56E-04
	step 2	1.41E-02	4.53E-08	8.68E-02	6.55E-07
106	original	2.69E-05	5.21E-05	7.19E-04	1.46E-03
	step 1	2.78E-03	1.59E-05	2.47E-02	7.61E-04
	step 2	2.99E-03	4.59E-11	4.44E-02	1.76E-08

theoretical value, the error of the magnetic field before and after each correction step decays as the mesh is further refined, as better shown in the left columns of Figure 9 and Figure 10. On the other hand, in the right columns of Figure 9 and Figure 10, the divergence of the magnetic field before and after each correction step also decays

with a finer mesh. More importantly, after the second-step correction, the divergence

goes down to the unnoticeable level compared to the divergence before the correction

steps. It shows that our global divergence cleaning technique is efficient when working

with spatial and temporal discretization schemes.

Table 8: Error of magnetic field **B** after divergence cleaning at $t = 0$ and its convergence rate for different orders of basis

$t = 0$ Mesh	$p = 2$ $\mathbf{B} - \mathbf{B}_h$	order	$p = 3$ $\mathbf{B} - \mathbf{B}_h$	order	$p = 4$ $\mathbf{B} - \mathbf{B}_h$	order	$p = 5$ $\mathbf{B} - \mathbf{B}_h$	order
2	2.14E-01		5.51E-01		2.11E-01		2.94E-01	
14	1.92E-02	2.67	1.47E-02	4.42	2.76E-02	2.13	1.63E-01	0.04
44	6.14E-03	1.99	5.41E-03	1.79	1.23E-02	1.52	1.41E-02	3.88
106	5.80E-03	0.82	3.30E-03	1.44	1.46E-03	3.81	2.99E-03	2.96

Table 9: Error of magnetic field **B** after divergence cleaning at $t = 1.0$ and its convergence rate for different orders of basis

$t = 1.0$ Mesh	$p = 2$ $\mathbf{B} - \mathbf{B}_h$	order	$p = 3$ $\mathbf{B} - \mathbf{B}_h$	order	$p = 4$ $\mathbf{B} - \mathbf{B}_h$	order	$p = 5$ $\mathbf{B} - \mathbf{B}_h$	order
2	1.22E-01		1.93E-01		5.53E-02		7.78E-02	
14	1.94E-02	1.84	1.95E-01	-0.81	3.08E-02	0.04	1.72E-01	-1.94
44	1.52E-02	0.70	1.29E-02	4.27	1.05E-02	1.90	8.68E-02	1.33
106	5.80E-02	-1.18	1.36E-02	0.65	1.45E-02	0.26	4.44E-02	1.70

Figure 11 shows the error and log error of magnetic field **B** before and after each divergence cleaning step from time $t = 0$ to $t = 2.0$. Figure 12 shows the divergence and log divergence of the magnetic field **B** before and after each divergence cleaning step from time $t = 0$ to $t = 2.0$. This is calculated over the domain $[0, 10] \times [0, 10]$ with a mesh of 106 triangular elements, using third order $\mathcal{H}(\mathbf{div})$-conforming basis and third order regular orthonormal hierarchical basis. As we can see in Figure 12, without any correction, the divergence can accumulate and grow very quickly. After two-step cleaning process, the global divergence is mostly eliminated compared to the initial divergence, and stays low as time evolves. On the other hand, the numerical solution of magnetic field **B** has a relative large error after the corrections. Particularly, the first step of the divergence cleaning, i.e., eliminating the high order terms of the divergence, will lead to a bigger error margin in the solution itself. The second step of the divergence cleaning has little impact on the solution itself, but largely eliminated the divergence. However, in spite of introducing extra errors of the numerical solution itself for the divergence cleaning, the numerical solution still stays close enough with the uncorrected one. It shows again that, as a post process, our divergence cleaning technique greatly serves our purpose, and can also work well with the spatial and temporal discretization schemes.
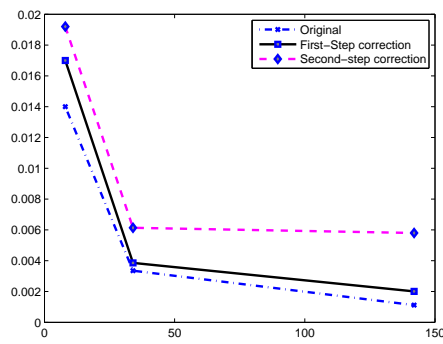
(a) Second order basis, L^2 error
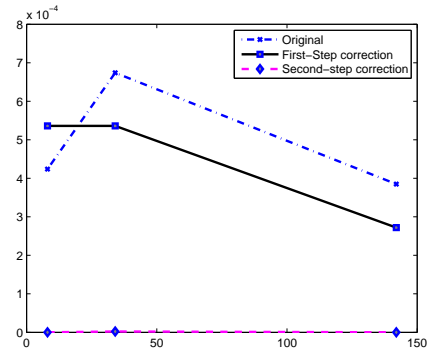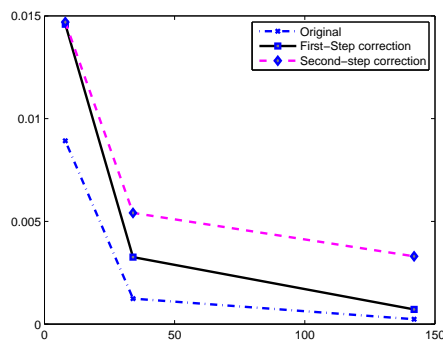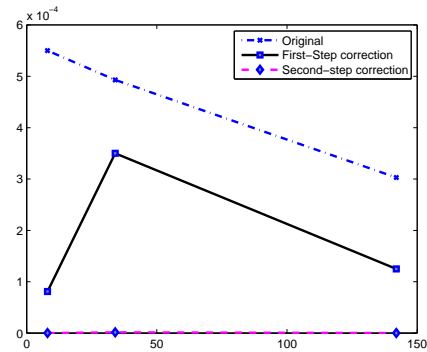
(b) Second order basis, divergence

(c) Third order basis, L^2 error

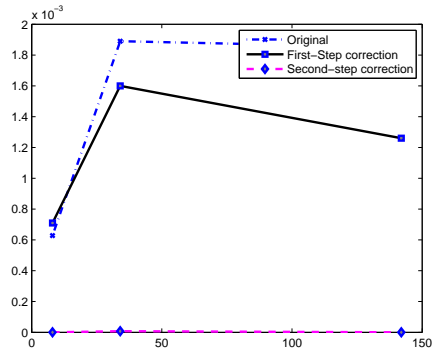(d) Third order basis, divergence
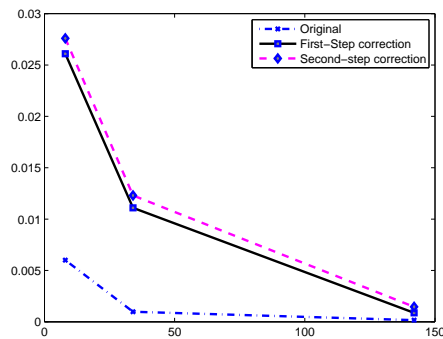
(e) Fourth order basis, L^2 error
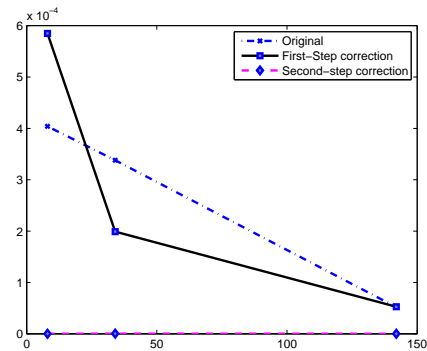
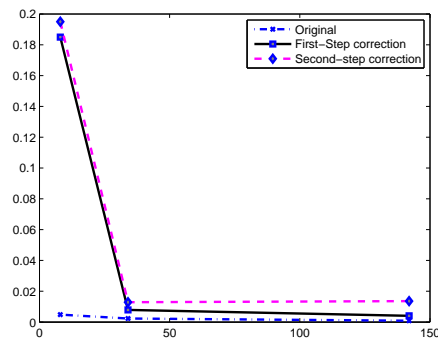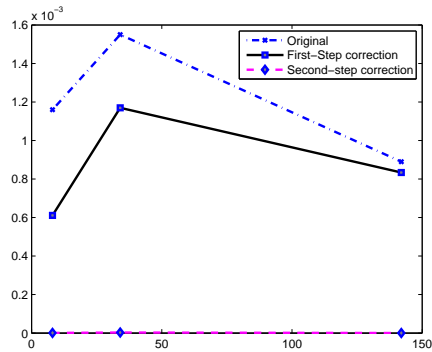(f) Fourth order basis, divergence
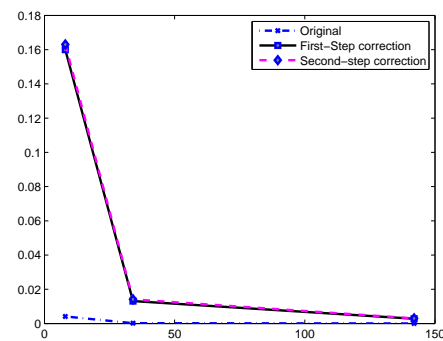
(g) Fifth order basis, L^2 error
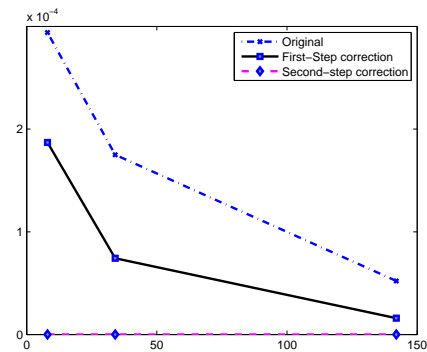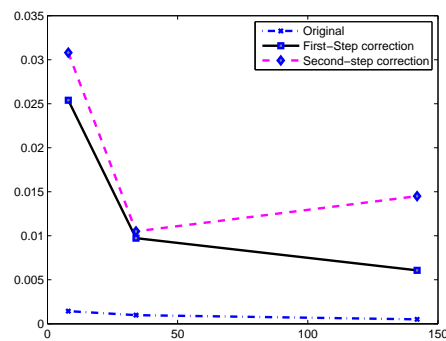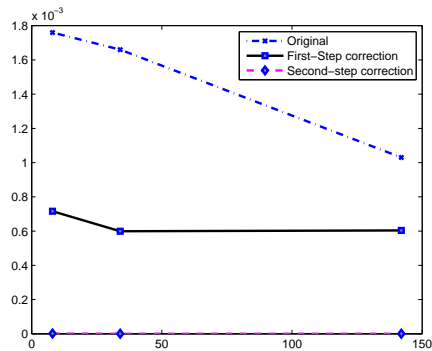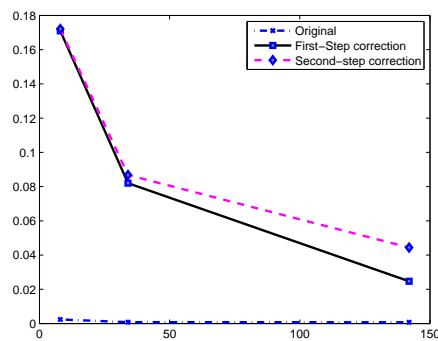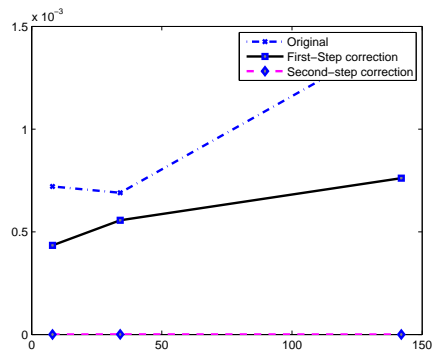
(h) Fifth order basis, divergence

Figure 9: Numerical error(left column) and divergence(right column) of magnetic field $\mathbf{B}$ on different size of meshes, using $\mathcal{H}(\mathbf{div})$ basis at $t = 0$
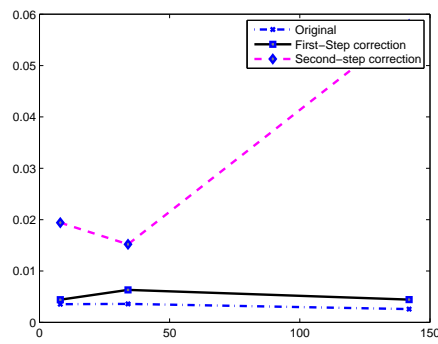
(a) Second order basis, L^2 error

(b) Second order basis, divergence

(c) Third order basis, L^2 error

(d) Third order basis, divergence

(e) Fourth order basis, L^2 error

(f) Fourth order basis, divergence

(g) Fifth order basis, L^2 error

(h) Fifth order basis, divergence

Figure 10: Numerical error(left column) and divergence(right column) of magnetic field $\mathbf{B}$ on different size of meshes, using $\mathcal{H}(\mathbf{div})$ basis at $t = 1.0$
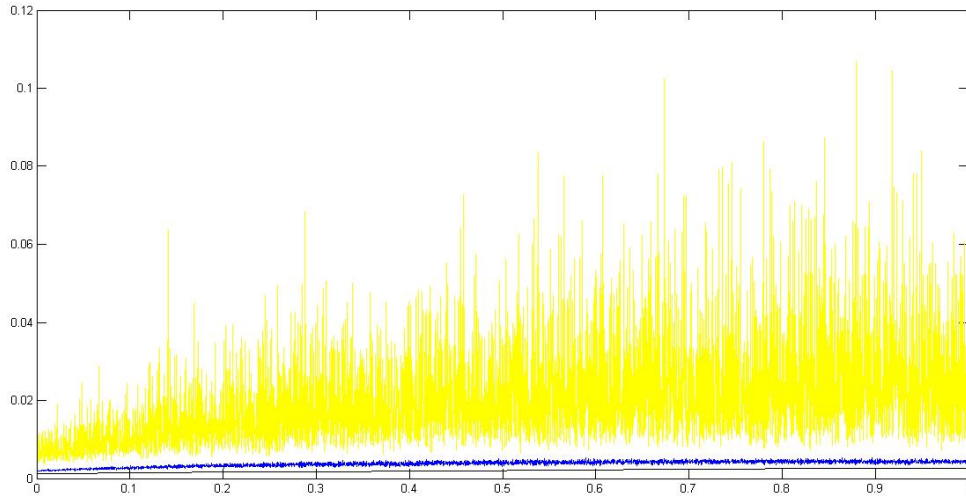
(a) Numerical error of magnetic field **B**
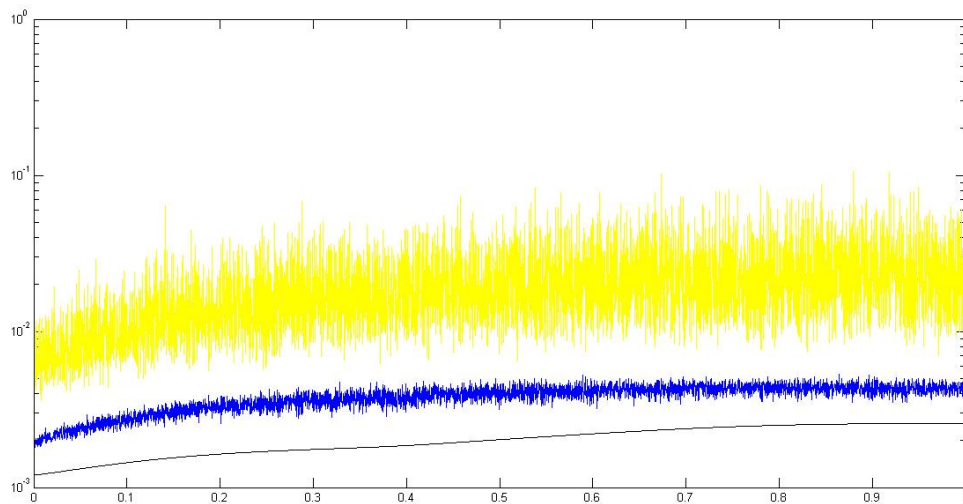
(b) Log of numerical error of magnetic field **B**

Figure 11: Numerical error of magnetic field **B** from $t = 0$ to $t = 2.0$ for 2-D smooth solution. Solid line is original, dash-dot line is **B** after first step correction, dash line is **B** after second step correction.
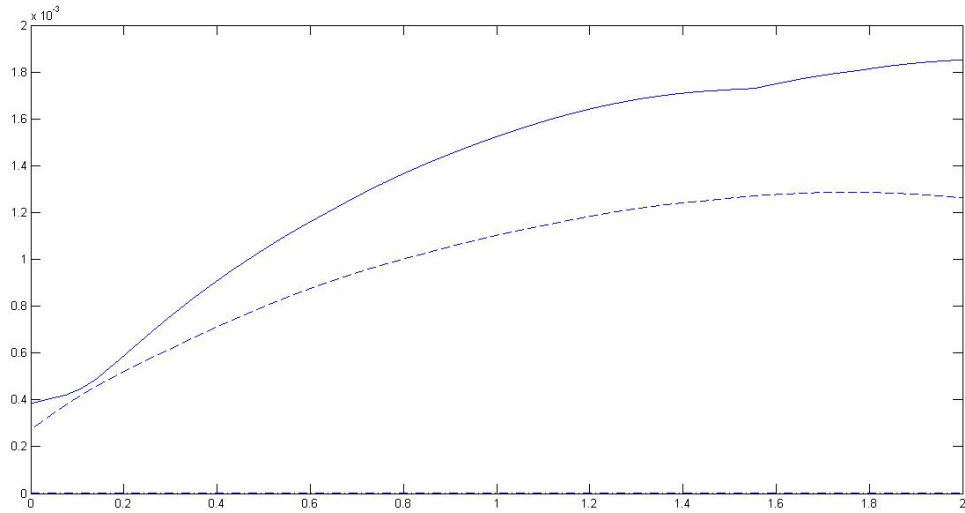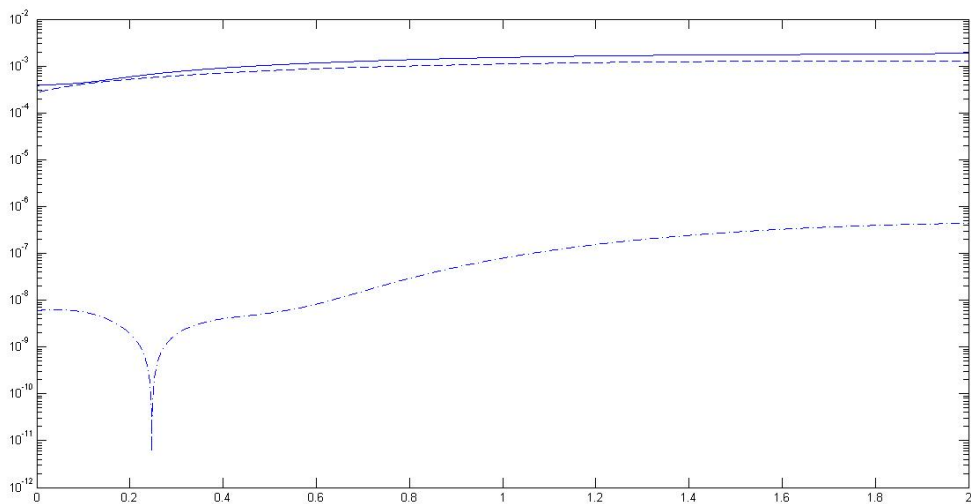
(a) Divergence of magnetic field **B**

(b) Log of Divergence of magnetic field **B**

Figure 12: Divergence of magnetic field **B** from $t = 0$ to $t = 2.0$ for 2-D smooth solution. Solid line is original, dash-dot line is **B** after first step correction, dash line is **B** after second step correction.

5.3   Orszag-Tang Vortex Example

We will study the development of the Orszag-Tang vortex example, see [31], which is a widely used test example in the literature because of the complex interaction between several shocks generated as the whole system evolves. Starting from a smooth state, after the transition period, the system will go to turbulence. The initial setup is

$$\mathbf{U}^p = (\gamma^2, -\sin y, \sin x, 0, -\sin y, \sin 2x, 0, \gamma) \tag{5.10}$$

with $\gamma = 5/3$, and the computational domain is $[0, 2\pi] \times [0, 2\pi]$ with periodic boundary conditions.

The time development of density is shown in Figure 13. This is calculated over the domain $[0, 2\pi] \times [0, 2\pi]$ with a mesh of 106 triangular elements, using second order $\mathcal{H}(\mathbf{div})$-conforming basis and first order regular orthonormal hierarchical basis. The figures show that the solution is quite smooth at the early stage. At $t = 2$, shocks have already appeared. At later times, for example, at $t = 3, 4$, the shocks interact each other and the structure gets quite complicated.

During the computation, the minmod TVB shlope limiter is applied to the components that will develop shocks, which can enhance the stability of the method and eliminate possible spurious oscillations in the approximate solution. The limiter is only designed for the first order basis, but for higher order basis, the limiter can still delay the blowing up. For example, with $M = 4.0$, on a mesh of 44 triangular elements, computation with third order $\mathcal{H}(\mathbf{div})$-conforming basis and first order regular
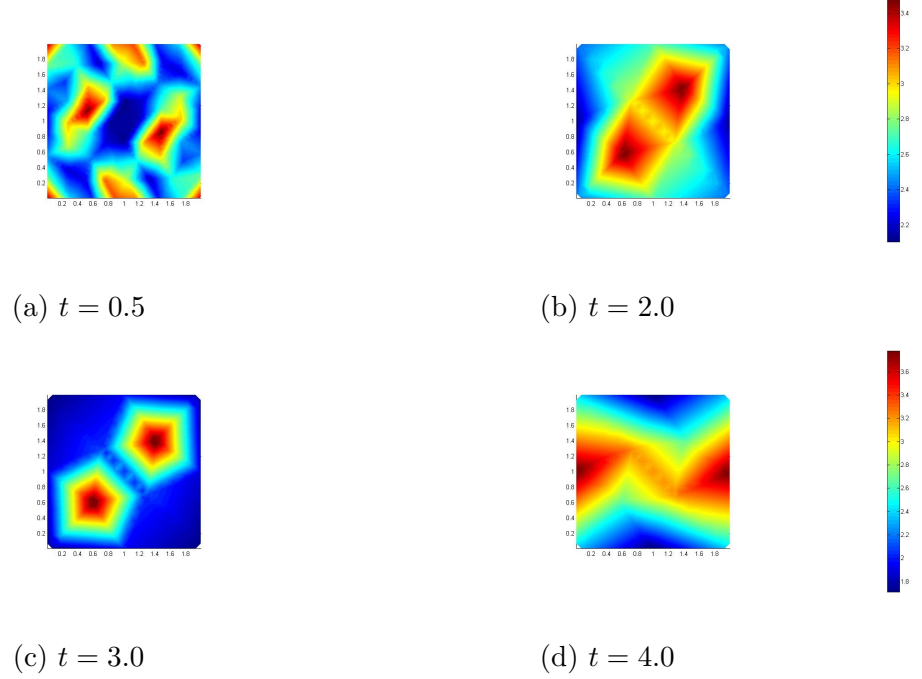
(a) $t = 0.5$ (b) $t = 2.0$

(c) $t = 3.0$ (d) $t = 4.0$

Figure 13: The development of ρ on a mesh of 106 triangular elements.

orthonomal hierarchical basis could reach $t = 20.0$. This stability is highly dependent on the choice of M. Li [26] also pointed out that the choice of limiters also has a big impact on the numerical stability.

Figure 14a shows the divergence of the magnetic field $\mathbf{B}$ before and after each divergence cleaning step from $t = 0$ to $t = 2.0$, and Figure 14b shows the log of the divergence. This is calculated on a mesh of 106 triangular elements, using second order $\mathcal{H}(\mathbf{div})$-conforming basis and first order regular orthonormal hierarchical basis. These two figures show that without any correction, the divergence RKDG solutions can quickly accumulate and grow, which will eventually lead to non-physical solutions. By applying our proposed divergence corrections, as a post process, the numerical divergence can be significantly eliminated, and maintained stably at a low level, even

over the time evolution. Therefore, our divergence cleaning technique is effective.
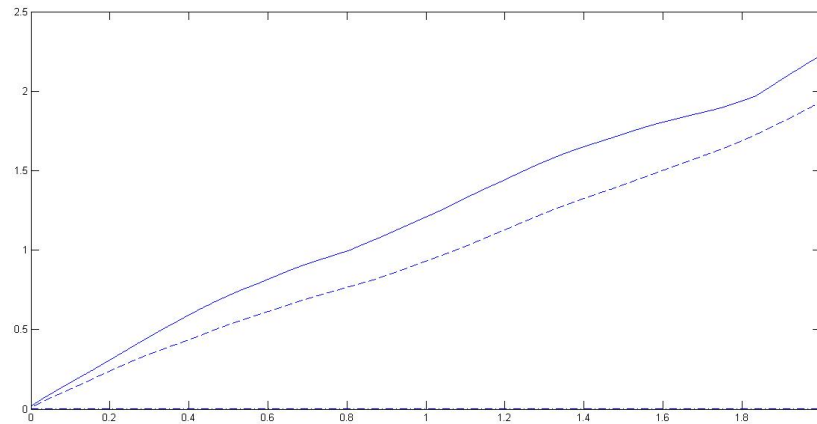
(a) Divergence of magnetic field $\mathbf{B}$
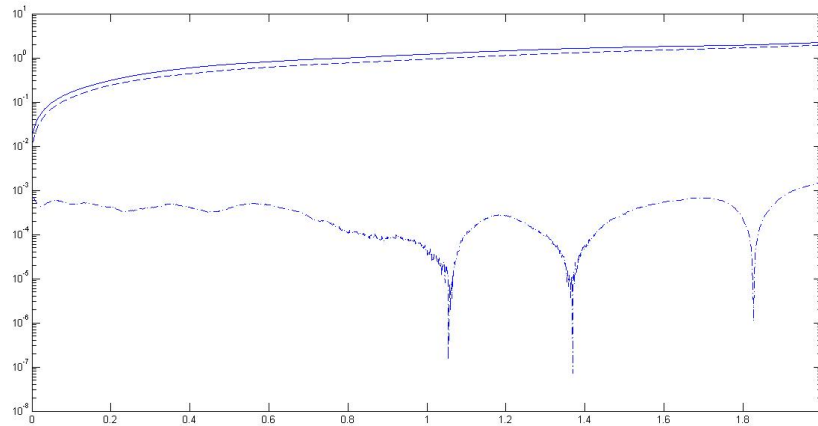
(b) Log of Divergence of magnetic field $\mathbf{B}$

Figure 14: Divergence of magnetic field $\mathbf{B}$ from $t = 0$ to $t = 2.0$ for 2-D Orszag-Tang vortex problem. Solid line is original, dash-dot line is $\mathbf{B}$ after first step correction, dash line is $\mathbf{B}$ after second step correction.

CHAPTER 6: CONCLUDING REMARKS

Discontinuous Galerkin method using $H(div)$-conforming basis seems to be very effective for solving the MHD equations. It can reduce the computational cost, and increase the flexibility, by providing the choice of different order of basis for magnetic field and the rest of the components. More importantly, the divergence cleaning techniques developed based on the $\mathcal{H}(\mathbf{div})$-conforming basis can greatly eliminate the divergence of the magnetic field on the global scope, while maintaining the solution itself stable with small sacrifice on the accuracy.

This method can be extend to three dimensional cases without essential difficulty.

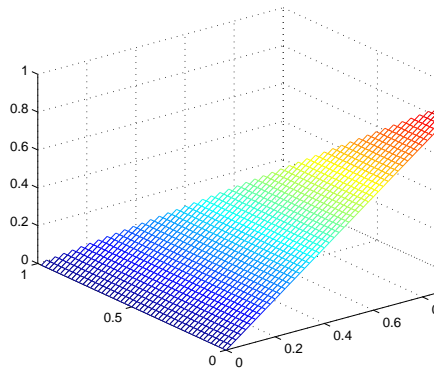## 7.1   List of 2-D $\mathcal{H}(\mathbf{div})$ Basis Functions

For the convenience of implementation, we list the $\mathcal{H}(\mathbf{div})$ basis function of 2-Dimensional triangles, up to order 5.

$\mathcal{H}(\mathbf{div})$ basis functions for 2-Dimension triangles

- **Zeroth order**

  Edge functions

$$
\psi^0_{e[0,1]} = \begin{bmatrix} x \\ y-1 \end{bmatrix} , \ \psi^0_{e[0,2]} = \begin{bmatrix} x-1 \\ y \end{bmatrix} , \ \psi^0_{e[1,2]} = \begin{bmatrix} x \\ y \end{bmatrix} , \tag{7.1}
$$

(a) x component   (b) y conponent
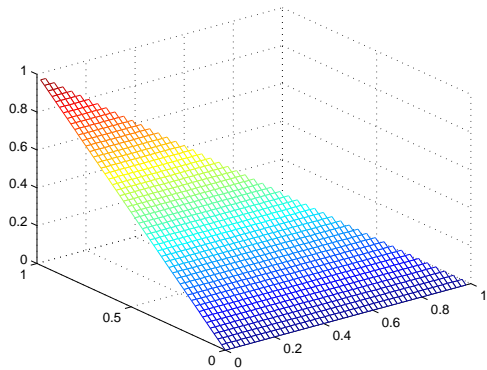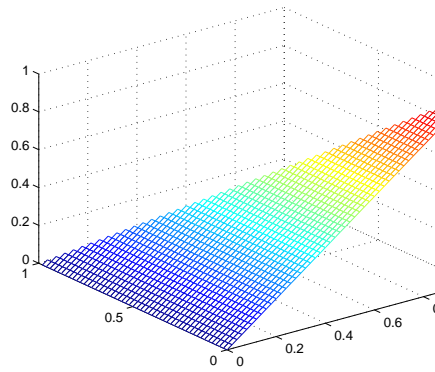
Figure 15: Graph of $\psi^0_{e[1,2]}$

- **First order**

Edge functions

$$\psi^1_{e[0,1]} = \begin{bmatrix} -x \\ 2x+y-1 \end{bmatrix} , \ \psi^1_{e[0,2]} = \begin{bmatrix} x+2y-1 \\ -y \end{bmatrix} , \ \psi^1_{e[1,2]} = \begin{bmatrix} x \\ -y \end{bmatrix} \tag{7.2}$$

(a) x component
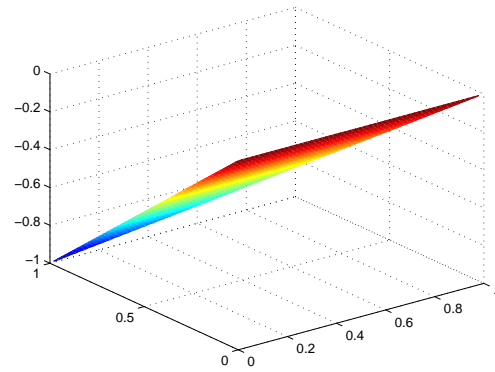
(b) y conponent

Figure 16: Graph of $\psi^1_{e[1,2]}$

- **Second order**

  Edge functions

$$\psi^2_{e[0,1]} = \begin{bmatrix} -2x^2 - xy \\ 4x^2 + y^2 + 4xy - 4x - 3y + 2 \end{bmatrix} ,$$

$$\psi^2_{e[0,2]} = \begin{bmatrix} -x^2 - 4y^2 - 4xy + 3x + 4y - 2 \\ 2y^2 + xy \end{bmatrix} , \tag{7.3}$$

$$\psi^2_{e[1,2]} = \begin{bmatrix} -x^2 + xy - x \\ -y^2 + xy - y \end{bmatrix}$$
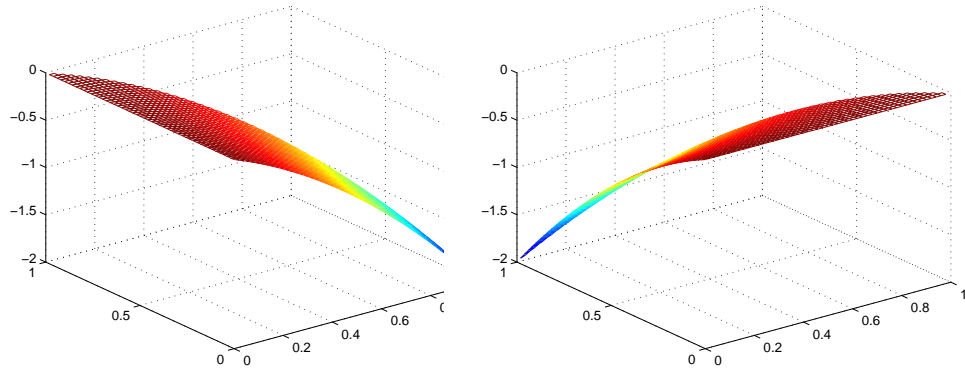
(a) x component   (b) y conponent

Figure 17: Graph of $\psi^2_{e[1,2]}$

<u>Interior functions</u>

$$\psi^{\mathbf{t},2}_{e[0,1]} = \begin{bmatrix} x(1-x-y) \\ \\ 0 \end{bmatrix},$$

$$\psi^{\mathbf{t},2}_{e[0,2]} = \begin{bmatrix} 0 \\ \\ y(1-x-y) \end{bmatrix}, \qquad (7.4)$$

$$\psi^{\mathbf{t},2}_{e[1,2]} = \begin{bmatrix} xy \\ \\ -xy \end{bmatrix}$$

- **Third order**

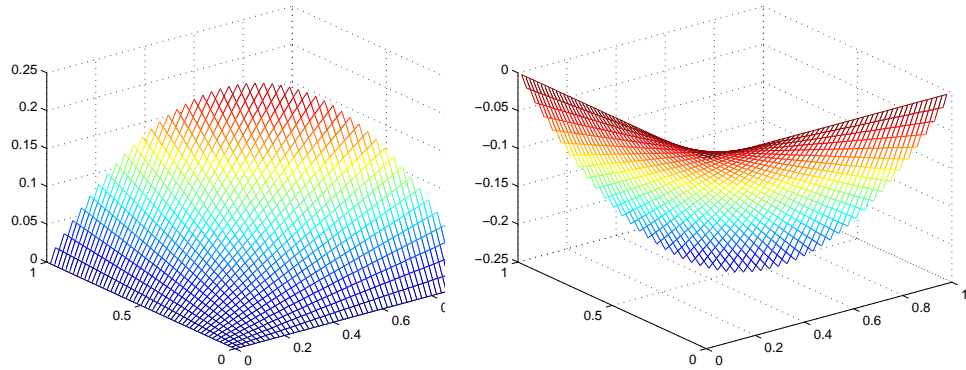(a) x component   (b) y conponent

Figure 18: Graph of $\psi_{e[1,2]}^{\mathbf{t},2}$

Edge functions

$$\psi_{e[0,1]}^3 = \begin{bmatrix} -6x^3 - 6x^2y - \dfrac{3}{2}xy^2 + 4x^2 + 2xy \\ 12x^3 + \dfrac{3}{2}y^3 + 18x^2y + 9xy^2 - 18x^2 - \dfrac{11}{2}y^2 - 20xy + 10x + 6y - 2 \end{bmatrix},$$

$$\psi_{e[0,2]}^3 = \begin{bmatrix} -\dfrac{3}{2}x^3 - 12y^3 - 9x^2y - 18xy^2 + \dfrac{11}{2}x^2 + 18y^2 + 20xy - 6x - 10y + 2 \\ 6y^3 + \dfrac{3}{2}x^2y + 6xy^2 - 4y^2 - 2xy \end{bmatrix},$$

$$\psi_{e[1,2]}^3 = \begin{bmatrix} \dfrac{3}{2}x^3 - 3x^2y + \dfrac{3}{2}xy^2 - y^2 - xy - \dfrac{1}{2}x \\ -dfrac32y^3 - \dfrac{3}{2}xy^2 + 3x^2y + x^2 + xy + \dfrac{1}{2}y \end{bmatrix}$$

$$(7.5)$$
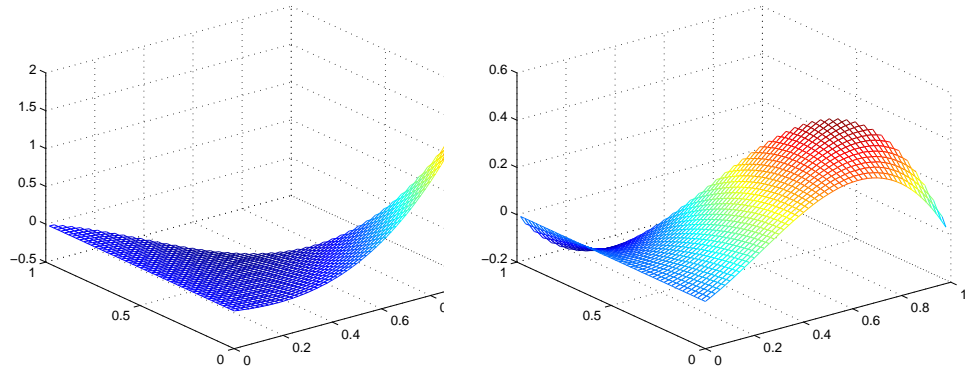
(a) x component (b) y conponent

Figure 19: Graph of $\psi^3_{e[1,2]}$

Interior functions

$$
\psi^{\mathbf{t},3}_{e[0,1]} = \begin{bmatrix} -x(x+y-1)(2x+y-1) \\ \\ 0 \end{bmatrix},
$$

$$
\psi^{\mathbf{t},3}_{e[0,2]} = \begin{bmatrix} 0 \\ \\ -y(x+y-1)(x+2y-1) \end{bmatrix}, \tag{7.6}
$$

$$
\psi^{\mathbf{t},3}_{e[1,2]} = \begin{bmatrix} -xy(x-y) \\ \\ xy(x-y) \end{bmatrix}
$$
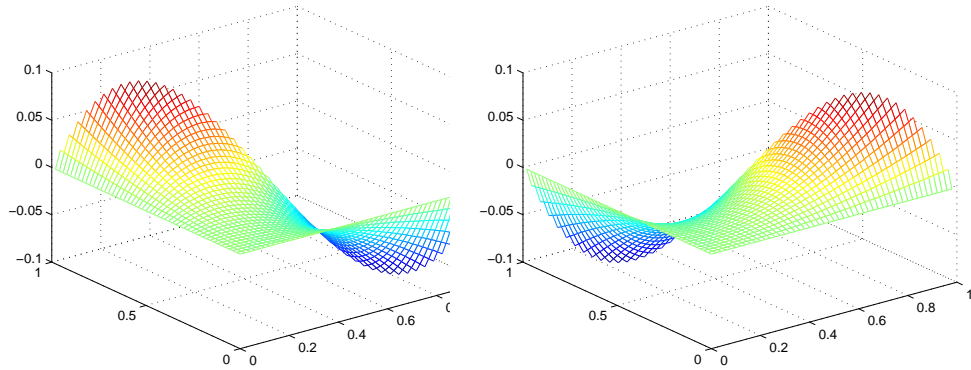
(a) x component

(b) y conponent

Figure 20: Graph of $\psi_{e[1,2]}^{\mathbf{t},3}$

Bubble functions

$$\psi_{0,0}^{\mathbf{t},\overrightarrow{e_1}} = \begin{bmatrix} xy(1 - x - y) \\ \\ 0 \end{bmatrix},$$

$$\psi_{0,0}^{\mathbf{t},\overrightarrow{e_2}} = \begin{bmatrix} 0 \\ \\ xy(1 - x - y) \end{bmatrix}$$

$$(7.7)$$
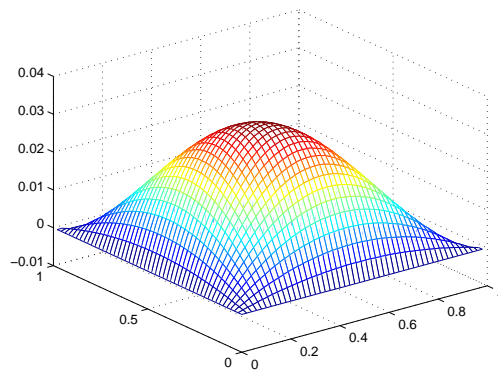
Figure 21: Graph of $\psi_{0,0}^{\mathbf{t},e_1}$, x component

- **Fourth order**

Edge functions

$$\psi^4_{e[0,1]} = \begin{bmatrix} -(\frac{5}{2}(2x+y-1)^3 + \frac{3}{2}(2x+y-1)^2 - 3x - \frac{3}{2}y + 1)x \\ (-3x + \frac{3}{2} - \frac{3}{2}y + \frac{5}{2}(2x+y-1)^3)(2x+y-1) + (-\frac{1}{2} + \frac{3}{2}(2x+y-1))(1-y) \end{bmatrix},$$

$$\psi^4_{e[0,2]} = \begin{bmatrix} (-3y + \frac{3}{2} - \frac{3}{2}x + \frac{5}{2}(x+2y-1)^3)(-x-2y+1) + (-\frac{1}{2} + \frac{3}{2}(x+2y-1)^2)(x-1) \\ (\frac{5}{2}(x+2y-1)^3 + \frac{3}{2}(x+2y-1)^2 - \frac{3}{2}x - 3y + 1)y \end{bmatrix},$$

$$\psi^4_{e[1,2]} = \begin{bmatrix} (\frac{5}{2}(y-x)^3 - \frac{3}{2}(y-x)^2 + \frac{3}{2}x - \frac{3}{2}y + \frac{1}{2})x \\ (-\frac{5}{2}(y-x)^3 - \frac{3}{2}(y-x)^2 - \frac{3}{2}x + \frac{3}{2}y + \frac{1}{2})y \end{bmatrix}$$

$$(7.8)$$
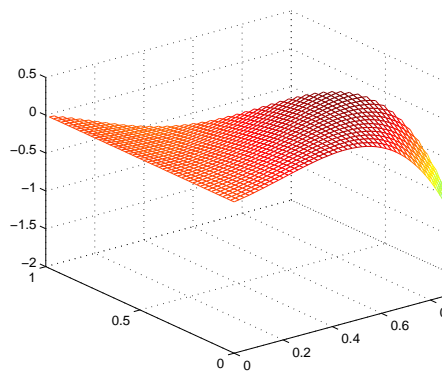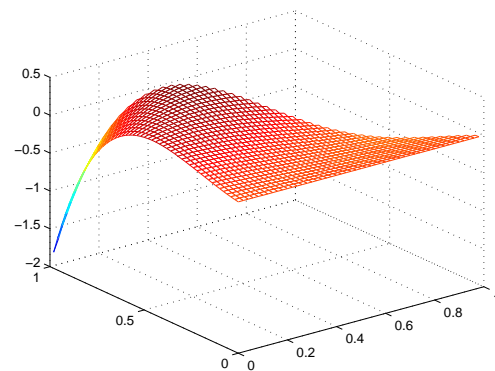
(a) x component (b) y conponent

Figure 22: Graph of $\psi^4_{e[1,2]}$

Interior functions

$$\psi^{\mathbf{t},4}_{e[0,1]} = \begin{bmatrix} x(1-x-y)(-3x+\dfrac{3}{2}-\dfrac{3}{2}y+\dfrac{5}{2}(2x+y-1)^3) \\ 0 \end{bmatrix},$$

$$\psi^{\mathbf{t},4}_{e[0,2]} = \begin{bmatrix} 0 \\ y(1-x-y)(-3y+\dfrac{3}{2}-\dfrac{3}{2}x+\dfrac{5}{2}(x+2y-1)^3) \end{bmatrix}, \qquad (7.9)$$

$$\psi^{\mathbf{t},4}_{e[1,2]} = \begin{bmatrix} xy(-\dfrac{3}{2}y+\dfrac{3}{2}x+\dfrac{5}{2}(y-x)^3) \\ -xy(-\dfrac{3}{2}y+\dfrac{3}{2}x+\dfrac{5}{2}(y-x)^3) \end{bmatrix}$$
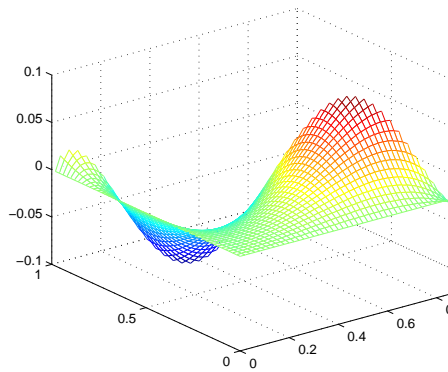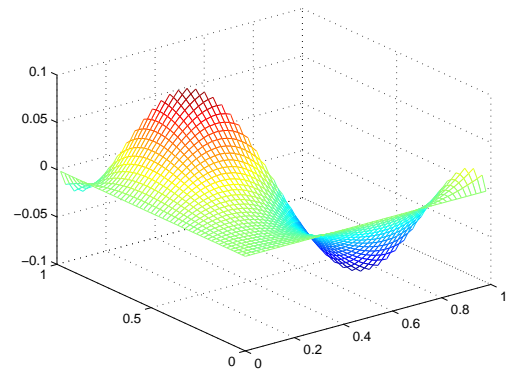
(a) x component (b) y conponent

Figure 23: Graph of $\psi^{\mathbf{t},4}_{e[1,2]}$

Bubble functions

$$\psi_{1,0}^{\mathbf{t},\overrightarrow{e_1}} = \begin{bmatrix} (1-x-y)xy(y-x) \\ \\ 0 \end{bmatrix},$$

$$\psi_{1,0}^{\mathbf{t},\overrightarrow{e_2}} = \begin{bmatrix} 0 \\ \\ (1-x-y)xy(y-x) \end{bmatrix}$$

$$\psi_{0,1}^{\mathbf{t},\overrightarrow{e_1}} = \begin{bmatrix} (1-x-y)xy(1-2x-y) \\ \\ 0 \end{bmatrix},$$

$$\psi_{0,1}^{\mathbf{t},\overrightarrow{e_2}} = \begin{bmatrix} 0 \\ \\ (1-x-y)xy(1-2x-y) \end{bmatrix}$$

$$(7.10)$$
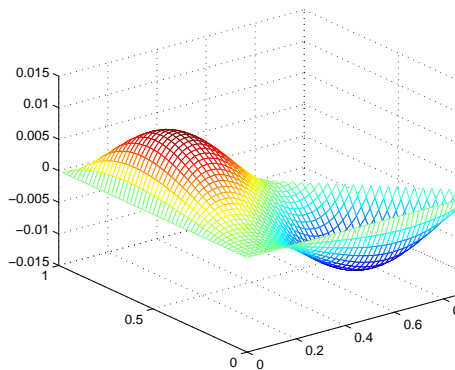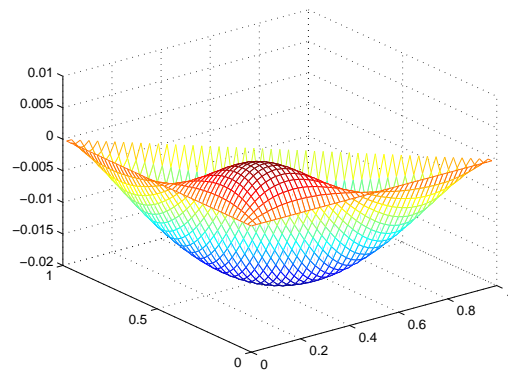
(a) Graph of $\psi_{1,0}^{\mathbf{t},e_1}$ (b) Graph of $\psi_{0,1}^{\mathbf{t},e_1}$

Figure 24: Graph of bubble functions, x component

- **Fifth order**

Edge functions

$$\psi^5_{e[0,1]} = \begin{bmatrix} -(\frac{35}{8}(2x+y-1)^4 + \frac{5}{2}(2x+y-1)^3 - \frac{15}{4}(2x+y-1)^2 - 3x - \frac{3}{2}y + \frac{15}{8})x \\ (\frac{3}{8} - \frac{15}{4}(2x+y-1)^2 + \frac{35}{8}(2x+y-1)^4)(2x+y-1) + (-3x + \frac{3}{2} - \frac{3}{2}y + \frac{5}{2}(2x+y-1)^3)(1-y) \end{bmatrix},$$

$$\psi^5_{e[0,2]} = \begin{bmatrix} (\frac{3}{8} - \frac{15}{4}(x+2y-1)^2 + \frac{35}{8}(x+2y-1)^4)(x+2y-1) + (-3y + \frac{3}{2} - \frac{3}{2}x + \frac{5}{2}(x+2y-1)^3)(x-1) \\ (\frac{35}{8}(x+2y-1)^4 \frac{5}{2}(x+2y-1)^3 - \frac{15}{4}(x+2y-1)^2 - \frac{3}{2}x - 3y + \frac{15}{8})y \end{bmatrix},$$

$$\psi^5_{e[1,2]} = \begin{bmatrix} (\frac{35}{8}(y-x)^4 - \frac{5}{2}(y-x)^3 - \frac{15}{4}(y-x)^2 - \frac{3}{2}x + \frac{3}{2}y + \frac{3}{8})x \\ (-\frac{35}{8}(y-x)^4 - \frac{5}{2}(y-x)^3 + \frac{15}{4}(y-x)^2 - \frac{3}{2}x + \frac{3}{2}y - \frac{3}{8})y \end{bmatrix}$$

$$(7.11)$$
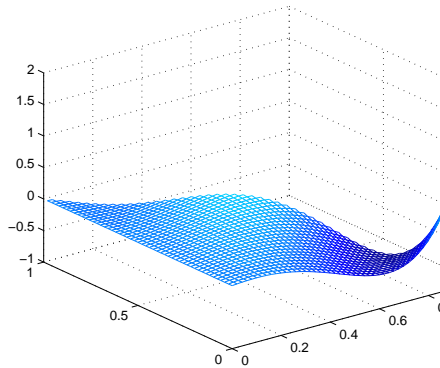
(a) x component
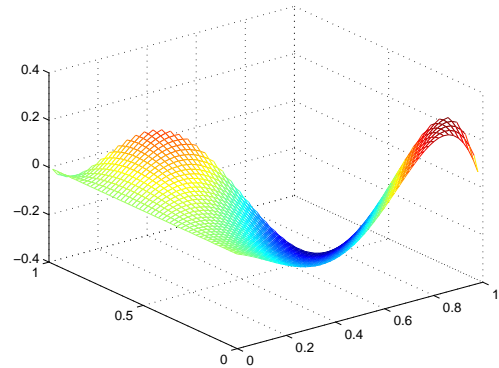
(b) y conponent

Figure 25: Graph of $\psi^5_{e[1,2]}$

Interior functions

$$\psi_{e[0,1]}^{\mathbf{t},5} = \begin{bmatrix} x(1 - x - y)(\dfrac{3}{8} - \dfrac{15}{4})(2x + Y - 1)^2 + \dfrac{35}{8}(2x + y - 1)^4 \\ 0 \end{bmatrix},$$

$$\psi_{e[0,2]}^{\mathbf{t},5} = \begin{bmatrix} 0 \\ y(1 - x - y)(\dfrac{3}{8} - \dfrac{15}{4}(x + 2y - 1)^2 + \dfrac{35}{8}(x + 2y - 1)^4) \end{bmatrix}, \quad (7.12)$$

$$\psi_{e[1,2]}^{\mathbf{t},5} = \begin{bmatrix} xy(\dfrac{3}{8} - \dfrac{15}{4}(y - x)^2 + \dfrac{35}{8}(y - x)^4) \\ -xy(\dfrac{3}{8} - \dfrac{15}{4}(y - x)^2 + \dfrac{35}{8}(y - x)^4) \end{bmatrix}$$
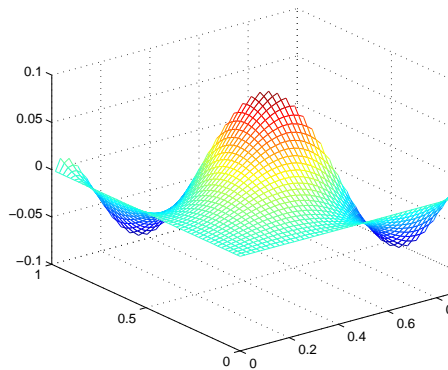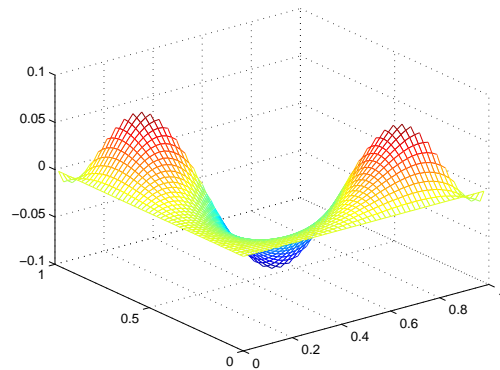
(a) x component　　　　(b) y conponent

Figure 26: Graph of $\psi_{e[1,2]}^{\mathbf{t},5}$
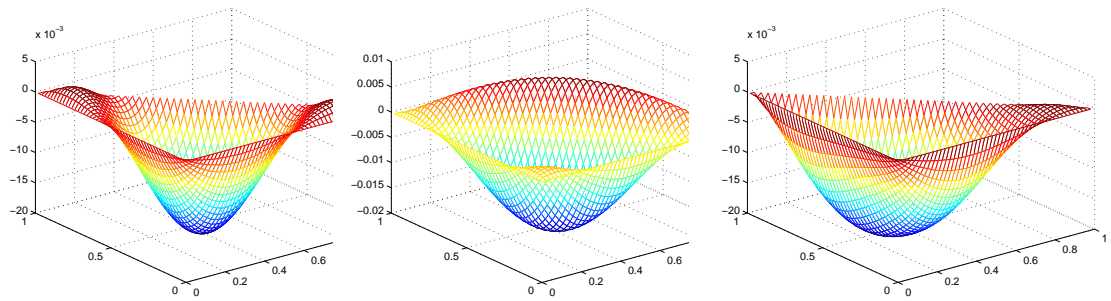
(a) Graph of $\psi_{2,0}^{\mathbf{t},e_1}$ (b) Graph of $\psi_{0,2}^{\mathbf{t},e_1}$ (c) Graph of $\psi_{1,1}^{\mathbf{t},e_1}$

Figure 27: Graph of bubble functions, x component

<u>Bubble functions</u>

$$\psi_{2,0}^{\mathbf{t},\overrightarrow{e_1}} = \begin{bmatrix} xy(1-x-y)(-\frac{1}{2} + \frac{3}{2}(y-x)^2) \\ 0 \end{bmatrix},$$

$$\psi_{2,0}^{\mathbf{t},\overrightarrow{e_2}} = \begin{bmatrix} 0 \\ xy(1-x-y)(-\frac{1}{2} + \frac{3}{2}(y-x)^2) \end{bmatrix},$$

$$\psi_{0,2}^{\mathbf{t},\overrightarrow{e_1}} = \begin{bmatrix} xy(1-x-y)(-\frac{1}{2} + \frac{3}{2}(1-2x-2y)^2) \\ 0 \end{bmatrix},$$

(7.13)

$$\psi_{0,2}^{\mathbf{t},\overrightarrow{e_2}} = \begin{bmatrix} 0 \\ xy(1-x-y)(-\frac{1}{2} + \frac{3}{2}(1-2x-2y)^2) \end{bmatrix},$$

$$\psi_{1,1}^{\mathbf{t},\overrightarrow{e_1}} = \begin{bmatrix} xy(1-x-y)(-\frac{1}{2} + (y-x)(1-2x-2y)) \\ 0 \end{bmatrix},$$

$$\psi_{1,1}^{\mathbf{t},\overrightarrow{e_2}} = \begin{bmatrix} 0 \\ xy(1-x-y)(-\frac{1}{2} + (y-x)(1-2x-2y)) \end{bmatrix}$$

7.2   Barycentric Coordinates

In the context of a triangle, barycentric coordinates are also known as area coordinates or areal coordinates, because the coordinates of P with respect to triangle ABC are equivalent to the (signed) ratios of the areas of PBC, PCA and PAB to

the area of the reference triangle ABC. Areal and trilinear coordinates are used for similar purposes in geometry.
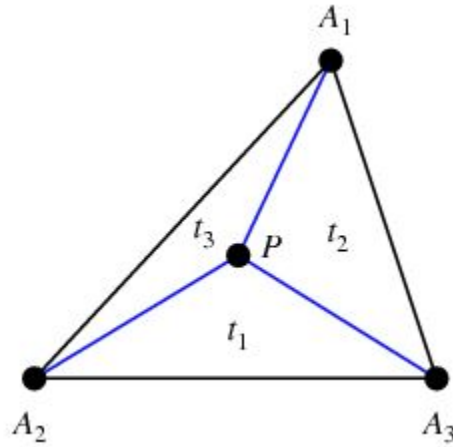
Figure 28: An example of patching two triangular elements

Barycentric or areal coordinates are extremely useful in engineering applications involving triangular subdomains. These make analytic integrals often easier to evaluate, and Gaussian quadrature tables are often presented in terms of area coordinates.

Conversion between barycentric and Cartesian coordinates

Given a point $\mathbf{r}$ in a triangle's plane one can obtain the barycentrick coordinates λ_1, λ_2 and λ_3 from the Cartesian coordinates (x, y) or vice versa.

We can write the Cartesian coordinates of the point $\mathbf{r}$ in terms of the Cartesian components of the triangle vertices $\mathbf{r}_1, \mathbf{r}_2, \mathbf{r}_3$, where $\mathbf{r}_i = (x_i, y_i)$ and in terms of the barycentric coordinates of $\mathbf{r}$ as

$$\mathbf{x} = \lambda_1 x_1 + \lambda_2 x_2 + \lambda_3 x_3$$
$$\mathbf{y} = \lambda_1 y_1 + \lambda_2 y_2 + \lambda_3 y_3$$

(7.14)

where $\lambda_1 + \lambda_2 + \lambda_3 = 1$. That is, the Cartesian coordinates of any point are a weighted average of the Cartesian coordinates of the triangle's vertices, with the weights being

the point's barycentric coordinates summing to unity.

To find the reverse transformation, from Cartesian coordinates to barycentric co-ordinates, it satisfies this linear transformation

$$\mathbf{T} \cdot \lambda = \mathbf{r} - \mathbf{r_3} \tag{7.15}$$

where

$$\mathbf{T} = \begin{bmatrix} x_1 - x_3 & x_2 - x_3 \\ y_1 - y_3 & y_2 - y_3 \end{bmatrix} \tag{7.16}$$

Now the matrix $\mathbf{T}$ is invertible. Thus, we can rearrange the above equation to get

$$\begin{bmatrix} \lambda_1 \\ \lambda_2 \end{bmatrix} = \mathbf{T}^{-1}(\mathbf{r} - \mathbf{r}_3) \tag{7.17}$$

Explicitly, the formulae for the barycentric coordinates of point $\mathbf{r}$ in terms of its Cartesian coordinates (x, y) and in terms of the Cartesian coordinates of the triangle's vertices are:

$$
\begin{aligned}
\lambda_1 &= \frac{(y_2 - y_3)(x - x_3) + (x_3 - x_2)(y - y_3)}{det(\mathbf{J})} = \frac{(y_2 - y_3)(x - x_3) + (x_3 - x_2)(y - y_3)}{(y_2 - y_3)(x_1 - x_3) + (x_3 - x_2)(y_1 - y_3)} \\
\lambda_2 &= \frac{(y_3 - y_1)(x - x_3) + (x_1 - x_3)(y - y_3)}{det(\mathbf{J})} = \frac{(y_3 - y_1)(x - x_3) + (x_1 - x_3)(y - y_3)}{(y_2 - y_3)(x_1 - x_3) + (x_3 - x_2)(y_1 - y_3)} \\
\lambda_3 &= 1 - \lambda_1 - \lambda_2
\end{aligned}
\tag{7.18}
$$

7.3 Numerical Integration and Numerical Quadrature

- Gaussian quadrature for general triangle elements K:

First of all, on the reference triangular element $T_S t$, the Gaussian quadrature

rules [16] are in the form

$$\int\int_{T_st} g(\xi,\eta)d\xi d\eta \approx \frac{1}{2}\sum_{i=1}^{N_g} \omega_i g(\xi_i,\eta_i) \qquad (7.19)$$

where N_g is the number of quadrature points, (ξ_i,η_i) are quadrature points located inside the reference triangular element and ω_i are weights (normalized with respect to the triangle area).

Let K be a triangular element with straight boundary lines and vertices $(x_i,y_i), i = 1,2,3$ arranged in the counter-clockwise order:

We would like to evaluate

$$I = \int\int_K F(x,y)dx dy, \qquad (7.20)$$

The idea is to first transform the triangular element K to the standard triangular element $T_s t$ and then apply the Gaussian quadrature for T_{st}.

The mapping can be achieved conveniently by using the nodal shape functions as follows:

$$x = P(\xi,\eta) = \sum_{i=1}^{3} x_i N_i(\xi,\eta) = x_1 N_1(\xi,\eta) + x_2 N_2(\xi,\eta) + x_3 N_3(\xi,\eta),$$
$$x = Q(\xi,\eta) = \sum_{i=1}^{3} y_i N_i(\xi,\eta) = y_1 N_1(\xi,\eta) + y_2 N_2(\xi,\eta) + y_3 N_3(\xi,\eta),$$
$$(7.21)$$

Then we have

$$\int\int_K F(x,y)dx dy = \int\int_{T_{st}} F(P(\xi,\eta),Q(\xi,\eta))|J(\xi,\eta)|d\xi d\eta \qquad (7.22)$$

where $J(\xi, \eta)$ is the Jacobian of the transformation, namely,

$$J(\xi, \eta) = \left| \frac{\partial(x, y)}{\partial(\xi, \eta)} \right| = \begin{vmatrix} \dfrac{\partial x}{\partial \xi} & \dfrac{\partial y}{\partial \xi} \\ \dfrac{\partial x}{\partial \eta} & \dfrac{\partial y}{\partial \eta} \end{vmatrix} = 2T \tag{7.23}$$

Here T represents the area of the triangle K, which is generalized in (), and can be evaluated here in $T_s t$ by

$$K = \frac{|x_1(y_2 - y_3) + x_2(y_3 - y_1) + x_3(y_1 - y_2)|}{2} \tag{7.24}$$

Therefore, we have

$$\int \int_K F(x, y) dx dy = 2K \int \int_{T_s t} F(P(\xi, \eta), Q(\xi, \eta)) d\xi d\eta \tag{7.25}$$

Applying the Gaussian quadrature of degree N for the standard triangular element yields

$$\int \int_K F(x, y) dx dy \approx K \sum_{i=1}^{N_g} \omega_i F(P(\xi_i, \eta_i), Q(\xi_i, \eta_i)) \tag{7.26}$$

- Legendre-Gauss quadrature for 1-D integration:

  Legendre-Gauss quadrature integral approximation tries to solve the following function

  $$\int_a^b f(x) dx = \sum_{i=1}^{\infty} \omega_i f(x_i) \approx \sum_{i=1}^{n} \omega_i f(x_i) \tag{7.27}$$

  by picking approximate values for n, ω_i and x_i. While only defined for interval $[-1, 1]$, this is actually a universal function, because we can convert the limits

of integration for any interval $[a, b]$ to the Legendre-Gauss interval $[-1, 1]$:

$$\int_{\partial K} \phi(x, y) ds = \frac{1}{2} d_r \cdot \sum_{i=1}^{N_r} \phi(x(\xi_i, \eta_i), y(\xi_i, \eta_i)) w_i \tag{7.28}$$

where (ξ_i, η_i) are the Gaussian quadrature points on reference triangle, and w_i are the weights. d_r is the length of the integrated edge, and N_r are the number of quadrature points on the edge.

Here we include some of the weights and abscissae tables for both 1-D and 2-D triangular elements that are used for our computation.

- 1-D Gaussian quadrature

Table 10: 1-D Gaussian quadrature

i	weight-ω_i	abscissa-x_i
n=2		
1	1.0000000000000000	-0.5773502691896257
2	1.0000000000000000	0.5773502691896257
n=3		
1	0.8888888888888888	0.0000000000000000
2	0.5555555555555556	-0.7745966692414834
3	0.5555555555555556	0.7745966692414834
n=4		
1	0.6521451548625461	-0.3399810435848563

(continued)

2	0.6521451548625461	0.3399810435848563
3	0.3478548451374538	-0.8611363115940526
4	0.3478548451374538	0.8611363115940526
n=5		
1	0.5688888888888889	0.0000000000000000
2	0.4786286704993665	-0.5384693101056831
3	0.4786286704993665	0.5384693101056831
4	0.2369268850561891	-0.9061798459386640
5	0.2369268850561891	0.9061798459386640
n=6		
1	0.3607615730481386	0.6612093864662645
2	0.3607615730481386	-0.6612093864662645
3	0.4679139345726910	-0.2386191860831969
4	0.4679139345726910	0.2386191860831969
5	0.1713244923791704	-0.9324695142031521
6	0.1713244923791704	0.9324695142031521
n=7		
1	0.4179591836734694	0.0000000000000000
2	0.3818300505051189	0.4058451513773972
3	0.3818300505051189	-0.4058451513773972

(continued)

4	0.2797053914892766	-0.7415311855993945
5	0.2797053914892766	0.7415311855993945
6	0.1294849661688697	-0.9491079123427585
7	0.1294849661688697	0.9491079123427585
n=8		
1	0.3626837833783620	-0.1834346424956498
2	0.3626837833783620	0.1834346424956498
3	0.3137066458778873	-0.5255324099163290
4	0.3137066458778873	0.5255324099163290
5	0.2223810344533745	-0.7966664774136267
6	0.2223810344533745	0.7966664774136267
7	0.1012285362903763	-0.9602898564975363
8	0.1012285362903763	0.9602898564975363
n=9		
1	0.3302393550012598	0.0000000000000000
2	0.1806481606948574	-0.8360311073266358
3	0.1806481606948574	0.8360311073266358
4	0.0812743883615744	-0.9681602395076261
5	0.0812743883615744	0.9681602395076261
6	0.3123470770400029	-0.3242534234038089

(continued)

7	0.3123470770400029	0.3242534234038089
8	0.2606106964029354	-0.6133714327005904
9	0.2606106964029354	0.6133714327005904
n=10		
1	0.2955242247147529	-0.1488743389816312
2	0.2955242247147529	0.1488743389816312
3	0.2692667193099963	-0.4333953941292472
4	0.2692667193099963	0.4333953941292472
5	0.2190863625159820	-0.6794095682990244
6	0.2190863625159820	0.6794095682990244
7	0.1494513491505806	-0.8650633666889845
8	0.1494513491505806	0.8650633666889845
9	0.0666713443086881	-0.9739065285171717
10	0.0666713443086881	0.9739065285171717

- 2-D Gaussian quadrature for triangle elements

Table 11: 2-D Gaussian quadrature for triangular elements

i	x	y	ω_i
n=1			
1	0.33333333333333	0.33333333333333	0.33333333333333
n=2			
1	0.16666666666667	0.16666666666667	0.33333333333333
2	0.16666666666667	0.16666666666667	0.33333333333333
3	0.16666666666667	0.16666666666667	0.33333333333333
n=3			
1	0.33333333333333	0.33333333333333	-0.56250000000000
2	0.20000000000000	0.20000000000000	0.52083333333333
3	0.20000000000000	0.60000000000000	0.52083333333333
4	0.60000000000000	0.20000000000000	0.52083333333333
n=4			
1	0.44594849091597	0.44594849091597	0.22338158967801
2	0.44594849091597	0.10810301816807	0.22338158967801
3	0.10810301816807	0.44594849091597	0.22338158967801

(continued)

4	0.09157621350977	0.09157621350977	0.10995174365532
5	0.09157621350977	0.81684757298046	0.10995174365532
6	0.81684757298046	0.09157621350977	0.10995174365532
n=5			
1	0.33333333333333	0.33333333333333	0.22500000000000
2	0.47014206410511	0.47014206410511	0.13239415278851
3	0.47014206410511	0.05971587178977	0.13239415278851
4	0.05971587178977	0.47014206410511	0.13239415278851
5	0.10128650732346	0.10128650732346	0.12593918054483
6	0.10128650732346	0.79742698535309	0.12593918054483
7	0.79742698535309	0.10128650732346	0.12593918054483
n=6			
1	0.24928674517091	0.24928674517091	0.11678627572638
2	0.24928674517091	0.50142650965818	0.11678627572638
3	0.50142650965818	0.24928674517091	0.11678627572638
4	0.06308901449150	0.06308901449150	0.05084490637021
5	0.06308901449150	0.87382197101700	0.05084490637021
6	0.87382197101700	0.06308901449150	0.05084490637021
7	0.31035245103378	0.63650249912140	0.08285107561837
8	0.63650249912140	0.05314504984482	0.08285107561837

(continued)

9	0.05314504984482	0.31035245103378	0.08285107561837
10	0.63650249912140	0.31035245103378	0.08285107561837
11	0.31035245103378	0.05314504984482	0.08285107561837
12	0.05314504984482	0.63650249912140	0.08285107561837
n=7			
1	0.33333333333333	0.33333333333333	-0.14957004446768
2	0.26034596607904	0.26034596607904	0.17561525743321
3	0.26034596607904	0.47930806784192	0.17561525743321
4	0.47930806784192	0.26034596607904	0.17561525743321
5	0.06513010290222	0.06513010290222	0.05334723560884
6	0.06513010290222	0.86973979419557	0.05334723560884
7	0.86973979419557	0.06513010290222	0.05334723560884
8	0.31286549600487	0.63844418856981	0.07711376089026
9	0.63844418856981	0.04869031542532	0.07711376089026
10	0.04869031542532	0.31286549600487	0.07711376089026
11	0.63844418856981	0.31286549600487	0.07711376089026
12	0.31286549600487	0.04869031542532	0.07711376089026
13	0.04869031542532	0.63844418856981	0.07711376089026
n=8			
1	0.33333333333333	0.33333333333333	0.14431560767779

(continued)

2	0.45929258829272	0.45929258829272	0.09509163426728
3	0.45929258829272	0.08141482341455	0.09509163426728
4	0.08141482341455	0.45929258829272	0.09509163426728
5	0.17056930775176	0.17056930775176	0.10321737053472
6	0.17056930775176	0.65886138449648	0.10321737053472
7	0.65886138449648	0.17056930775176	0.10321737053472
8	0.05054722831703	0.05054722831703	0.03245849762320
9	0.05054722831703	0.89890554336594	0.03245849762320
10	0.89890554336594	0.05054722831703	0.03245849762320
11	0.26311282963464	0.72849239295540	0.02723031417443
12	0.72849239295540	0.00839477740996	0.02723031417443
13	0.00839477740996	0.26311282963464	0.02723031417443
14	0.72849239295540	0.26311282963464	0.02723031417443
15	0.26311282963464	0.00839477740996	0.02723031417443
16	0.00839477740996	0.72849239295540	0.02723031417443
n=16			
1	0.33333333333333	0.33333333333333	0.14431560767779
2	0.08141482341455	0.45929258829272	0.09509163426729
3	0.45929258829272	0.45929258829272	0.09509163426729
4	0.45929258829272	0.08141482341455	0.09509163426729

(continued)

5	0.65886138449648	0.17056930775176	0.10321737053472
6	0.17056930775176	0.17056930775176	0.10321737053472
7	0.17056930775176	0.65886138449648	0.10321737053472
8	0.89890554336594	0.05054722831703	0.03245849762320
9	0.05054722831703	0.05054722831703	0.03245849762320
10	0.05054722831703	0.89890554336594	0.03245849762320
11	0.00839477740996	0.26311282963464	0.02723031417444
12	0.26311282963464	0.72849239295540	0.02723031417444
13	0.72849239295540	0.00839477740996	0.02723031417444
14	0.26311282963464	0.00839477740996	0.02723031417444
15	0.72849239295540	0.26311282963464	0.02723031417444
16	0.00839477740996	0.72849239295540	0.02723031417444
n=19			
1	0.33333333333333	0.33333333333333	0.097135796282799
2	0.02063496160253	0.48968251919874	0.031334700227139
3	0.48968251919874	0.48968251919874	0.031334700227139
4	0.48968251919874	0.02063496160253	0.031334700227139
5	0.12582081701413	0.43708959149294	0.077827541004774
6	0.43708959149294	0.43708959149294	0.077827541004774
7	0.43708959149294	0.12582081701413	0.077827541004774

(continued)

8	0.62359292876193	0.18820353561903	0.079647738927210
9	0.18820353561903	0.18820353561903	0.079647738927210
10	0.18820353561903	0.62359292876193	0.079647738927210
11	0.91054097321109	0.04472951339445	0.025577675658698
12	0.04472951339445	0.04472951339445	0.025577675658698
13	0.04472951339445	0.91054097321109	0.025577675658698
14	0.03683841205474	0.22196298916077	0.043283539377289
15	0.22196298916077	0.74119859878450	0.043283539377289
16	0.74119859878450	0.03683841205474	0.043283539377289
17	0.22196298916077	0.03683841205474	0.043283539377289
18	0.74119859878450	0.22196298916077	0.043283539377289
19	0.03683841205474	0.74119859878450	0.043283539377289
n=25			
1	0.33333333333333	0.33333333333333	0.09081799038275
2	0.02884473323269	0.48557763338366	0.03672595775647
3	0.48557763338366	0.48557763338366	0.03672595775647
4	0.48557763338366	0.02884473323269	0.03672595775647
5	0.78103684902993	0.10948157548504	0.04532105943553
6	0.10948157548504	0.10948157548504	0.04532105943553
7	0.10948157548504	0.78103684902993	0.04532105943553

(continued)

8	0.14170721941488	0.30793983876412	0.07275791684542
9	0.30793983876412	0.55035294182100	0.07275791684542
10	0.55035294182100	0.14170721941488	0.07275791684542
11	0.30793983876412	0.14170721941488	0.07275791684542
12	0.55035294182100	0.30793983876412	0.07275791684542
13	0.14170721941480	0.55035294182100	0.07275791684542
14	0.02500353476269	0.24667256063990	0.02832724253106
15	0.24667256063990	0.72832390459741	0.02832724253106
16	0.72832390459741	0.02500353476269	0.02832724253106
17	0.24667256063990	0.02500353476269	0.02832724253106
18	0.72832390459741	0.24667256063990	0.02832724253106
19	0.02500353476269	0.72832390459741	0.02832724253106
20	0.00954081540030	0.06680325101220	0.00942166696373
21	0.06680325101220	0.92365593358750	0.00942166696373
22	0.92365593358750	0.00954081540100	0.00942166696373
23	0.06680325101220	0.00954081540030	0.00942166696373
24	0.92365593358750	0.06680325101220	0.00942166696373
25	0.00954081540030	0.92365593358750	0.00942166696373

REFERENCES

[1] M. Ainsworth and J. Coyle. Hierarchic finite element bases on unstructured tetrahedral meshes. *Internat. J. Numer. Methods Engrg.*, 58:2103–2130, 2003.

[2] H. Alfvén. Existence of electromagnetic-hydrodynamic waves. *Nature*, 150:405–406, 1942.

[3] D. S. Balsara. Divergence-free adaptive mesh refinement for magnetodydrodynamics. *J. Comput. Phys.*, 174:614–648, 2001.

[4] D. S. Balsara. Second order accurate schemes for magnetohydrodynamics with divergence-free reconstruction. *Astrophys. J.*, 151:149–184, 2004.

[5] D. S. Balsara and D. S. Spicer. A staggered mesh algorithm using high order Godunov fluxes to ensure solenoidal magnetic fields in magnetohydrodynamic simulatios. *J. Comput. Phys.*, 149:270–292, 1999.

[6] B.Cockburn and C.-W. Shu. The Runge-Kutta discontinuous Galerkin method for conservation laws V: Multidimensional systems. *J. Comput. Phys.*, 141:199–224, 1998.

[7] J. U. Brackbill and D. C. Barnes. The effect of nonzero $\nabla \cdot \mathbf{B}$ on the numerical solution of the magnetohydrodynamic equations. *J. Comput. Phys.*, 35:426–430, 1980.

[8] J. Xin; W. Cai and N. Guo. On the construction of well-conditioned hierarchical bases for $h(div)$-conforming $\mathbb{R}^n$ simplicial elements. *Commun. Comput. Phys.*, 14:621–638, 2013.

[9] W. Cai. *Computational Methods for electromagnetic Phenomena*. Cambridge, 2013.

[10] B. Cockburn and C.-W. Shu. The Runge-Kutta local projection discontinuous Galerkin finite element method for conservation laws II: General framework. *Math. Comput.*, 52:411–435, 1989.

[11] B. Cockburn and C.-W. Shu. The Runge-Kutta local projection discontinuous Galerkin finite element method for conservation laws III: One-dimensional systerms. *J. Comput. Phys.*, 84:90–113, 1989.

[12] B. Cockburn and C.-W. Shu. The Runge-Kutta local projection discontinuous Galerkin finite element method for conservation laws IV: The multidimensional case. *Math. Comput.*, 54:545–581, 1990.

[13] B. Cockburn and C.-W. Shu. Runge-Kutta discontinuous Galerkin method for convection-dominated problems. *J. Comput. Phys.*, 16:173–261, 2001.

[14] W. Dai and P. R. Woodward. A simple finite difference scheme for multidimensional magnetohydrodynamic equations. *J. Comput. Phys.*, 142:331–369, 1998.

[15] R. Dautray and J.-L. Lions. *Mathematical Analysis and Numerical Methods for Science and Technology, Vol 3. Spectral Theory and Applications.* Springer-Verlag, 1990.

[16] D. A. Dunavant. High degree efficient symmetrical gaussian quadrature rules for the triangle. *Int. J. Num. Meth. Engng,*, 21:1129–1148, 1985.

[17] C. R. Evans and J. F. Hawley. Simulation of magnetohydrodynamic flows: A constrained transport method. *Astrophys. J.*, 332:659–677, 1988.

[18] S. H. Brecht; J. G. Lyon; J. A. Fedder and K. Hain. A simulation study of eastwest IMF effects on the magnetosphere. *Geophys. Res. Lett.*, 8:397–400, 1981.

[19] W. Cai; J. Hu and S. Zhang. High order hierarchical divergence-free constrained transport H(div) finite element method for magnetic induction equation. *Numerical Mathematics: Theory, Methods and Applications*, 2016.

[20] G. S. Jiang and C. C. Wu. A high-order WENO finite difference scheme for the equations of ideal magnetodydrodynamics. *J. Comput. Phys.*, 150:561–594, 1996.

[21] D. Ryu; F. Miniat; T. W. Joens and A. Frank. A divergence-free upwind code for multi-dimensional magnetohydrodynamic flows. *Astrophys. J.*, 509:244–255, 1998.

[22] G. A. Baker; W. N. Jureidini and O. A. Karakashian. Piecewise solenoidal vector fields and the stokes problem. *SIAM J. Numer. Anal.*, 27:1466–1485, 1990.

[23] O. A. Karakashian and W. N.Jureidini. A nonconforming finite element method for the stationary Navier-Stokes equations. *SIAM J. Numer. Anal.*, 35:93–120, 1998.

[24] B. Cockburn; F. Li and C.-W. Shu. The Runge-Kutta local projection p^1 discontinuous Galerkin finite element method for scalar conservation laws. *Math. Model. Num. Analy.*, 25:337–361, 1991.

[25] B. Cockburn; F. Li and C.-W. Shu. Locally divergence-free discontinuous Galerkin methods for the Maxwell equations. *J. Comput. Phys.*, 194:588–610, 2004.

[26] F. Li and C.-W. Shu. Locally divergence-free discontinuous Galerkin methods for MHD equations. *J. Sci.Comput.*, 22:413–442, 2003.

[27] F. Li and L. Xu. Arbitrary order exactly divergence-free central discontinuous Galserkin methods for ideal MHD equations. *J. Comput. Phys.*, 231:2655–2675, 2012.

[28] J. C. Nédélec. Fixed finite elements in $\mathbb{R}^3$. *Nuner. Math.*, 35:315–341, 1980.

[29] J. C. Nédélec. A new family of mixed finite elements in $\mathbb{R}^3$. *Nuner. Math.*, 50:57–81, 1986.

[30] W. Magnus; F. Oberhettinger and R. P. Soni. *Formulas and Theorems for the Special Functions of Mathematical Physics*. Springer-Verlag, 1966.

[31] S. A. Orszag and C.-M. Tang. Small-scale structure of two-dimensional magnetohydrodynamic turbulence. *J. Fluid. Mech.*, 90:129–143, 1979.

[32] K. G. Powell. An approximate riemann solver for Magnetohydrodynamics (that works in more than one dimension). *ICASE report*, pages 94–24, 1994.

[33] J. Qiu and C.-W. Shu. Hermite WENO schemes and their application as limiters for Runge-Kutta discontinuous Galerkin method: One dimensional case. *J. Comput. Phys.*, 193:115–135, 2003.

[34] J. Qiu and C.-W. Shu. Runge-Kutta discontinuous Galerkin method using WENO limiters. *SIAM J. Sci. Comput.*, 26:907–929, 2005.

[35] W. H. Reed and T. R. Hill. Triangular mesh methods for the neutron transport equation. *Tech. Report $LA_U R - 73 - 479$*, 1973.

[36] A. Dedner; F. Kemm; D. Kröner; C.-D. Munz; T. Schnitner and M. Wesenberg. Hyperbolic divergence cleaning for the MHD equations. *J. Comput. Phys.*, 175:654–673, 2002.

[37] C.-W. Shu. TVB uniformly high-order schemes for conservation laws. *Math. Comput.*, 49:105–121, 1987.

[38] C.-W. Shu. *Essentially non-oscillatory and weighted essentially non-oscillatory schemes for hyperbolic conservation laws. In Cockburn, B., Johnson, C., Shu, C.-W., and Tadmor, E., Quarteroni, A. (eds.), Advanced Numerical Approximation of Nonlinear Hyperbolic Equations. Lecture Notes in Mathematics*, volume 1697, pages 325–432. Springer, Berlin, 1998.

[39] C. D. Munz; P. Omnes; R. Schneider; E. Sonnendrücker and U. Voβ. Divergence correction techniques for Maxwell solvers based on a hyperbolic model. *J. Comput. Phys.*, 161:484–511, 2000.

[40] J. M. Stone and M. L. Norman. A radiation magnetohydrodynamics code for astrophysical flows in two space dimensions II: The magnetohydrodynamics algorithms and tests. *Astrophys. J. Suppl. Ser.*, 80:791–818, 1992.

[41] G. Tóth. The $\nabla \cdot \mathbf{B} = 0$ constraint in shock-capturing magnetohydrodynamics codes. *J. Comput. Phys.*, 161:3042–3060, 2000.

[42] B. N. Jiang; J. Wu and L. A. Provinelli. The origin of spurious solutions in computational electromagnetics. *J. Comput. Phys.*, 125:104–123, 1996.

[43] W. Cai; J. Wu and J. Xin. Divergence-free $h(div)$-comforming hierarchical bases for magnetohydrodynamics. *Commun. Math. Stat.*, 1:19–35, 2013.

[44] F. Li; L. Xu and S. Yakovlev. Central discontinuous Galerkin methods for ideal MHD equations with the exactly divergence-free magnetic field. *J. Comput. Phys.*, 230:4828–4847, 2011.

[45] K. S. Yee. Numerical solution of initial boundary value problems involving Maxwell's equations in isotropic media. *IEEE Trans. on antenna Propagation*, AP-14:302–307, 1966.

[46] S. Zaglmayr. *High order finite element methods for electromagnetic field computation.* PhD thesis, Johannes Kepler Universität, Linz, 2006.

[47] K. G. Powell; P. L. Row; R. S. Myong; T. Gombosi; D. D. Zeeuw. An upwind schemee for magnetohydrodynamics. *Num. Meth.for Flu. D*, 5:163, 1994.